

TECHNICAL REPORT  
OCTOBER 1975

DISTRIBUTION STATEMENT A  
Approved for public release;  
Distribution Unlimited

SLL 80-046/LO  
cy 1

V.H. Reiss

54-160

# FEASIBILITY OF A 30-METER SPACE BASED LASER TRANSMITTER

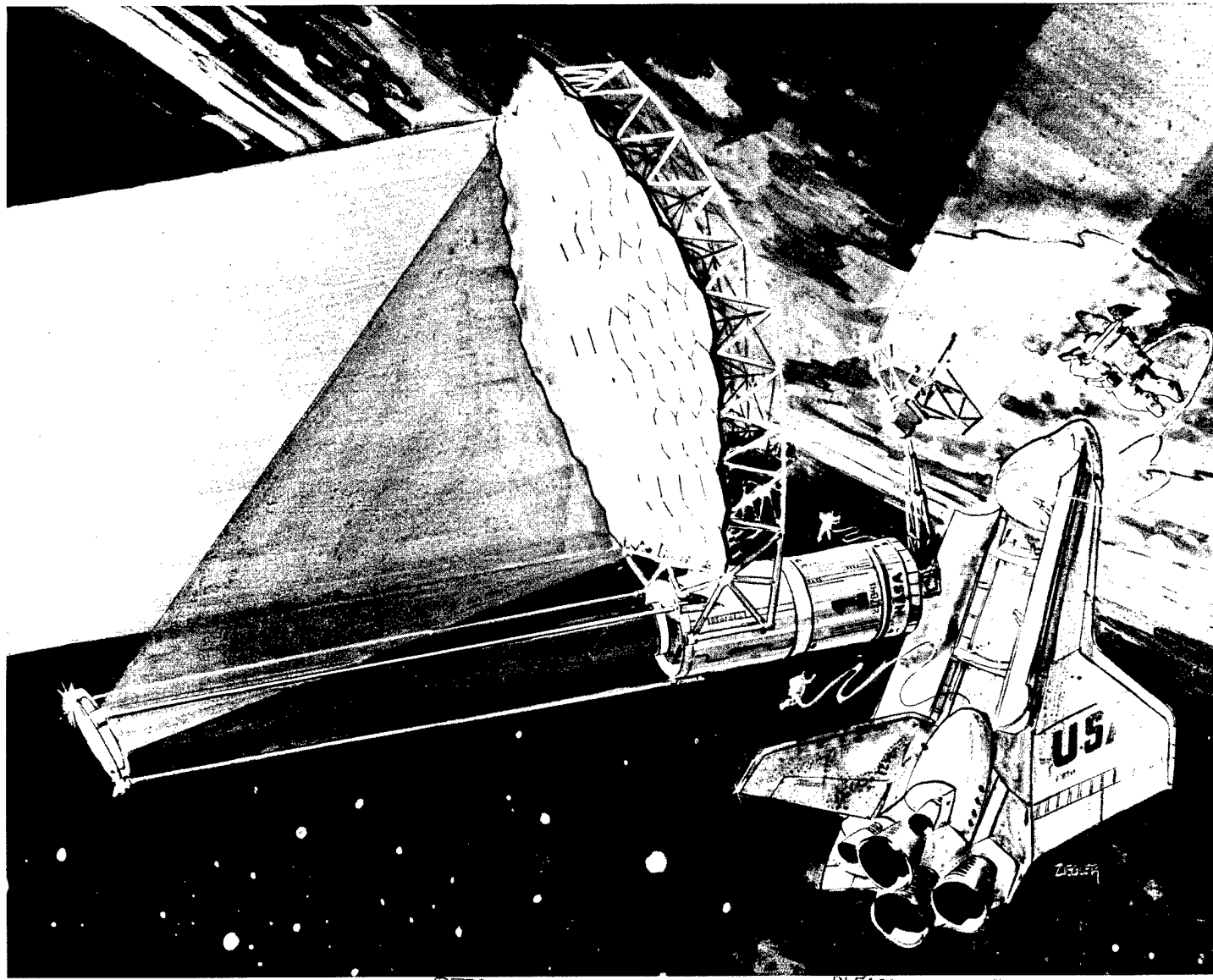
Authors: R. R. Berggren and G. E. Lenertz

Prepared for

NATIONAL AERONAUTICS AND SPACE ADMINISTRATION  
NASA LEWIS RESEARCH CENTER

Contract NAS 3-19400

19980513 293



PLEASE RETURN TO:

BMD TECHNICAL INFORMATION CENTER  
BALLISTIC MISSILE DEFENSE ORGANIZATION  
7100 DEFENSE PENTAGON  
WASHINGTON D.C. 20301-7100

u5764

Itek  
Optical  
Systems

A Division of Itek Corporation  
10 Maguire Road  
Lexington, Massachusetts 02173

Accession Number: 3764

Publication Date: Oct 01, 1975

Title: Feasibility of a 30-Meter Space Based Laser Transmitter - Technical Report

Personal Author: Berggren, R.R.; Lenertz, G.E.

Corporate Author Or Publisher: Itek Corporation, 10 Maguire Road, Lexington, MA 02173 Report Number: NASA CR-134903

Report Prepared for: National Aeronautics and Space Administration, Washington, DC Report Number Assigned by Contract

Monitor: SLL 80-046/LO; 8254-1

Comments on Document: Archive, RRI, DEW

Descriptors, Keywords: Directed Energy Weapon DEW Measurement Feasibility 30-Meter Space Based Laser Transmitter  
Expandable Structure Mirror Deployable Diffraction Technology Geometry Segment

Pages: 110

Cataloged Date: Sep 29, 1992

Contract Number: NAS 3-19400

Document Type: HC

Number of Copies In Library: 000001

Record ID: 24843

Source of Document: DEW

## CONTENTS

1.	Summary and Introduction . . . . .	1
1.1	Summary. . . . .	1
1.2	Introduction. . . . .	1
2.	System Considerations . . . . .	3
2.1	Discussion . . . . .	3
2.2	System Configuration . . . . .	3
2.3	System Tolerances . . . . .	7
2.4	Asphericity. . . . .	13
2.5	Conclusions. . . . .	13
3.	Faceplate Parametric Analysis . . . . .	16
3.1	Discussion . . . . .	16
3.2	Material Properties . . . . .	16
3.3	Coating Properties . . . . .	16
3.4	Thermal Effects on the Faceplate . . . . .	19
3.5	Faceplate Thickness . . . . .	23
3.6	Conclusions—Faceplate Design . . . . .	28
4.	Mirror Figure Control . . . . .	33
4.1	Discussion . . . . .	33
4.2	Applying the Correction . . . . .	33
4.3	Sensing the Error . . . . .	48
4.4	Control Logic . . . . .	49
4.5	Summary. . . . .	50
5.	Stow and Deployment Concepts . . . . .	51
5.1	Discussion . . . . .	51
5.2	Deployment Concepts . . . . .	51
5.3	Support Concepts. . . . .	56
5.4	Surface Concepts. . . . .	57
6.	30-Meter Mirror Concepts. . . . .	61
6.1	Discussion . . . . .	61
6.2	30-Meter Inflatable Concept . . . . .	61
6.3	30-Meter Variable Geometry Concept. . . . .	68
6.4	Assembled in Space Concept . . . . .	73
6.5	Concept Evaluation . . . . .	74
7.	Conclusions and Recommendations. . . . .	84
7.1	Conclusions. . . . .	84
7.2	Recommendations . . . . .	84
8.	References. . . . .	86
	Appendix—Real-Time Lateral Shearing Interferometry . . . . .	88

## FIGURES

1	Optical System Concepts . . . . .	4
2	Energy Within First Dark Ring as a Function of Central Obstruction Diameter Ratio, $\epsilon$ . . . . .	6
3	Allowable Defocus Error at Secondary Mirror or at Prime Focus . . . . .	9
4	Allowable Lateral Displacement and Tilt of Secondary Mirror or of Prime Focus Optics. . . . .	11
5	Allowable Uniform Temperature Change of Metering Structure . . . . .	12
6	Allowable Temperature Difference Between Struts of a Tripod-Type Metering Structure . . . . .	14
7	Asphericity of Off-Axis Mirror Segments . . . . .	15
8	Metallic Reflecting Envelopes on the Extraterrestrial Solar Spectrum. . . . .	17
9	Sag Deformation of Mirror Faceplate Segments Caused by Steady-State Gradient Through Faceplate. . . . .	20
10	Allowable Power Variations on Segments Based on Sag Change Caused by Change in Gradient . . . . .	21
11	Allowable Uniform Temperature Change of Segments of Faceplate . . . . .	22
12	Temperature Versus Absorbed Energy, Radiative Rejection . . . . .	24
13	Mirror Weight Versus Material Thickness . . . . .	26
14	Support Requirements for Faceplate . . . . .	27
15	Natural Frequency of Faceplate . . . . .	29
16	Natural Frequency of Faceplate Versus Support Span . . . . .	30
17	Design Frequency Versus Excitation Acceleration . . . . .	31
18	Support Requirement for Dynamic Input . . . . .	32
19	Schematic Diagram of Techniques to Obtain Figure Correction . . . . .	35
20	Piezoelectric Displacement Actuators . . . . .	37
21	Spring and Screw Force Actuators . . . . .	39
22	Application of a Piezoelectric Device as a Self-Reacting Actuator . . . . .	40
23	Application of Piezoelectric Moment Actuator . . . . .	41
24	Thermal Deformation of a Truss . . . . .	43
25	Active Control Concepts for Supporting Structure . . . . .	44
26	Residual Error After Correction of Faceplate Figure Errors by Actuators. . . . .	47
27	Shuttle Bay-Mirror Area Relationship. . . . .	52
28	Balloon-Mirror Concept . . . . .	54
29	Toroidal Balloon-Mirror Concept . . . . .	55
30	Double Paraboloid Inflatable Mirror . . . . .	55
31	Inflatable Deployment Concept. . . . .	63
32	30-Meter Inflated Mirror Concept . . . . .	65
33	Airmat Folding Sequence . . . . .	67
34	Nitinol Plate Thickness Versus Bend Radius . . . . .	69
35	30-Meter Variable Geometry Concept . . . . .	71

36	30-Meter Assembled in Space Concept. . . . .	75
37	Surface Obtained for Graphite-Epoxy/ULE Sphere . . . . .	79
38	Effect of Humidity on Composite Integral Laminated Flat. . . . .	80
39	Effect of Temperature on Composite Blank . . . . .	81
40	Graphite-Epoxy Mirror Developed Under IR&D by Convair Aerospace and Itek Corporation. . . . .	82

## TABLES

1	Laser-Transmitter Specifications. . . . .	2
2	Material Properties . . . . .	17
3	Reflectance and Absorptance of Various Metals Over the Solar Spectrum. . . . .	18
4	Indicated Specular Reflectance Measured at 0.6328 Micrometers by N.W.C. . . . .	58
5	Indicated Specular Reflectance Measured at 10.6 Micrometers by N.W.C. . . . .	59
6	Indicated Surface Roughness, Å. . . . .	60
7	Evaluation Matrix, 30-Meter Mirror Concept . . . . .	83

## 1. SUMMARY AND INTRODUCTION

### 1.1 SUMMARY

This report presents the results of Itek Corporation's program effort conducted under contract NAS3-19400 for the NASA Lewis Research Center. The study investigated the application of large expandable mirror structure in future space missions. Specifically, scientists and engineers at NASA Lewis have embarked on a program to establish the feasibility and define the potential of high-power lasers for space vehicle propulsion and power generators. Application of these concepts requires a 30-meter-diameter, diffraction limited mirror for transmission of the laser energy.

Three concepts for the laser-transmitter are presented, encompassing the major stow-deployment categories of inflatable, variable geometry, and assembled-in-space mirror structures. Each mirror configuration is based on existing aerospace state-of-the-art technology to establish the feasibility of implementation.

The assembled-in-space concept appears to be the more practical approach at this time. This mirror configuration is based on the concept of partial assembly in space. The aperture would be formed from a number of hexagonal segments which are attached to an expandable truss structure by EVA operations. The reflecting surface would be of low thermal expansion glass/ceramic materials and the supporting structures fabricated from a graphite/epoxy lay-up of matching low expansion characteristics.

First-order system and parametric analysis was performed in order to obtain an understanding of the scope of the problems associated with the deployment of a large diffraction limited mirror in space. Several representative optical configurations for the laser-transmitter were briefly considered and evaluated for possible impact on the design of the 30-meter mirror.

In order to maintain diffraction limited performance, 0.5 micrometer, of such a large mirror in the harsh space environment, it is necessary to incorporate active control of the reflective surface into the mirror assembly.

Control of the figure of the mirror involves the separate operations of sensing the figure errors, computing the corrections to be made, and applying the correction by means of appropriate actuators. The control logic and computation process is simple and is easily within the capability of a small on-board computer. The figure sensing technology is also straightforward, a number of possible sensors having been developed in recent years. Consideration of techniques available for control of the figure indicates that this too is feasible. The techniques that are available, the control ranges required, and indication of the number of actuators required is given in this report.

### 1.2 INTRODUCTION

Potential applications for high-power lasers are being investigated at NASA's Lewis Research Center (ref. 1). Space vehicle propulsion and conversion of laser radiation into electrical

power are examples of the concepts being pursued. Large 30-meter-diameter mirrors, capable of diffraction limited performance at 10.6-micrometer wavelength, will be needed as part of the laser-transmitter space station. To deploy a reflector of this size in space, deviation from the current technology of mirror fabrication is required in that the mirror structure must be expanded from a relatively small launch volume to its operational configuration.

Extensive research and development of expandable structures has been directed toward the applications of solar energy collectors and space communication antennas. This technology forms a valuable basis for formulating concepts for the 30-meter transmitter. From an optical standpoint, the key factor which makes a 30-meter diffraction limited mirror practical is the recent developments in the theory of actively controlling the shape of the mirror surface. This is essential for a mirror of this size, due to the interactions of material properties and the harsh space environment, particularly thermal loads.

The task of formulating a feasible design for the 30-meter diffraction limited mirror is not considered trivial. More than a decade has been required to develop materials, fabrication procedures, and analytical techniques for diffraction limited mirrors, working at the visible wavelengths, to the point where the optical industry is ready to undertake the production of a 3-meter-diameter mirror for NASA's Large Space Telescope program.

The objective of this study was to explore transmitter concepts meeting the specifications of Table 1. A minimum of two basic mirror systems were to be evaluated, a mirror having an expandable, continuous, actively-controlled surface and a multisegmented mirror where the phase of each segment must also be controlled.

Concepts for these mirrors and means of effecting the active figure control are discussed in this report. The philosophy adopted for this study was to understand and stress basic principles and technology applicable to the requirements. From this foundation, development and detailed design activities can progress to the implementation of a viable laser-transmitter in the relatively near future.

Table 1 — Laser-Transmitter Specifications

Item	Value	Remarks
Beam wavelength	$10.6(10^{-6})$ meter	
Mirror heat flux	$100 \text{ kW/m}^2$	Laser output
Beam distribution	Uniform	
Mirror reflectivity	99 percent	
Overall mirror accuracy	$\lambda/20$ p-p, surface	Diffraction limited performance
Transmitter mirror diameter	30 meters	
Pointing stability	$2(10^{-7})$ radian	
Stowed length (maximum)	18.28 meters	Space shuttle limitation (ref. 2)
Stowed diameter (maximum)	4.57 meters	Space shuttle limitation (ref. 2)
Stowed weight (maximum)	28123.2 kg	Space shuttle limitation (ref. 2)

## 2. SYSTEM CONSIDERATIONS

### 2.1 DISCUSSION

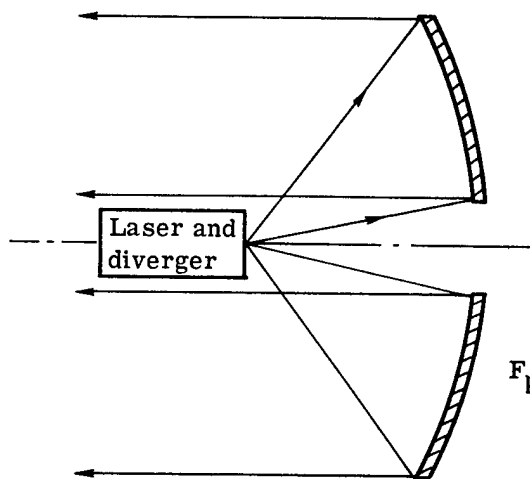
The optical system design will have a strong impact on the structural and thermal requirements of the primary mirror, and thus must be considered as part of the 30-meter mirror design. Of particular concern is the type of system—prime focus, Newtonian, Cassegrain, off-axis, or other—and the first-order parameters establishing mirror focal ratios (f/number) and separations. In this section several such configurations for the laser-transmitter are considered and evaluated for possible impact on the design of the 30-meter mirror. In addition, preliminary tolerance data for system alignment and thermal control were formulated as a function of the focal ratio of the primary mirror.

The system design is of particular importance as it affects heat transfers to and from the large primary mirror. It is shown in later sections that the primary mirror can be uncooled if it is free to radiate to space from the rear face, and if unusual heating gradients are absent. For many system configurations, the laser or other equipment may partially obscure the radiation from the rear face, or may shade sunlight, causing uneven heating. Since it is too early to select a system design, the configurations and tolerances are presented as an aid in understanding laser-transmitter system interactions.

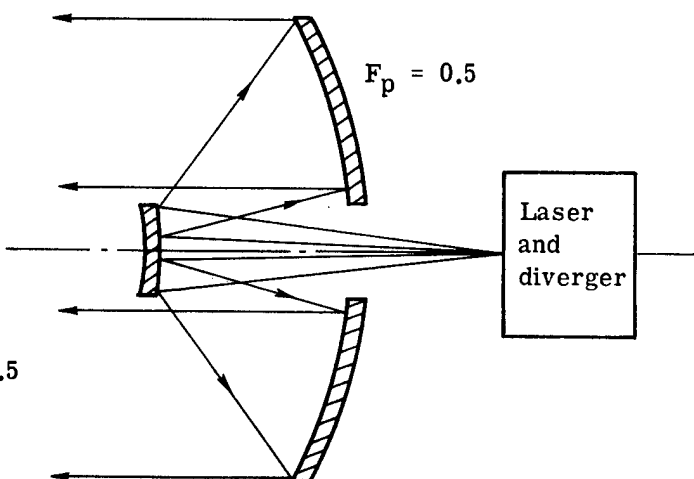
### 2.2 SYSTEM CONFIGURATIONS

The possible optical systems are generalized into prime focus, Cassegrain, Newtonian, and eccentric aperture systems. Other arrangements are possible, but these cover a sufficient range to explore the effects of changing system geometry. A schematic of each of these systems is shown in Fig. 1.

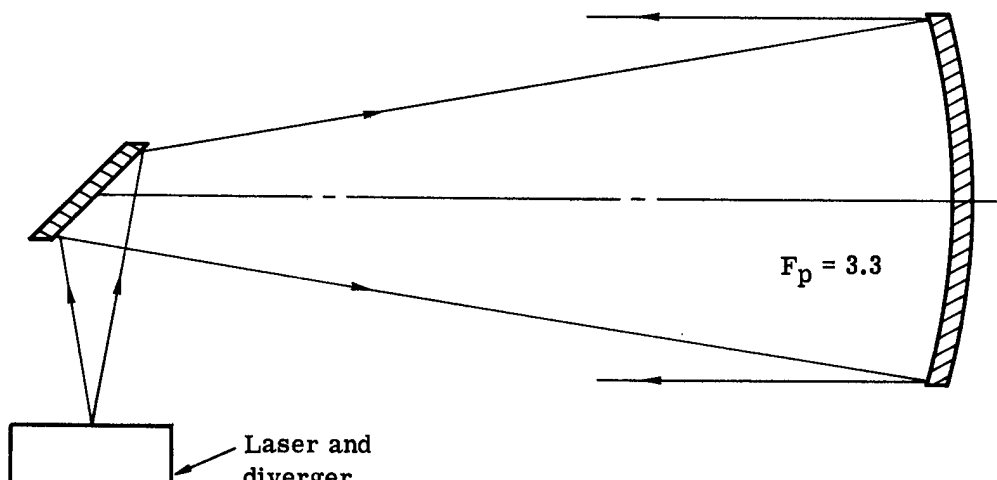
All but the eccentric aperture system have an obscuration of the center of the aperture. This must be kept small in order to maximize the energy delivered to a receiving mirror. For a perfect transmitter, the illumination pattern (diffraction pattern) focused on the receiver will consist of a bright spot, called the Airy disk, surrounded by concentric light and dark rings. At best, about 83 percent of the total energy transmitted will be received within the first dark ring. If the center of the transmitting aperture is obscured, even though the energy is redistributed over the unobscured area so that the same total energy is transmitted, the energy falling within the Airy disk will be decreased. A graph of the energy falling within the first dark ring, as a fraction of the total energy transmitted, is shown in Fig. 2. The energy lost is redistributed well out in the diffraction pattern, and is not captured by slight increases in the size of the receiving aperture. If the central obscuration is less than 20 percent of the diameter of the mirror, only about 5 percent of the available 83 percent of the energy will be lost; but for larger obscurations the energy loss is great. This curve represents only the diffraction effects of the obscuration—it is assumed that all of the laser power is distributed over the annulus outside of obscuration, so that there is no loss of power in the telescope.



(a) Prime-focus system

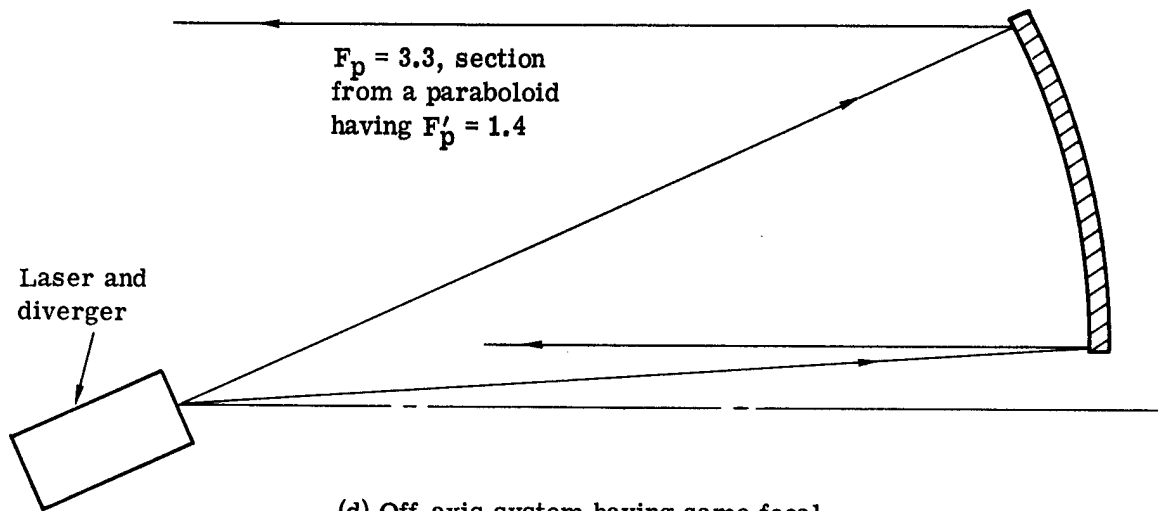


(b) Cassegrain system

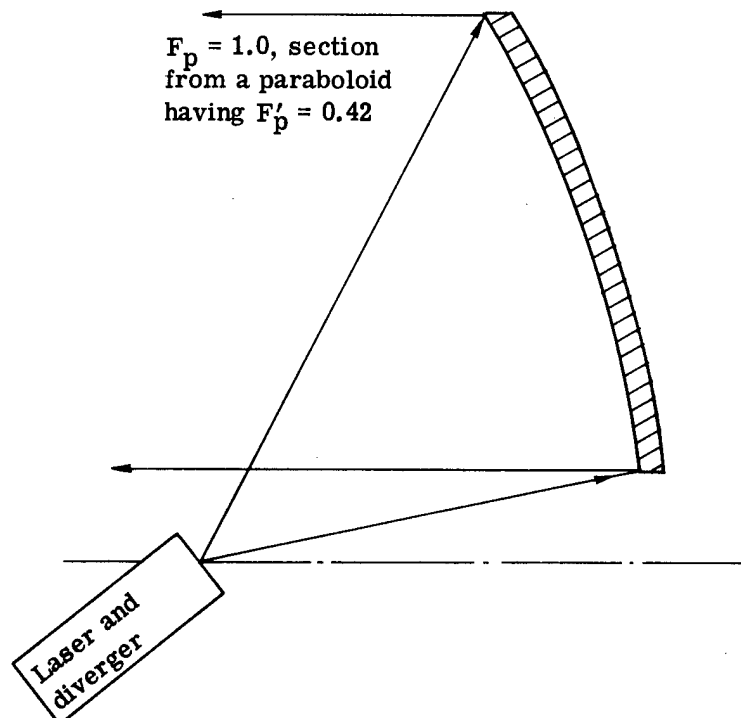


(c) Newtonian system

Fig. 1 — Optical system concepts ( $F_p$  = focal ratio of primary mirror)



(d) Off-axis system having same focal ratio as Newtonian



(e) Minimum length off-axis system

Fig. 1 — Optical system concepts ( $F_p$  = focal ratio of primary mirror) (Cont.)

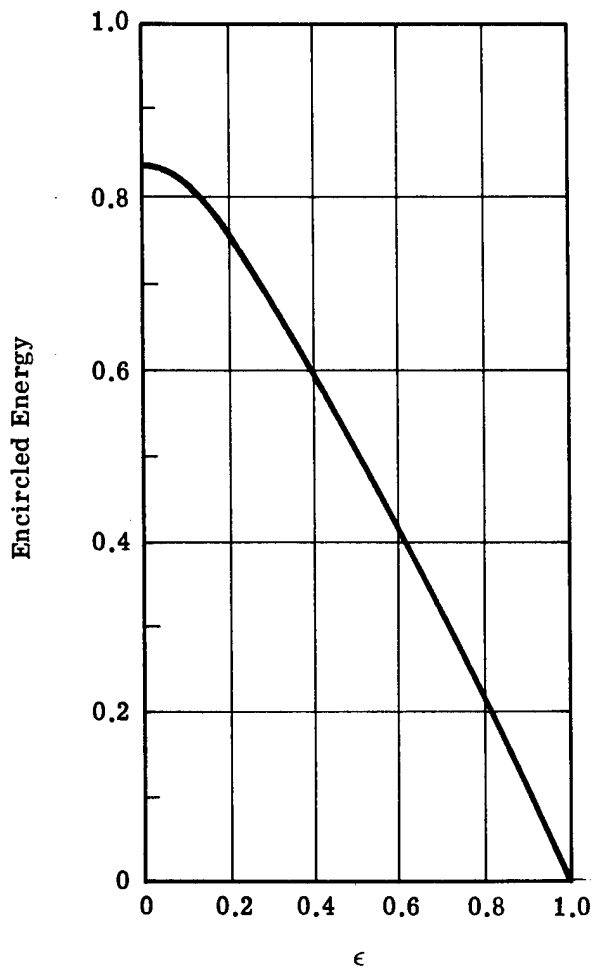


Fig. 2 — Energy within first dark ring as a function of central obstruction diameter ratio,  $\epsilon$

In the prime focus system, there will be a large central obscuration unless the laser is quite small (6-meter diameter or less for a 20 percent diameter obscuration). We expect the laser system to be such that a prime focus system will not be acceptable. The Cassegrain configuration solves this problem, leaving plenty of room for the laser in back of the mirror. If the laser and supporting equipment are large, however, this would seriously restrict the radiation from the back of the mirror and would result in a substantial increase in the temperature of the mirror. This would be true even if a thermally controlled plate is used to accept heat radiated from the mirror, since a two-step radiating process would then be required.

The laser can be placed out of the way by using a Newtonian telescope, which is made by placing a flat folding mirror in the converging beam. This is a good, simple approach, but requires a higher focal ratio, and thus a long system, if a small obscuration is desired. The illustration shows a system having a 20 percent diameter obscuration and the focal point about 5 meters outside the beam (20 meters from the optical axis). The focal ratio of the primary mirror must then be about  $F_p = 3.3$ .

Both the Newtonian and Cassegrain configurations use a small mirror which will see a high heat load and will require cooling. The use of a cooled mirror at a distance from the laser can be avoided by employing an off-axis primary mirror, as shown in Fig. 1(d). If the focal ratio is large,  $F_p = 3.3$ , the system will have about the same properties as the Newtonian system. The primary mirror is now a portion of a larger paraboloidal shape; the asphericity at the edge corresponds to that of a mirror having  $F_p = 1.4$ .

The off-axis system cannot be made as short as an on-axis Cassegrain. Fig. 1(b) shows a short Cassegrain with  $F_p = 0.5$  and Fig. 1(e) shows an off-axis parabola with  $F_p = 1.0$ . The focal ratio of the paraboloidal shape from which the latter is made would be about 0.42, which is even faster than that for the Cassegrain.

It is concluded that the most compact and stable configuration is the short Cassegrain, but that the size of the laser and its shadowing effects on radiation from the mirror must be considered. The off-axis system could not be as compact, but it would eliminate the shadowing and improve the diffraction point spread of the beam. If a longer system ( $F_p = 3$  or greater) is acceptable for the off-axis case, the asphericity of the faceplate of the mirror would be less than for a fast Cassegrain, and thus fabrication of the faceplate segments or of a continuous sheet would not be any more difficult.

### 2.3 SYSTEM TOLERANCES

It is useful to consider how the mirror shape is affected by systems considerations, particularly those relating to alignment requirements. The applications being considered for this 30-meter mirror are so different from those of a conventional optical system, that our general rules regarding tolerances and appropriate system focal ratios (f/numbers) are no longer valid. This is particularly true since we are assuming an actively controlled system and nonconventional structural concepts for the large mirror assembly. It could be expected that the result could be a system with a much faster primary mirror (lower f/number) than those considered feasible for conventional optical telescopes.

Equations and notations for the system tolerance analysis were taken from ref. 3. It is assumed that the laser is either at the prime focus of a parabolic mirror, or that the optical system takes the Cassegrain form, in which the secondary (smaller) mirror is either a traditional secondary mirror (if the laser diverger has a point focus), or is the first element in an afocal beam expander (if the laser optics supply a collimated beam). The results of the tolerance analysis will be similar for almost any other configuration (Newtonian, Gregorian, etc.).

The notation used here is as follows:

$D_p$  = diameter of the primary mirror (30 meters)

$D_{sec}$  = diameter of the secondary mirror

$F_p$  = focal ratio (f/number) of the primary mirror

$F$  = focal ratio of the system

$\epsilon$  = diameter ratio of the central obscuration

$\omega$  = allowable wavefront error. This may be taken either as rms error or as peak-to-peak error, and is always labeled if rms. This is usually assumed to be 0.02 wave rms or 0.10 wave peak-to-peak.

$\sigma$  = mirror surface error, usually taken as 0.05 wave peak-to-peak

$m$  = magnification of the secondary mirror. This is  $F/F_p$  for a system having a focus, or  $D_p/D_{sec}$  for an afocal expander system.

$D_s$  = diameter of a segment of the primary mirror.

Other terms are defined as used.

### 2.3.1 Defocus Tolerance

For either a prime focus or Cassegrain system, the axial displacement,  $\delta_p$ , which can be accepted at the prime focus or at the secondary mirror, is related to the allowable wavefront error by the equation:

$$\delta_p = \frac{\pm 16 \sqrt{3} \omega F_p^2}{1 - \epsilon^2}$$

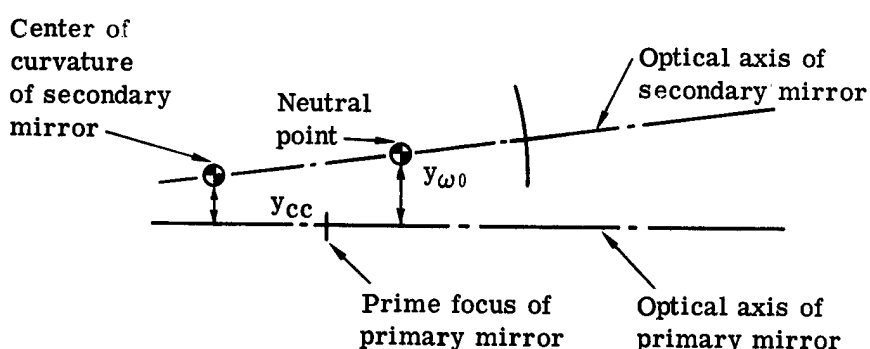
A plot of allowable defocus versus focal ratio of the primary is shown in Fig. 3. Position tolerance ranges are from 1.5 to 25 micrometers over the range of focal ratios from  $F_p = 0.5$  to  $F_p = 2$ .

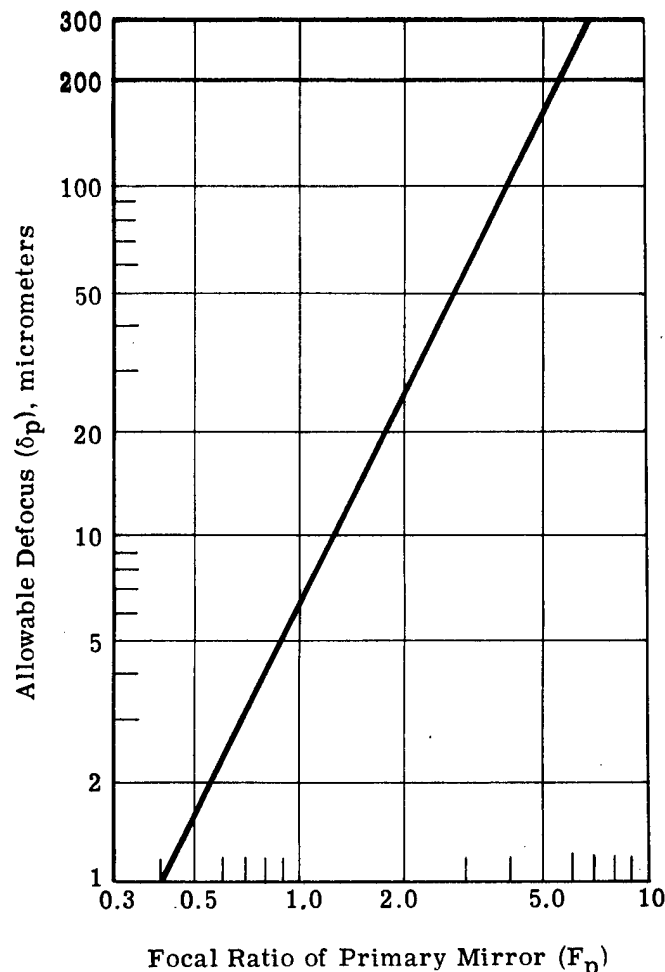
The value of  $\epsilon$  is taken as 0.3, allowing for a diverging beam from well behind the primary. In any case, the allowable defocus is not sensitive to the value of  $\epsilon$ .

These tolerances, while small, are probably acceptable, since they will be maintained by active control. The wavefront error sensor can measure the error which occurs and the proper correction can be applied. However, the tolerances show that a large focal ratio is preferred.

### 2.3.2 Tilt and Decenter Tolerance

Tip or lateral misalignment of the secondary mirror will also seriously degrade the wavefront. To analyze this, it is necessary to note the dimensions  $\Delta y_{cc}$  and  $y_{\omega_0}$  below.





$$\delta_p = \frac{\pm 16\sqrt{3} \omega F_p^2}{1 - \epsilon^2}$$

$$\omega = 0.2 \text{ } \mu\text{m rms}$$

$$\epsilon = 0.3$$

Fig. 3 — Allowable defocus error at secondary mirror or at prime focus

There are two characteristic points on the axis of the secondary mirror. Rotation about one, the center of curvature, results in no displacement of the image, but causes coma. Rotation about the second point, called the neutral point, causes no coma but gives an image shift. The misalignment of the secondary mirror is thus best described in terms of the displacement of these two points from the axis of the primary mirror. Coma is given by

$$\omega(\text{coma}) = \frac{0.0037\Delta y_{\omega_0}}{F_p^3}$$

and image displacement is expressed as:

$$\Delta\theta = \frac{\Delta y_{CC} (1 - m)}{D_p F_p m}$$

Fig. 4 shows a plot of the allowable displacement. Active control must be used, as needed, to prevent the separations  $\Delta y_{CC}$  or  $\Delta y_{\omega_0}$  from exceeding these allowable values.

Here we have assumed that the image motion is limited to  $0.2 \times 10^{-6}$  radian, the rms wave-front error is 0.2 micrometer, and the magnification of the Cassegrain system is taken as 6. It can be seen that the results are insensitive to the value of the magnification. For a prime focus system, the pointing error and coma caused by displacement from the axis are the same as given in these equations, with the condition that  $m \gg 1$ .

The data again indicates a preference for the large focal ratio primary.

### 2.3.3 Thermal Tolerances

If active control is to be used to correct or prevent defocus and alignment errors, then we must know how sensitive the system is to perturbations, and how frequently control will be necessary. Thermal perturbations are usually among the most important causes of system degradation and are considered in this section. The dynamic response of the system is also important, but is outside the scope of this effort.

First we must consider the defocus tolerance. If we assume the structure supporting the secondary mirror extends from the primary mirror, its length will be:

$$L = D_p F_p (1 - \epsilon)$$

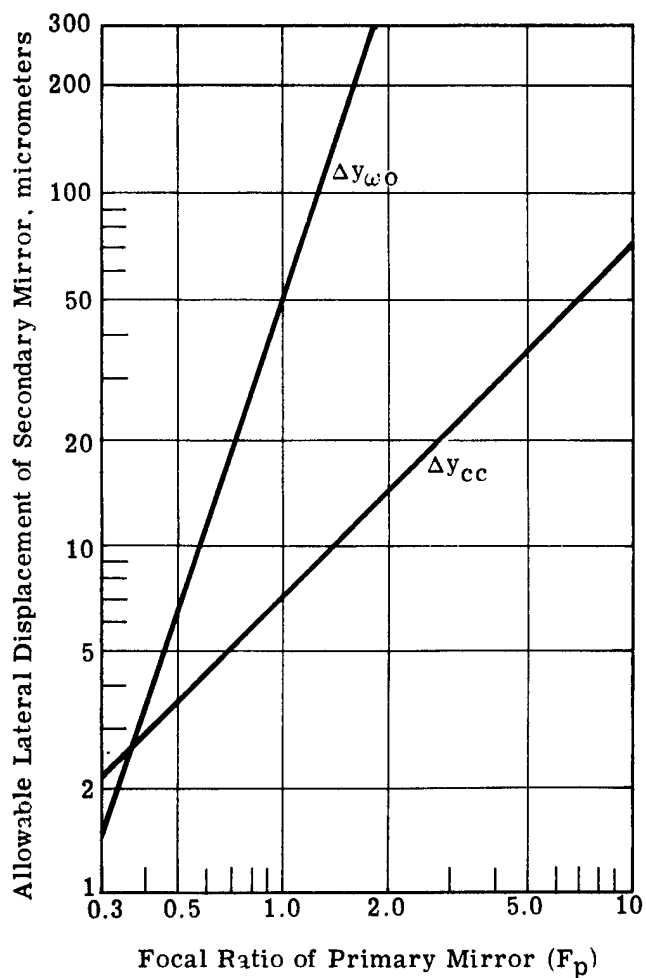
and the change of length with a uniform temperature change would be

$$\Delta L = \alpha L \Delta T$$

where  $\alpha$  is the linear coefficient of thermal expansion for the supporting structure. Substituting these expressions into the equation for allowable defocus, we can solve for the allowable uniform temperature change of the metering structure. The resulting equation is:

$$\Delta T = \frac{\pm 16 \sqrt{3} \omega F_p}{\alpha D_p (1 - \epsilon^2) (1 - \epsilon)}$$

The results are shown in Fig. 5. Here we have assumed that the metering structure is a graphite/epoxy composite having an expansion coefficient  $\alpha = 5(10^{-8})/^\circ\text{C}$ . The allowable uniform temperature change, before correction is required, ranges upward from a low of  $3^\circ\text{C}$  for a focal ratio of 0.5. Further studies should determine, for a selected system design, the rate of change of temperature that would occur and the frequency of correction that would be required.



Focal Ratio of Primary Mirror ( $F_p$ )

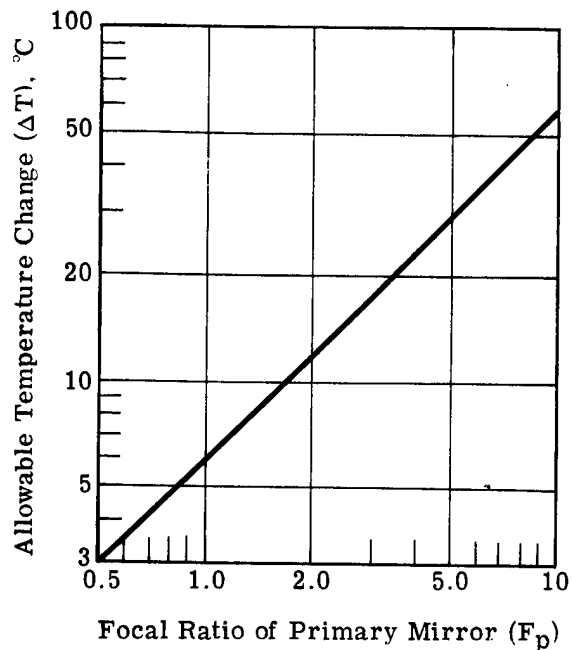
$$\Delta y_{cc} = \frac{\Delta\theta D_p F_p m}{1 - m} \text{ (causes pointing error)}$$

$$\Delta y_{\omega_0} = \frac{\omega F_p^3}{0.0037} \text{ (causes coma)}$$

$$\Delta\theta = 0.2 \times 10^{-6} \quad D_p = 30 \text{ meters}$$

$$m = 6 \quad \omega = 0.2 \mu\text{m}$$

Fig. 4 — Allowable lateral displacement and tilt of secondary mirror or of prime focus optics



Focal Ratio of Primary Mirror ( $F_p$ )

$$\Delta T = \frac{\pm 16\sqrt{3}\omega F_p}{\alpha D_p(1 - \epsilon^2)(1 - \epsilon)}$$

$\omega = 0.2 \text{ } \mu\text{m rms}$        $\alpha = 5 \times 10^{-8}/^{\circ}\text{C}$

$D_p = 30 \text{ meters}$        $\epsilon = 0.3$

Fig. 5 — Allowable uniform temperature change of metering structure (based on allowable defocus)

Thermal tolerances can also be obtained from the coma and pointing tolerances. For this we have assumed that the secondary mirror is supported on three legs extending from three equally spaced points on the edge of the primary mirror. Changing the temperature of all three legs uniformly would give defocus, as described above. Changing the temperature of one leg relative to the other two will result in a misalignment. A real temperature change would probably not be uniform over one leg; still, it serves to indicate the sensitivity to thermal perturbations.

The equation obtained for the allowable temperature difference between legs is then:

$$\Delta T_{cc} = \frac{3\Delta\theta}{4F_p \alpha[G(F_p)]} \quad (\text{based on pointing})$$

$$\Delta T_{\omega_0} = \frac{3\omega F_p}{4(0.0037) D_p \alpha[G(F_p)]} \quad (\text{based on coma})$$

$$\text{where } G(F_p) = 1 + \frac{1}{8F_p^2} + \frac{1}{256F_p^4}$$

We have assumed:

$$\Delta\theta = 0.2 \times 10^{-6}$$

$$\alpha = 5 \times 10^{-8} \text{ for graphite/epoxy}$$

$$\omega = 0.2 \mu\text{m}$$

It is seen from the plot of Fig. 6 that the allowable temperature variation based on pointing error is a maximum of 4 °C for a primary focal ratio of 0.5 and decreases for larger focal ratios.

In this case, the tolerance based on pointing error is the more critical and increases with decreasing focal ratio. This is true even though the allowable displacement is smaller for small focal ratios; the thermal distortions of the support increase with length faster than the alignment tolerance increases.

#### 2.4 ASPHERICITY

The steepness of the aspheric on the surface could have an effect on the ease and cost of fabrication. The contour of the outer edge of the mirror can be represented by two curvatures in perpendicular directions. The equation for the differential sag at the edge of the aperture is:

$$\delta_{\text{sag}} = \frac{D_s^2}{16F_p D_p} \left[ \left(1 + \frac{1}{16F_p^2}\right)^{-1/2} - \left(1 + \frac{1}{16F_p^2}\right)^{-3/2} \right]$$

The results are shown in Fig. 7 for the three values of  $F_p$ . Considering a 3-meter segment, for example, we see differential sags of up to 5 millimeters, or 500 waves. For larger focal ratios, the asphericity is less.

#### 2.5 CONCLUSIONS

The type of optical system which is selected will depend on the nature of components which are not now defined—for example, on the laser size and beam geometry, and on the cooling method used for the smaller, high-flux-density mirrors. A Cassegrain system is one of the simplest and most easily constructed types, and would usually be chosen if cooling the secondary mirror and radiating heat from the rear of the primary mirror do not cause problems. For the purpose of this study it is not necessary to choose a system configuration. We have, however, assumed that the rear face of the primary mirror, our major area of study, is free to radiate without serious obstructions.

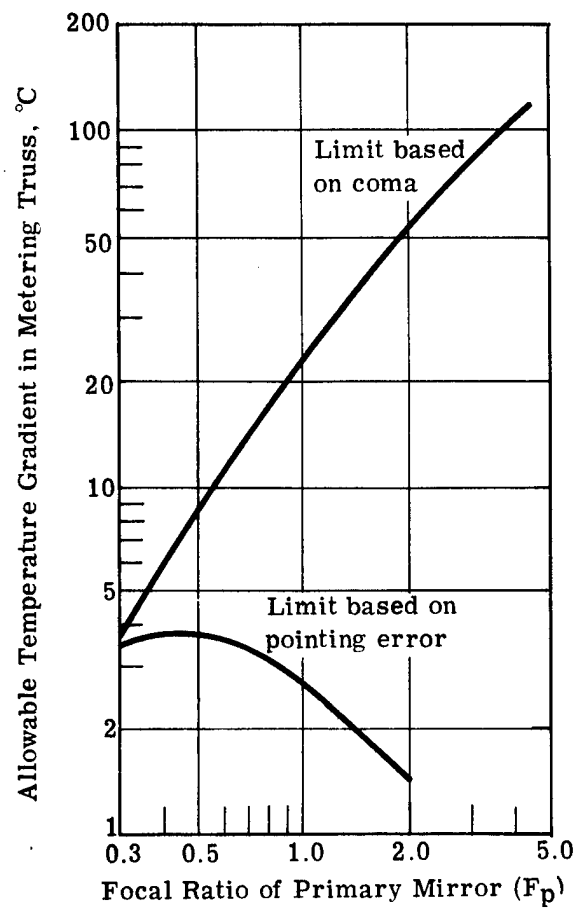
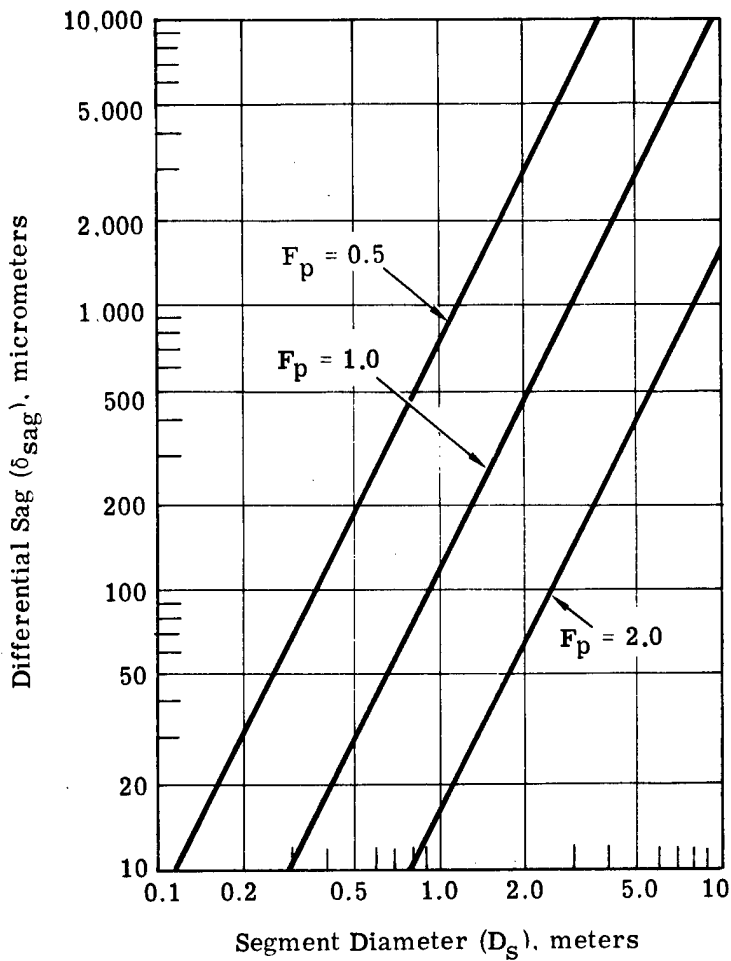


Fig. 6 — Allowable temperature difference between struts of a tripod-type metering structure



$$\delta_{\text{sag}} = \frac{D_s^2}{16F_p D_p} \left[ \left( 1 + \frac{1}{16F_p^2} \right)^{-1/2} - \left( 1 + \frac{1}{16F_p^2} \right)^{-3/2} \right]$$

Fig. 7 — Asphericity of off-axis mirror segments

In considering design concepts for the primary mirror structure, the focal ratio was not found to be a critical parameter and thus does not need to be specified at this time. It also will be dependent on system considerations, one of the most important being the maximum length of a secondary mirror supporting structure which can be launched and deployed. For the purpose of establishing a baseline design, we have chosen a primary mirror focal ratio (f/number) of 2.0. This represents a "fast" mirror by conventional optical standards, but probably represents the "slowest" (highest focal ratio) that would be acceptable for a 30-meter mirror. Values as low as 0.5 appear to be feasible.

The focal ratio is usually chosen on the basis of asphericity and alignment tolerances which affect the ease of making the mirror and maintaining the system quality. Active control concepts will make maintaining the alignment feasible, leaving dynamic response of the structure as a major problem area. Figuring very large, very aspheric, off-axis mirror segments will provide a challenge to optical fabrication technology; it is too early now to identify tradeoffs between cost, quality, and focal ratio.

### 3. FACEPLATE PARAMETRIC ANALYSIS

#### 3.1 DISCUSSION

This analysis was performed to evaluate the potentials of various materials which could be used as the reflecting surface (faceplate) of the mirror assembly. Useful information is provided in a form applicable to either segmented or continuous surface design concepts. Thermal effects of the laser and solar heating on the back of the mirror were considered and the allowable variations in heat inputs evaluated. The structural and dynamic characteristics were analyzed to determine support requirements for a faceplate based on fabrication, testing, or dynamic response requirements.

#### 3.2 MATERIAL PROPERTIES

In studying the faceplate, the more conventional mirror substrate materials were considered. Material properties, as listed in Table 2, are essentially for room temperature, 35 °C. Properties will vary with temperature and should be adjusted as concepts are refined. Justification of the low coefficient of expansion for ULE, Cer-Vit, and graphite/epoxy is based on current technology which allows the tailoring of the expansivity curve. Properties of Owens-Illinois' Cer-Vit and Corning's ULE fused silica are considered to be identical for this analysis.

#### 3.3 COATING PROPERTIES

Coating options presently available for the 30-meter deployable mirror were briefly considered. The mirror must have high reflectance (low absorptance) in both the 10.6-micrometer region and the solar region of 0.25 through 2.5 micrometers. Because of this broad band requirement, multilayer dielectric type mirrors are impractical, since they will exhibit regions of high transmittance which will be subject to solar absorption in the glass. A review of high reflectance metals was made using data from several sources (ref. 4 and 5). Aluminum, silver, copper and gold were reviewed for reflectance as shown in Table 6g-2, of ref. 4, for the complete spectrum. Their approximate reflectivity envelopes were superimposed on a curve of the extra terrestrial solar spectrum in Fig. 8 to show the areas of high absorption overlap. Using solar spectral irradiance data (ref. 5), the percent of solar spectrum falling within 500 Angstrom bands from 0.25 to 0.7 micrometer was calculated. These values were multiplied by the reflectance in that region as defined by the wavelength values. These products were added to a single value calculated for the 0.7- to 7.0-micrometer region, yielding an average weighted reflectance for the solar spectrum. The data is presented in Table 3 along with calculated absorption values. The use of protective overcoatings will further increase the absorption and this factor coupled with less ideal coatings than reported will produce a doubling of the loss in the solar region. It can be seen that, although all four metals provide high infrared reflectance, copper and gold exhibit high solar absorptivities and should be excluded from consideration where solar loads are anticipated.

Table 2 — Material Properties

Material/Property	Cer-Vit	Aluminum	Beryllium	Graphite/Epoxy	Copper	Gold
Young's modulus (E), Newton/m <sup>2</sup> ( $10^{10}$ )	6.74	7.31	28.96	6.89	11.72	8.28
Poisson's ratio ( $\nu$ )	0.18	0.36	0.2	0.2	0.3	—
Density ( $\rho$ ), kg/m <sup>3</sup> ( $10^3$ )	2.20	2.77	1.85	1.72	8.94	19.3
Coefficient of expansion ( $\alpha$ ), strain/ $^{\circ}$ C ( $10^{-6}$ )	0.03	23.22	11.52	0.03	17.74	14.2
Specific heat (c), Joules/kg $^{\circ}$ C	765.6	921.2	1880.3	1030.1	385.0	126.0
Thermal conductivity (k), W/m $^{\circ}$ C	1.31	188.9	150.5	41.5	391.0	290.0
Thermal diffusivity ( $k/c\rho$ ), m <sup>2</sup> /sec	0.79	74.1	44.5	23.5	113.6	121.0
( $\alpha/k$ ), W/m $^{\circ}$ C ( $10^{-8}$ )	2.3	12.3	7.7	0.07	4.5	4.9

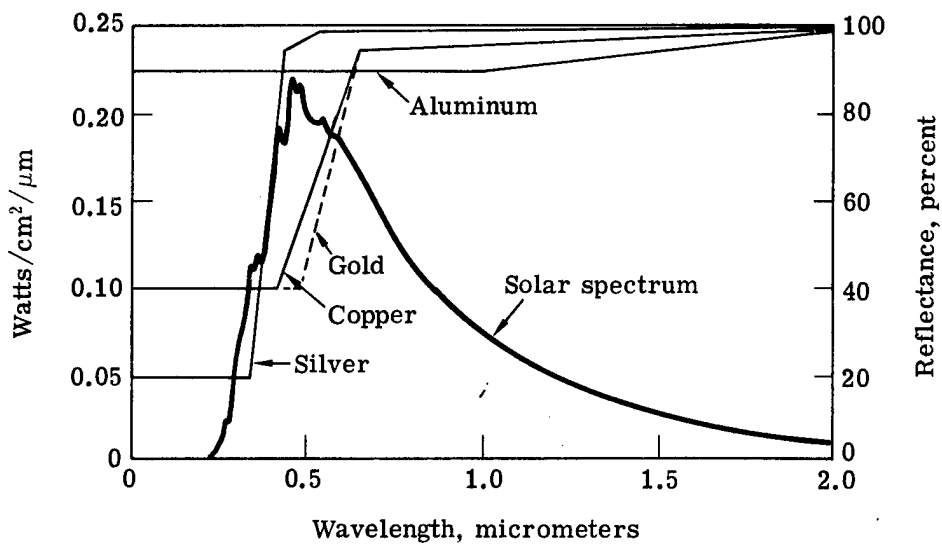


Fig. 8 — Metallic reflecting envelopes on the extraterrestrial solar spectrum

Table 3 — Reflectance and Absorptance of Various Metals Over the Solar Spectrum

Wavelength Range, $\mu\text{m}$	Percent Solar Energy	Reflectance $\times$ Percent Energy in Range			
		Al	Ag	Au	Cu
Below - 0.25	0.13	0.12	0.04	0.04	0.05
0.26 - 0.3	1.10	1.02	0.19	0.42	0.37
0.31 - 0.35	3.4	3.15	2.74	1.23	1.36
0.36 - 0.4	4.4	4.07	4.21	1.76	2.09
0.41 - 0.45	6.87	6.33	6.67	2.66	3.79
0.46 - 0.5	7.60	6.98	7.44	3.63	4.56
0.51 - 0.55	7.00	6.41	6.88	5.72	4.68
0.56 - 0.6	6.70	6.10	6.61	6.16	6.25
0.61 - 0.65	6.10	5.52	6.03	5.83	5.89
0.66 - 0.7	5.50	4.93	5.44	5.34	5.36
0.7 - 7.0	51.2	48.59	50.89	50.59	50.43
Reflectance (weighted)		93.20	97.14	83.38	84.83
Absorptance		6.80	2.86	16.62	15.17

### 3.4 THERMAL EFFECTS ON THE FACEPLATE

To evaluate the thermal effects on the faceplate of the mirror, we postulate a mirror in which the energy is absorbed from the laser on the front face, solar energy is absorbed on the rear face, and the combined heat load is radiated to space from the back surface of the mirror. When the laser and mirror have reached a steady state, the front face of the mirror will be hotter than the back and the temperature difference will be:

$$\Delta T_f = \frac{qk}{h}$$

where  $q$  is the heat absorbed in the front face,  $k$  is the thermal conductivity of the faceplate, and  $h$  is the thickness. This will be the maximum temperature difference that will occur; before steady-state has been reached the gradients in the mirror will be somewhat less.

If the mirror is made of segments of diameter  $D_s$ , the sag induced in that element by the gradient through the faceplate will be:

$$\delta = \frac{\alpha q D_s^2}{8k}$$

These deformations, shown in Fig. 9, are large; the results indicate the magnitude of active figure correction which may have to be effected.

Inverting this equation, we can solve for the change in absorbed power over a mirror segment which would result in an acceptable surface deformation of 0.5 micrometer, see Fig. 10. From this plot we see that, for example, a 4-meter-diameter segment would remain within tolerance, with no active control, in spite of a variation in input power level of 0.2 to 1 percent, depending on the mirror material.

ULE or Cer-Vit are always good mirror materials from the standpoint of insensitivity to thermal changes. Beryllium has as good properties when thermal gradients are important, because of its high conductivity. Its high stiffness is another desirable property. Aluminum, gold, and copper are included because they would make satisfactory mirror faceplates even without coating, and thus may be able to withstand higher faceplate temperatures, if that should be a limiting factor.

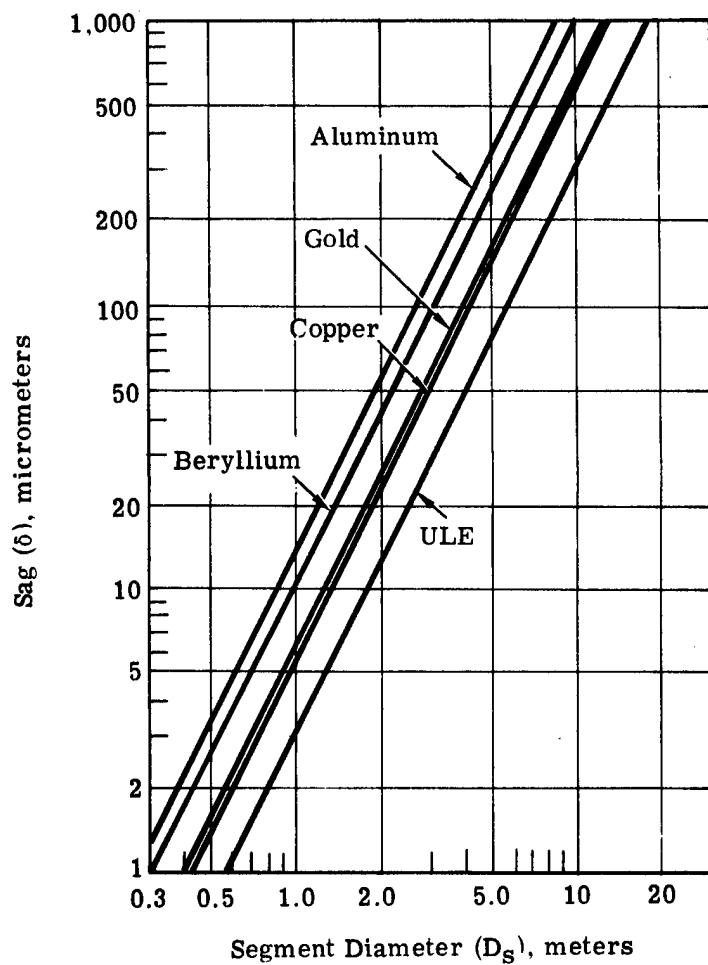
This graph considers only the effect of a gradient through the faceplate. The effect of a uniform temperature rise is also important. As the mirror or mirror segments are heated, their radius of curvature changes linearly with temperature as the entire mirror or segment expands. The sag of the surface of a segment is given approximately as:

$$\text{Sag} = \frac{D_s^2}{8R}$$

Thus, increasing the radius results in a sag change. The expression for the allowable temperature change as a function of the sag is:

$$\Delta T = \frac{16F_p D_p \sigma}{\alpha D_s^2}$$

The allowable temperature change increases with  $F_p$ , again showing that a slower system (larger f/number) results in larger tolerances. The curves of Fig. 11 are plotted for  $F_p = 1$  and for an allowable sag change of  $\sigma = 0.5 \mu\text{m}$ . For larger temperature changes, and thus larger sag changes, active control would be required.



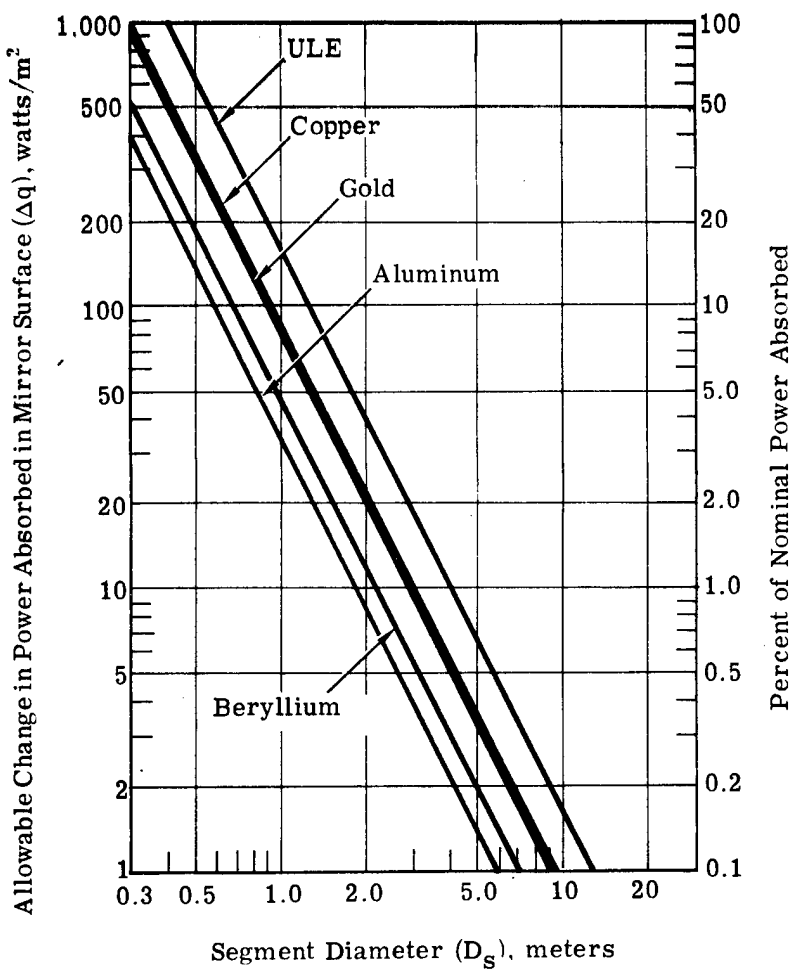
$$\delta = \frac{\alpha q D_s^2}{8k}$$

$\alpha$  = expansion coefficient,  $^{\circ}\text{C}^{-1}$

q = absorbed heat, 1,000 watts/m<sup>2</sup>

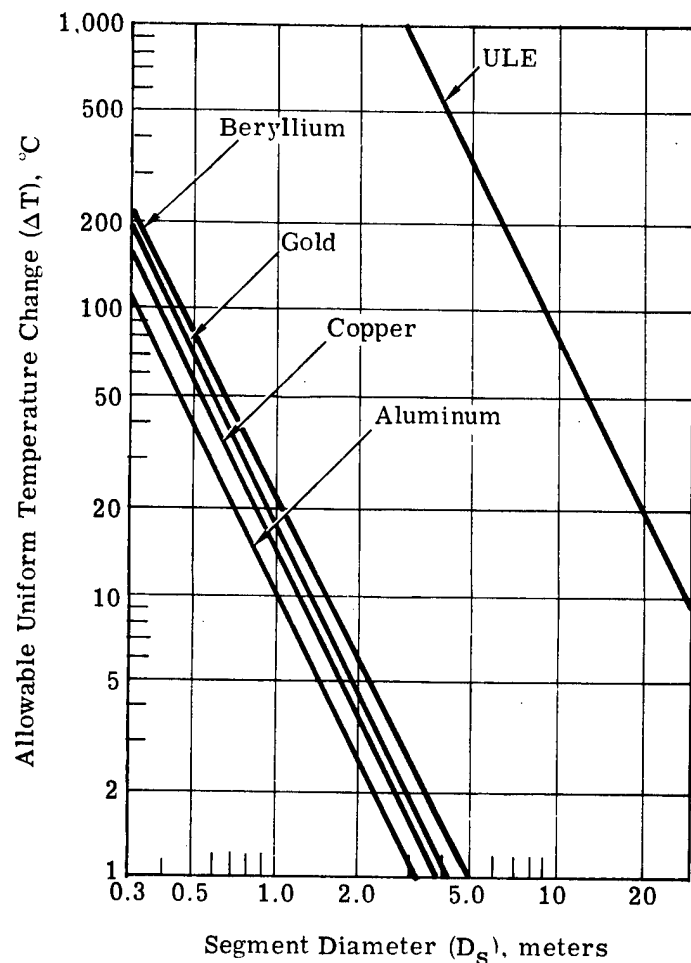
k = conductivity, watts/m  $\cdot$   $^{\circ}\text{C}$

Fig. 9 — Sag deformation of mirror faceplate segments caused by steady-state gradient through faceplate



$$\Delta q = \frac{8k\sigma}{\alpha D_s^2} \quad \sigma = \text{allowable peak surface deformation} = 0.5 \mu\text{m}$$

Fig. 10 — Allowable power variations on segments based on sag change caused by change in gradient



$$\Delta T = \frac{16F_p D_p \sigma}{\alpha D_s^2}$$

$$F_p = 1 \quad D_p = 30 \text{ meters}$$

$$\sigma = 0.5 \times 10^{-6} \text{ m}$$

Fig. 11 — Allowable uniform temperature change of segments of faceplate

Now the advantage of the low expansion glasses becomes evident, for with segments as large as 3 meters, the temperature of the mirror can be virtually ignored. For ULE or Cer-Vit faceplate, destruction of the coating would establish the limiting temperature. It is also interesting to consider the use of graphite/epoxy composite material for the mirror faceplate. It has a thermal expansion coefficient similar to that of ULE, but with higher conductivity. As a result, the effects of gradients through the material would be even smaller than those shown for ULE in Fig. 9.

If metals are used, figure control must be used for 3-meter segments if there is a temperature change of only a few degrees. It becomes clear that designing to minimize the effect of variations in the solar heating, either by the use of low expansion faceplates or by other design approaches, is a prime design consideration.

The temperature changes caused by variation of sunlight on the back surface are thus important and are treated in the next figure. Fig. 12 shows the average temperature of the faceplate which has reached steady state and is radiating to space, from the back surface, the total energy absorbed from the laser and from the sun. This is an optimistic prediction in that a more refined analysis of the mirror assembly will probably tend to increase the average faceplate temperature.

The design of the rear of the mirror is quite critical since the heat that is absorbed on the front must pass through the mirror by conduction and leave the rear of the mirror, by radiation, to deep space either directly or indirectly.

In addition, solar radiation which is not a problem when it is incident on the front of the mirror may be a problem on the rear, especially if the thermal finish is black over the entire solar spectrum. The most obvious solution is to coat the rear of the mirror with a material having as low  $\alpha/\epsilon$  such as either a white paint or an optical solar reflector. Such a material would have a solar absorptance on the order of 10 percent.

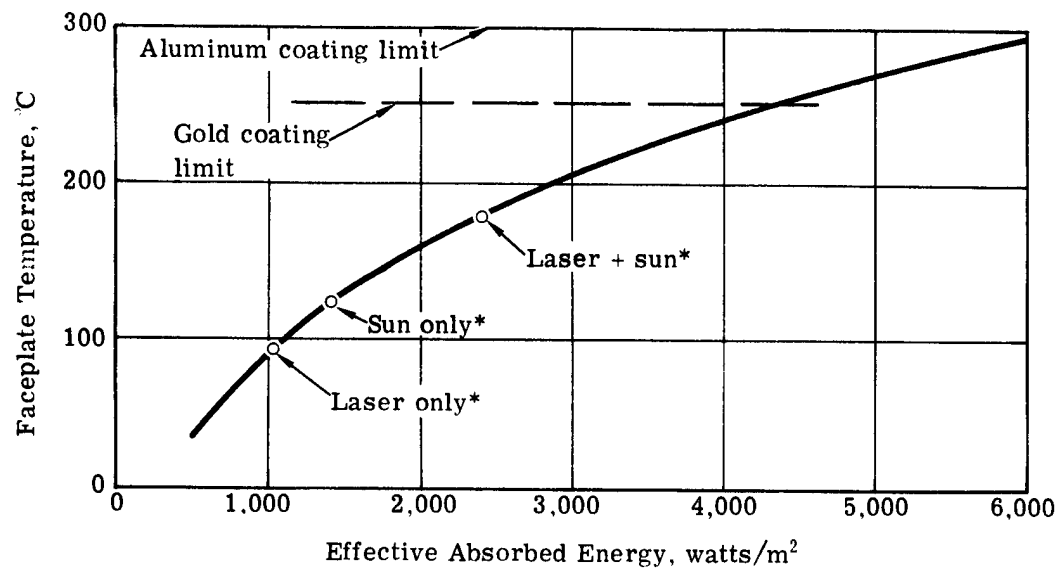
If direct radiation to space is utilized, then not only must the IR emissivity be high, but so must be the view factor. This indicates that any structure at the rear of the mirror must be low density, such as a truss. It also indicates that as much of the control hardware such as attitude engines, CMG's, and other electronic black boxes should be mounted where it does not affect the rear of the mirror.

Several possible solutions are available in order to decrease the solar energy input to the mirror assembly. One method would be to erect a steerable sun shield which would serve as an awning to keep solar energy from striking the rear of the mirror. If the distance between the sun shield and the mirror is large compared to its diameter, the view factor from the mirror to space will not be greatly reduced. Furthermore, it is conceivable that this sun shield can incorporate other functional subassemblies of the laser-transmitter.

Another method would be the use of a fixed cylindrical sun shield extending either completely around or partially around the rear of the mirror. Such a device would require either limited operations during full sun or extensive maneuvers to avoid the incident solar energy. It would also decrease the view factor to space. It is recognized that this may impose severe limitations on the mission.

### 3.5 FACEPLATE THICKNESS

In evaluating the structural characteristics of the faceplate, the first question to be determined is how thick the mirror faceplate can be. We have considered four factors which will be important in setting the faceplate thickness. From this analysis the general nature of the faceplate can be determined. It is assumed here that the faceplate is a uniform thickness sheet of material having some stiffness (not a membrane). The plate must be supported on some structure; the



$$T = \left( \frac{q\alpha A_A}{\sigma\epsilon A_R} \right)^{1/4} K$$

\*Assuming  $A_A = A_R$  absorbed or reflecting area, blackbody surface,  $\alpha/E = 1$

Fig. 12 — Temperature versus absorbed energy, radiative rejection

object of the study is to determine how thick the plate should be and what spacing between supports can be accepted. The factors which must be considered in determining the faceplate parameters include the shuttle payload limit, the stiffness requirements for polishing and testing the mirror, and the dynamic (vibration-limiting) requirements.

### 3.5.1 Weight Limit

The limit weight of the mirror assembly is assumed to be the allowable payload of the shuttle, i.e., 28,123 kg. To provide a boundary, half of the shuttle payload was arbitrarily assigned to the substrate and the remaining weight to the supporting structure, and deployment and control mechanism. The limiting thicknesses can then be seen in Fig. 13. It is concluded that thicknesses of up to 10 millimeters may be acceptable for the common substrate materials.

### 3.5.2 Polishing Loads

The faceplate thickness and the spacing that can be allowed between supporting points are important design considerations from an optical fabrication standpoint.

In an analysis by Timoshenko (ref. 6), we find that (using his standard structural notation):

$$w = \frac{\alpha_s q b^4}{D}$$

where  $\alpha_s$  takes on different values for different support configurations. In this equation,  $w$  is the deflection,  $q$  is the load per unit area,  $b$  is the space between supports,  $D$  is the plate stiffness,

$$D = \frac{Eh^3}{12(1 - \nu^2)}$$

$E$  is Young's modulus,  $\nu$  is Poisson's ratio, and  $h$  is the faceplate thickness. The value of  $\alpha_s$  is 0.0026 for equally spaced lines of support.

One requirement for optical fabrication of a high quality mirror is that the surface should not deform excessively during the polishing process. The magnitude of this resultant higher order ripple is the limiting surface quality. Typical lap loads for conventional mirror figuring are about 3,000 Newtons/meter<sup>2</sup> and, keeping with the restriction of  $\sigma = 0.5 \mu\text{m}$ , we obtain the three lefthand curves in Fig. 14. Other fabrication techniques can be postulated or tradeoffs between fabrication time and lap loading can be made which may minimize this consideration.

### 3.5.3 Gravity Load During Test

A more critical design requirement is that the mirror be of sufficient integrity such that the surface quality can be proven by testing in the 1-g gravity environment. Substituting  $\rho h$  for  $q$ , where  $\rho$  is the material density, and  $h$  the thickness gives the three righthand curves for the allowable support spacing based on gravity sag.

All curves in Fig. 14 are based on equally spaced line supports. These results are not intended to define a design, but to provide information in parametric form for a series of possible design concepts.

### 3.5.4 Dynamic Characteristics

A second requirement on faceplate thickness is developed from its dynamic characteristics. The laser and pointing control, for example, are sources of vibration excitation to the mirror structure during operation. It will probably be desirable to control the resultant magnitude of the surface deformation, passively, via the design of the mirror configuration.

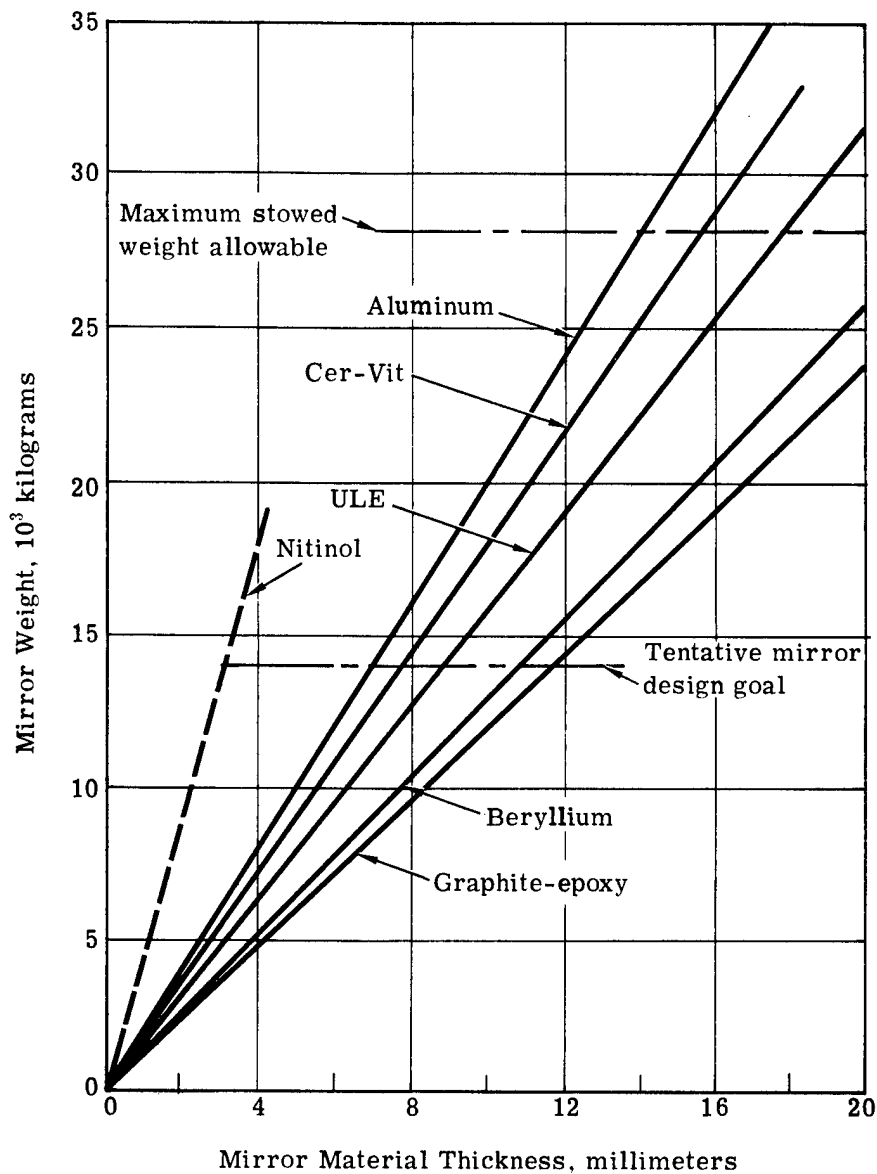


Fig. 13 — Mirror weight versus material thickness

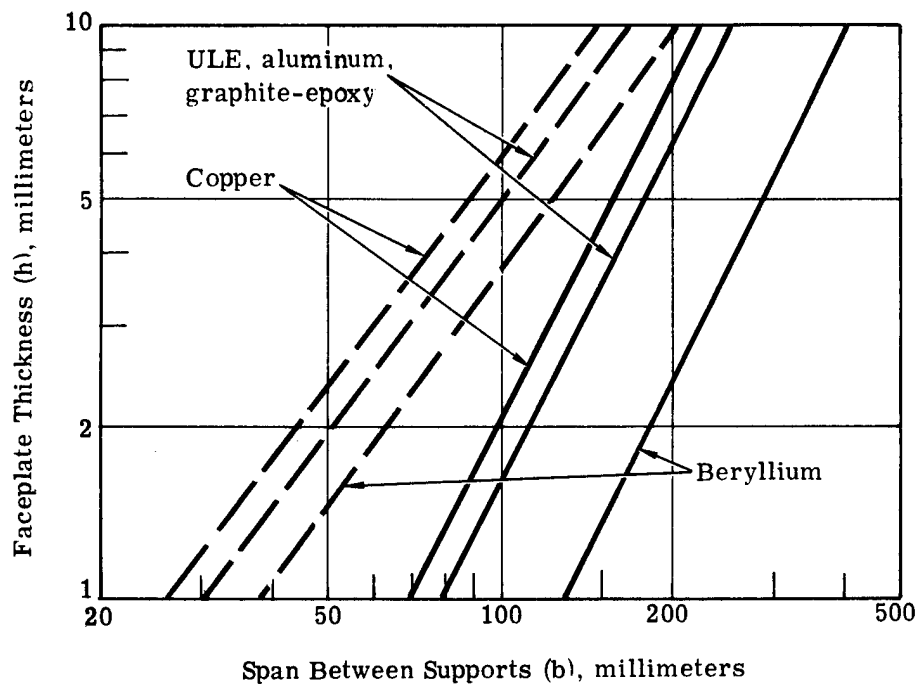


Fig. 14 — Support requirements for faceplate

The natural frequency for the mirror faceplate is:

$$f_n = \frac{2}{\pi} (\alpha) \left[ \frac{h}{(b)^2} \right] \left[ \frac{E}{12\rho} \right]^{1/2}$$

where  $(\alpha)$  is the mode constant which is a function of the plate format and boundary support conditions. For this analysis we have assumed  $(\alpha)$  of 5 to be representative of the possible faceplate/support configurations. Figs. 15 and 16 show the natural frequency of the faceplate per millimeter of thickness as a function of span between supports.

For a simple system excited by motion at its base, the ratio of response amplitude to input amplitude is referred to as the transmissibility ( $T$ ). The greatest transmissibility occurs when  $\omega = \omega_n$  (resonance) and for low damping factors.

If we assume a worst case condition of resonance, forcing frequency equals natural frequency, and a damping factor of 0.5 percent, then the transmissibility is about 100. Specifying that the allowable response amplitude  $\delta_r$  to be limited to  $0.5 \mu\text{m}$ , a relationship of design frequency versus operational forcing acceleration can be formulated as shown in Fig. 17.

The input spectral density due to the laser, pointing control, and other dynamic sources will be a critical factor in the design of the 30-meter transmitter. Assuming, for now, that the forcing acceleration is no more than  $10^{-4} \text{ m/sec}^2$ , the allowable spacing between support points is as shown in Fig. 18.

From Fig. 14 and 18, it is concluded that the lap loads or 1-g test requirements may size the faceplate thickness and support spacing. The dynamic characteristics of the faceplate would be the next design consideration. Solar pressure, which is only  $5(10^{-6}) \text{ Newtons/m}^2$ , is not considered critical to the design of the mirror structure at this time.

### 3.6 Conclusions—Faceplate Design

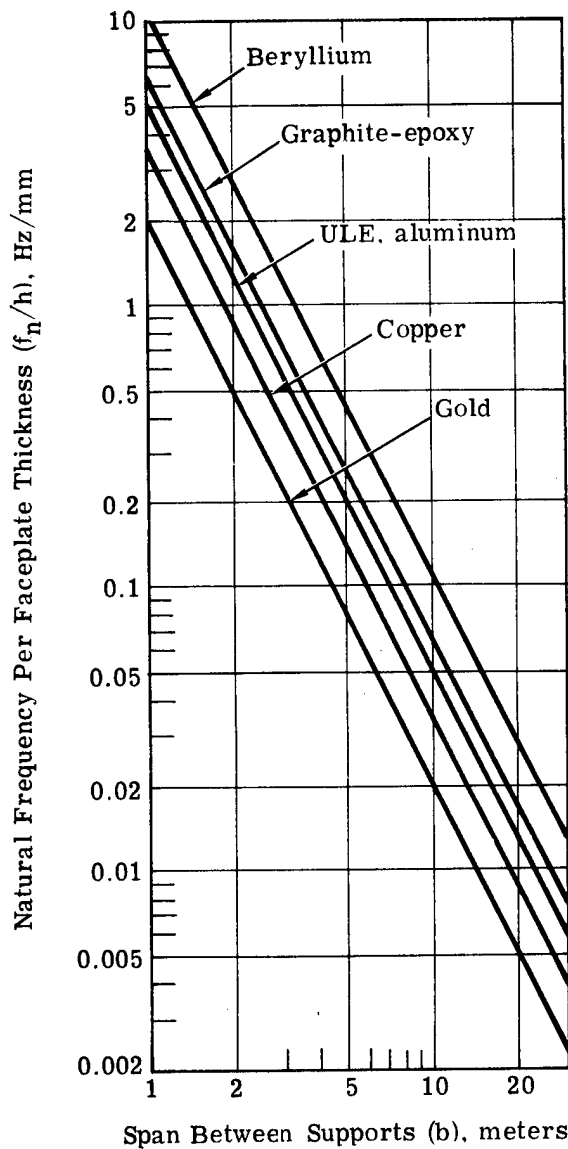
The basic requirements for the reflective surface (faceplate) have been established by analyzing fundamental structural and thermal properties. Segmented or continuous surfaces were considered; but membranes, held in shape by in-plane tensile forces, were not specifically included.

At the power levels per unit area required, it is found that special cooling techniques, other than radiative cooling to space from the rear surface of the mirror, are not required. Temperature of less than  $200^\circ\text{C}$  are reached even with fairly simple coatings that absorb as much as 1 percent of the laser energy, and with full solar energy absorbed. With some shading of sunlight, or with a coating on the rear surface having substantial reflectance in the visible and good emittance in the long infrared, temperatures closer to  $100^\circ\text{C}$  will be achieved.

The value of materials having a low coefficient of thermal expansion is easily seen; a 4-meter segment of aluminum can accept less than a 1-degree change, while a ULE segment could tolerate several hundred degrees. Thus, a prime consideration for system design is either that low expansion materials (ULE, Cer-Vit, graphite/epoxy composites) be used exclusively, or that careful thermal control, minimizing the effects of varying solar heating, be planned. Active control of the mirror figure will be required even with low expansion materials, but can be minimized if, in addition, some thermal control is used.

The required faceplate thickness will be determined by polishing load requirements, by the need to test the mirror in a normal gravity environment, and by dynamic limitations. These requirements limit the allowable unsupported span. Considering one-half the shuttle payload used just for a ULE faceplate allows a 9-millimeter thickness; Fig. 14 then indicates a maximum unsupported span of about 1.5 meters, based on rather small dynamic inputs.

The overall weight can then be greatly reduced by decreasing both the faceplate thickness and the support spacing. We have selected a baseline design of a 1.3-millimeter faceplate supported at intervals of 100 millimeters in order to simplify the fabrication and test requirements, as well as to avoid all possible dynamic difficulties. The supporting structure, for the baseline concept, consists of a graphite/epoxy grid with 100-millimeter spacing. All faceplate requirements are then met, with an overall mass well within limits.



$$f_n = \left( \frac{2}{\pi} \right) \left( \alpha \right) \left( \frac{h}{D_s^2} \right) \left( \frac{E}{12\rho} \right)^{1/2}$$

Fig. 15 — Natural frequency of faceplate

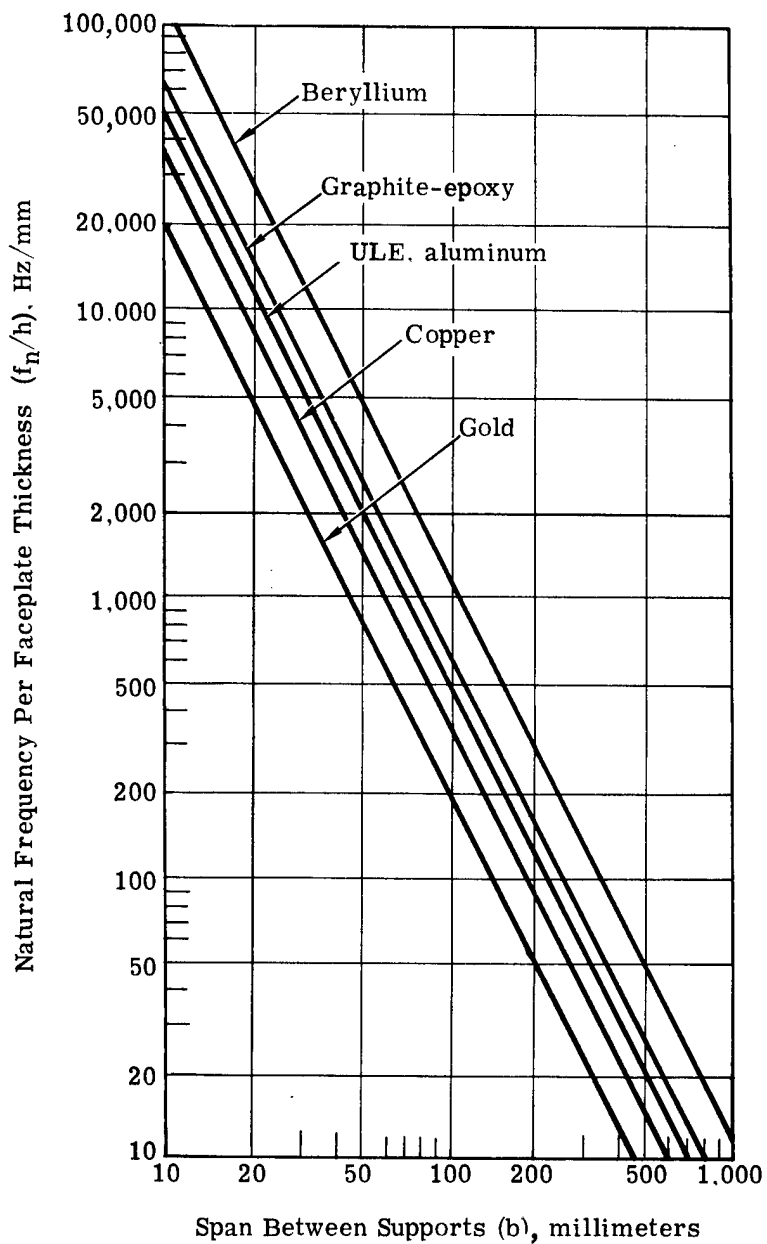
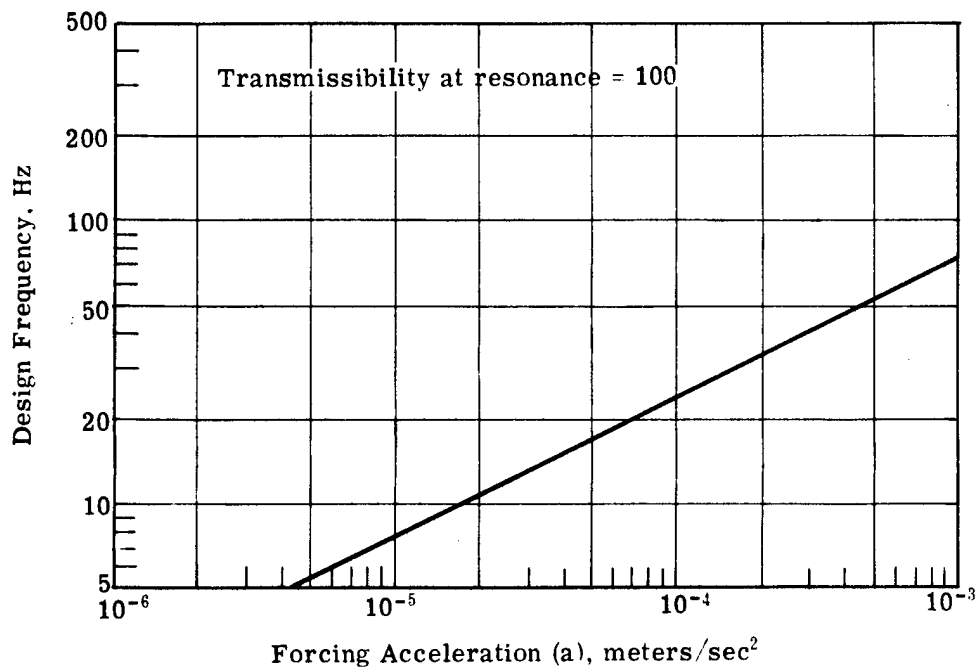
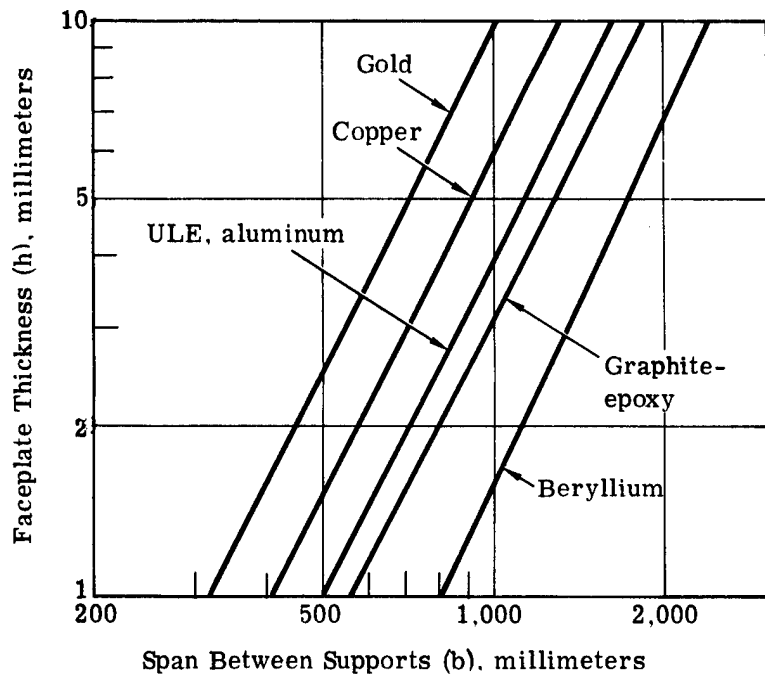


Fig. 16 — Natural frequency of faceplate versus support span



$$f_D = \frac{1}{2\pi} \left( \frac{a}{\delta_R/T} \right)^{1/2}$$

Fig. 17 — Design frequency versus excitation acceleration



Forcing acceleration at resonance =  $10^{-4}$   
 Transmissibility = 100  
 Response amplitude =  $0.5 \mu\text{m}$

Fig. 18 — Support requirement for dynamic input

## 4. MIRROR FIGURE CONTROL

### 4.1 DISCUSSION

Based on the analyses of system tolerances and faceplate parameters, we conclude that it is possible to place a large mirror in space. We also conclude that the figure will not remain passively stable to the close tolerance of 0.5 micrometer which is required. To keep this accuracy, active control of the mirror figure will be required, compensating for material changes or instabilities, and for thermal expansion. An initial alignment phase will also be needed in order to eliminate gross manufacturing or deployment errors. After considering techniques available for control of the figure, we have concluded that this, too, is feasible. The techniques that are available, the control ranges required, and some indication of the required number of devices (actuators) are discussed in this section.

Control of the figure of the mirror involves the separate operations of sensing the figure errors, computing the corrections to be made, and applying the correction by means of appropriate actuators. We have considered each of these problems. The control logic and computation process is simple and, for most possible mirror configurations, is easily within the capability of a small on-board computer. The figure sensing technology is also straightforward, a number of possible sensors having been developed in recent years. The set of sensors that will be used depends on the selected system configuration, which is not a part of this study. Therefore, our emphasis has been on the techniques to apply the correction to the mirror. This is an integral part of the mirror design, and is described in Section 4.2. The following sections, 4.3 and 4.4, treat briefly the figure sensing and the logic and computation problems.

### 4.2 APPLYING THE CORRECTION

This section presents the information which has led us to believe that accurate control of the figure of a large mirror in space is feasible. A variety of concepts and data, much of which has been generated at Itek in continuing studies into active control concepts, is summarized and applied to the specific requirements and structures being considered in the current program, as described in Section 5 (Stow and Deployment Concepts).

First we present a discussion of the ways correction can be applied (Types of Correction, 4.2.1) and of the significance of force and displacement actuators (4.2.2). This is followed by a description of a number of particular actuator types (4.2.3) including piezoelectric displacement and moment actuators, screw and spring force actuators, thermal actuators, and others. This illustrates the capabilities which can be available and which could be incorporated into mirror designs. The section includes representative examples; it is not a complete list of all possible concepts. A study of the characteristics of the actuator types and the control range required (4.2.4) leads us to conclude that control is feasible. Specific design of space-qualified equipment we leave to the future.

A question which must always be considered is the number of actuators which will be needed. It is even better to ask the number which should be used, since some redundancy will probably be desirable. Unfortunately, this is a question which cannot be answered until a final system and mirror design is developed. To determine the number of actuators, we must estimate the perturbations (thermal changes, material creep, and any other effects), determine the sensitivity of the mirror figure to these perturbations, and then compute the number of actuators needed to correct the predicted figure errors. Often, the predicted errors are very small. Additional actuators are then added to the system design; these are then insurance against system failures or unpredicted perturbations.

A determination of the number of actuators then requires a failure mode analysis for the system, including analysis of the possible failure of some of the actuators. If the system is properly designed, the result of the failure of an increasing number of actuators, as time passes, will be only a small and gradual deterioration of system quality, with no abrupt increase in wave-front error. For the concepts described in the following sections, no single actuator failure or combination of failures would be critical to system operation.

Even though a complete analysis is not possible at this time, we have generated, in Section 4.2.5, estimates of the number of actuators which will be desirable, and have included this in the presentation of selected system concepts, Section 6.

#### 4.2.1 Types of Correction

Whether the mirror is an assembly of semi-rigid faceplates or a large thin plate or membrane, there are three different ways of applying actuator control: positioning segments or membrane areas; bending of the faceplate or deflection of the membrane; and control of the supporting truss structure. Most actuator applications can be related to these types, which are shown schematically in Fig. 19.

If a segmented faceplate is used, each segment must be attached to the supporting truss at three points, these points providing proper alignment. For an array of hexagonal segments, three segments will meet at each support point. Since the three segments must match in height above the truss at the support, and since there will be some differences in the structure and material properties of the three supports, active position control will be needed to maintain matching surface heights. If the faceplate is a continuous plate or membrane, it may also be desirable to support it over a similar array of fixed reference points, and position control actuators would be required in this case too.

The second application for actuators is for control of the faceplate shape within a segment or in the region of a continuous plate or membrane between the supported reference points. It is possible, of course, that the faceplate will be a single continuous element supported on only three points. The three position actuators are then alignment (pointing) devices, and all other actuators would be faceplate bending devices. The actuators used to control bending will operate by applying a force to the faceplate or membrane; in the case of a rigid faceplate, they may provide either forces or moments to control the shape, and they may react against the underlying support structure or they may be self-reacting between pairs of points on the faceplate.

The third application for actuators is for control of the shape of the truss which supports either the segmented faceplate or a continuous thin plate or membrane. The purpose of such actuators is to correct for the figure error in the truss where it occurs.

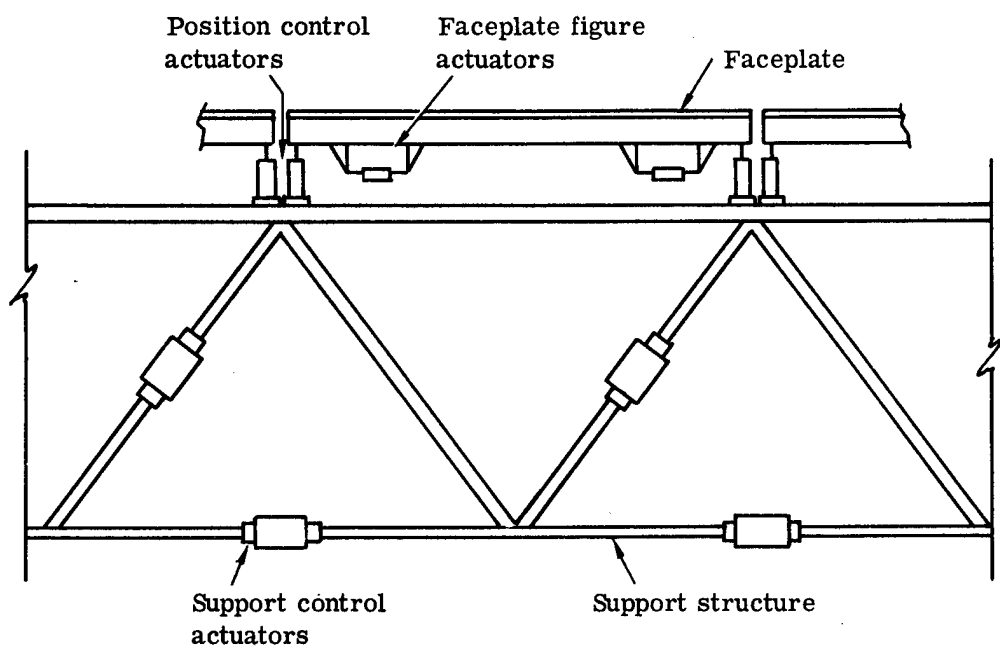


Fig. 19 — Schematic diagram of techniques to obtain figure correction

#### 4.2.2 Force and Displacement Actuators

It is convenient to discuss control in terms of force and displacement actuators. This is a distinction which is useful, even though the two types cannot be rigorously defined. A displacement actuator usually operates directly on the mirror surface, and requires a rigid support structure. It provides tight coupling between the surface and the support structure, and thus the surface figure depends, at each point, on the corresponding shape of the support. A force actuator includes a relatively soft spring or equivalent device. As long as the support plate is stiff compared to the actuator spring constant, the force applied by the actuator will not vary as the system deflects.

As an example, a piezoelectric element pushing against a light load is a clear case of a displacement device, and the segment positioning actuators described above fall into this category.

For the control of the shape of an individual segment, force actuators are usually more appropriate. In this case a device having a soft spring constant applies a force to the faceplate, and the force applied is nearly independent of small changes in the shape of the faceplate or of the supporting structure. The use of a force actuator eliminates the requirement that the force-reacting structure maintain a perfect shape. It is only necessary that the supporting structure be stiffer than the spring constant of the force actuator.

#### 4.2.3 Actuator Descriptions

##### Piezoelectric Actuators

Many types of actuators, of both the force and displacement mode of operation, have been built and demonstrated. The most common, of course, are the piezoelectric positioners which are available commercially in a variety of configurations and which can readily be made for a specific application from available piezoelectric-ceramic bars, plates, and cylinders. Two examples are shown in Fig. 20.

For the simple plate device in Fig. 20(a), the displacement is given by

$$\Delta z = Ed_{33}t$$

where  $E = \frac{V}{t}$  = field (volts/meter)

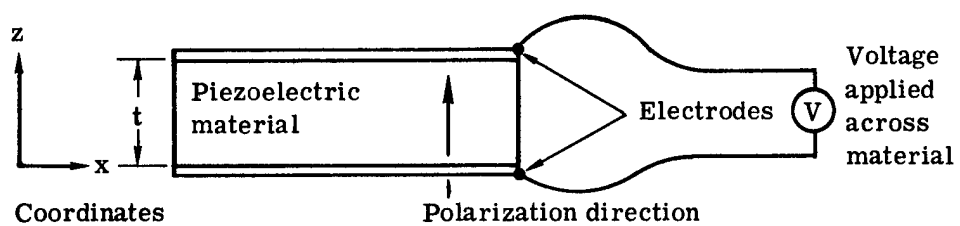
$d_{33}$  = piezoelectric coefficient for field and strain in the polarization direction (meters/volt)  
 $t$  = thickness (meters)

The maximum allowable field is typically  $10^6$  volts/meter; a typical value\* for  $d_{33}$  is  $3.7 \times 10^{-10}$  meter/volt; the maximum deflection is then 3.7 micrometers per centimeter of thickness. A potential of 10 kv across a 1-centimeter plate would give 3.7 micrometers deflection. If several plates are stacked with opposite polarizations, with electrodes of opposite polarity between alternate layers, they will be in series mechanically and in parallel electrically, allowing larger deformations with smaller voltages. However, the mechanical properties of the bond between layers must be considered in the device design.

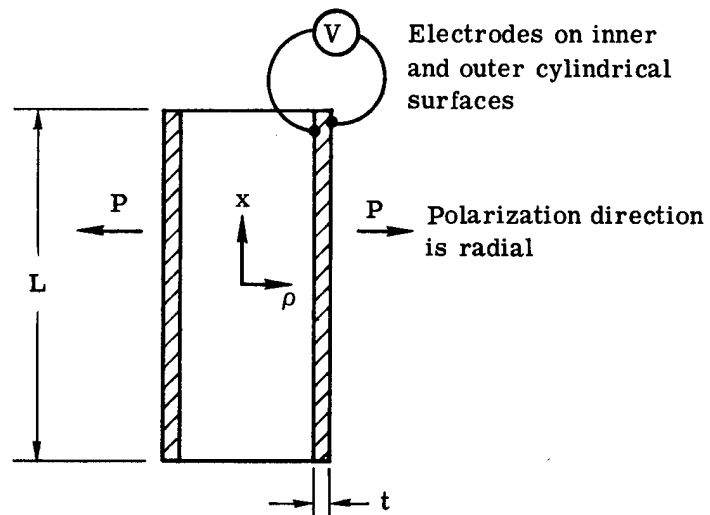
A large displacement can also be achieved by using the tube configuration, Fig. 20(b). Here the polarization and the field are in the radial direction; the thin wall allows high fields with low voltages, while the long tube gives a large length change for a small lengthwise strain. The dis-

---

\* Clevite Corporation ceramic material PZT-5A.



(a) Plate device



(b) Tube device

Fig. 20 — Piezoelectric displacement actuators

placement is:  $\Delta z = Ed_{31}L$ , where  $d_{31}$  is the coefficient describing strain in the long direction for a field in the radial polarization direction. Since the magnitude of  $d_{31}$  is less than that of  $d_{33}$ , the displacement is less than that for a stacked plate of equal thickness, but the mechanical properties may be better. For the same material,  $d_{31} = -1.7 \times 10^{-10}$  meter/volt. The coefficient is negative—as the material expands in thickness due to the applied field, it contracts in length. For a 10-cm long tube, the deflection would be as great as  $\pm 17 \mu\text{m}$ ; for a 1- to 2-mm wall thickness ( $t$ ), the maximum field of  $10^6$  volts per meter would be achieved at  $\pm 1$  to 2 kv.

Other piezoelectric devices provide a long range of travel, with fine resolution, by causing successive applications of voltage to produce stepwise translation in a kind of creeping motion. The "Inchworm"\*\* has a claimed resolution of  $0.006 \mu\text{m}$ , a travel range of 25 mm, a load capability of 5 pounds, and is available commercially. A piezoelectric peristaltic device has been announced by Bell Laboratories. It is said to be capable of 0.05- to  $2 \mu\text{m}$  increments over a range of several cm, with a load capability of up to 40 pounds.

#### Screw and Spring Force Actuators

The simplest implementation of a force actuator uses a stepping motor to drive a screw and compress or extend a spring. Since the spring constant is variable over a wide range, the actuators can be made with almost any desired property. Fig. 21 illustrates the concepts and shows one that was built to specifications appropriate for use with the very stiff primary mirror of a large space telescope. This design represents one extreme of the force design range which is possible. It will provide a force of  $\pm 500$  Newtons ( $\pm 100$  pounds), and a fineness of adjustment of less than 0.1 percent of its maximum force. Prototypes have been built and tested. An operational unit would probably have a mass of less than 2 kg for the 500-Newton device, and much less for low-force units.

#### Self-Reacting Actuators

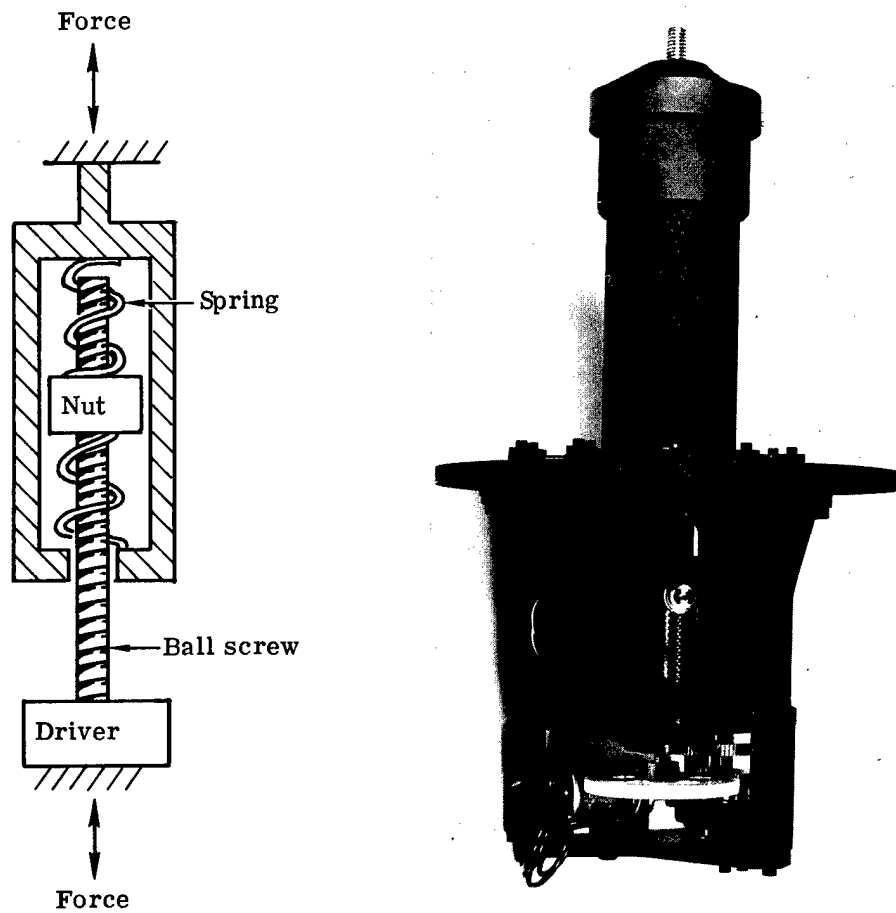
The use of either of the actuators illustrated in Figs. 20 or 21 requires the presence of a supporting structure as a base for the actuator. This is not always necessary—a wide range of devices can be conceived if one thinks in terms of self-reacting actuators operating to generate localized moments in the mirror plate.

As an example, a piezoelectric actuator acting to apply a moment to a faceplate is shown in Fig. 22. In this case, a disk of piezoelectric material about 2.5 cm in diameter and 1 cm thick was bonded to the thin circular plate. The electrodes were connected across the piezoelectric disk, as in Fig. 20(a). Expansion of the material in thickness has no effect, but the tendency to shrink in the radial direction (because of the  $d_{31}$  piezoelectric coefficient) is resisted by the plate and results in the application of a localized moment. Approximating this as a positive normal force at the center of the actuator and an equal negative normal force distributed on a circle having the diameter of the actuator gave a predicted deformation shape which closely matched the measured shape [Fig. 22(b)].

In using piezoelectric actuators, thermal effects must be considered. A change in temperature can easily cause a length change greater than the piezoelectric effect. For the segment position actuators of Fig. 19, temperature changes will cause adjacent segments to be displaced equally; only gradients will cause errors across the boundary. In the case of Fig. 22, however, the effect of a temperature change would be the same as that caused by the piezoelectric effect. Fig. 23(a) shows an actuator using three small piezoelectric plate elements which apply a localized

---

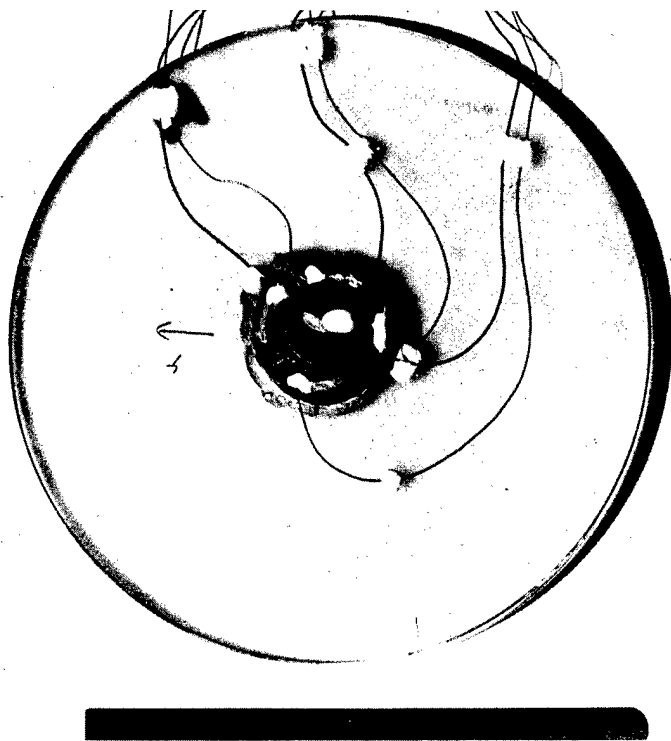
\* Patent pending, Burleigh Instruments, Inc.



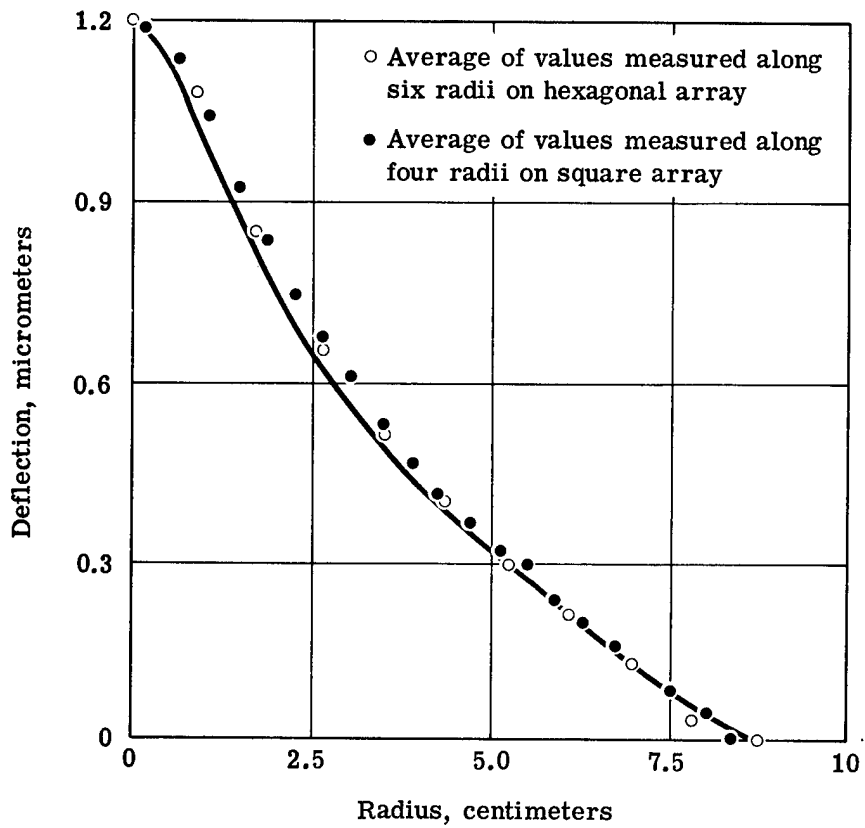
**Advantages:**

- Holds force, power off
- Soft spring allows large structural deflections without affecting applied force
- Can provide fine force increments (0.1% of maximum force)

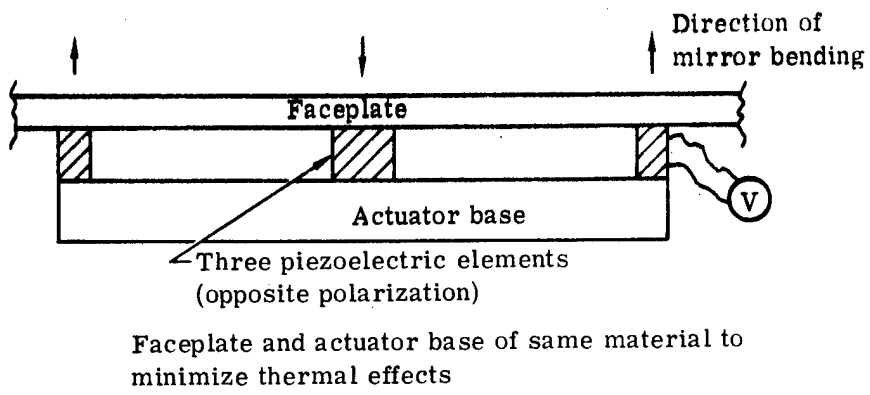
Fig. 21 — Spring and screw force actuators



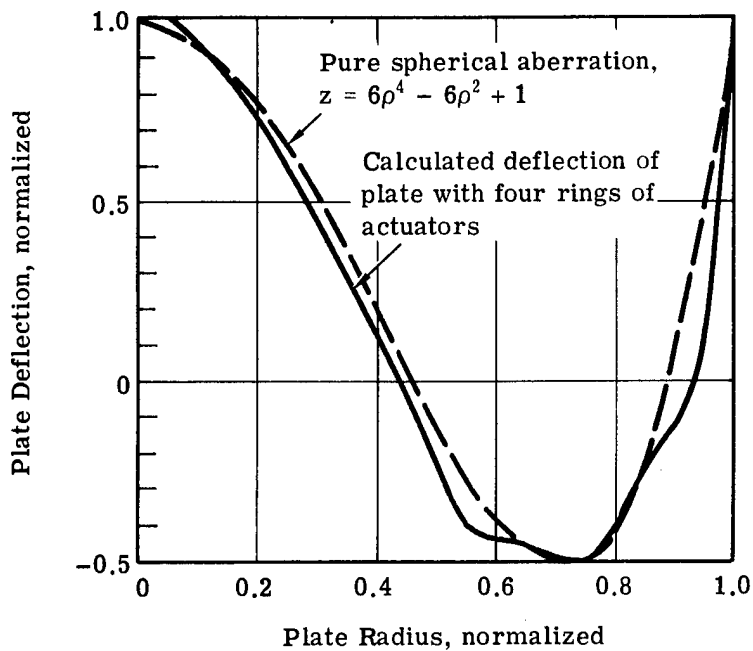
(a) Piezoelectric force actuator on a thin mirror



(b) Measured and predicted deflection for mirror with piezoelectric force actuator



(a) Piezoelectric moment actuator



(b) Example of calculated control of a thin mirror

Fig. 23 — Application of piezoelectric moment actuator

moment to the mirror. By using the same material for the faceplate and the base, preferably a low expansion material, thermally induced moments are nearly avoided. Fig. 23(b) illustrates an approximate calculation of an example of the type of deformation which can be corrected with such actuators, and will be referred to in Section 4.2.5. The actuator of Fig. 23(a) has been tested successfully.

A variety of other actuating principles may also be effective. With a very small heat input, thermal actuators could provide control in the same manner as that shown for the piezoelectric actuator. We have also built an electromagnetic driver capable of applying up to 35 Newtons of force, but this is more applicable for cases requiring large force and relatively rapid control.

#### 4.2.4 Control Range Required

The range of control required for each actuator is not large if control of the truss structure itself is provided. This approach is applicable to either segmented or continuous mirrors backed by a supporting truss; it is not directly applicable to an inflatable structure. Fig. 24 illustrates schematically a lightweight truss which could serve as the radial rib for a continuous surface mirror mounted on an umbrella-type support; or it could be the radial truss member of a continuous 3-dimensional truss. The figure also shows the deformation that would occur if there were an axial thermal gradient on the structure. As expected, a small strain in the rear truss members results in a small curvature change but a large deflection at the outer edge of the mirror. Correcting this by position actuators on the faceplate would require a long correction range. Instead, the truss itself should be controlled by changing the length of the diagonal or rear members, where it is only necessary to compensate for the thermal growth of the member itself. Two suggested ways are shown in Fig. 25. Changing the length of a rear element provides a uniform slope change for the rest of the structure; changing the diagonal provides a uniform displacement. Either thermal or force actuators can be used to accomplish this dimensional change, as illustrated.

If the truss material is low-expansion graphite/epoxy, the amount of correction required will be small. The thermal strain will be  $\epsilon_t = \Delta\alpha T$  and the length change  $\Delta d = d\alpha\Delta T$

where  $\alpha$  = coefficient of thermal expansion,  $5(10^{-8})$  per degree C

$\Delta T$  = temperature change,  $\pm 100^\circ\text{C}$

$d$  = length of a truss member, 3 meters.

In this case, the strain,  $\epsilon_t$ , is  $\pm 5(10^{-6})$ ; the length change,  $\Delta d$ , is  $\pm 15 \mu\text{m}$ .

The truss can be deformed by using force parallel to a member to expand or compress the truss member. The resulting stress in the material would be

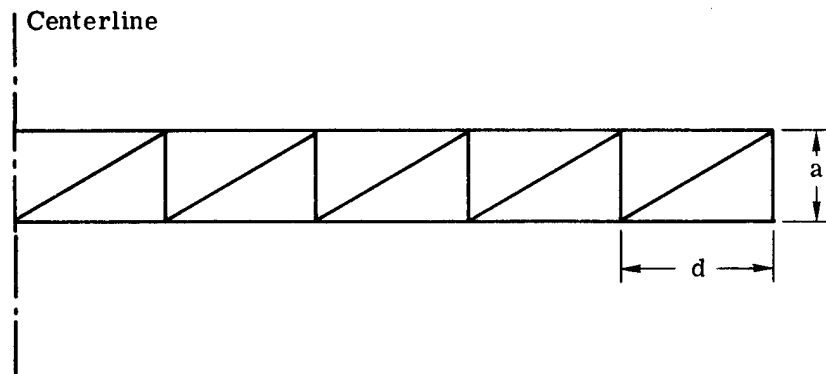
$$\sigma = \epsilon E$$

where  $E$  = Young's modulus. Taking  $E \approx 14 \times 10^{10}$  Newtons/m<sup>2</sup> ( $20 \times 10^6$  psi) gives a stress of only  $\pm 700,000 \text{ N/m}^2$  (100 psi), a trivial value. The actuator force required would be

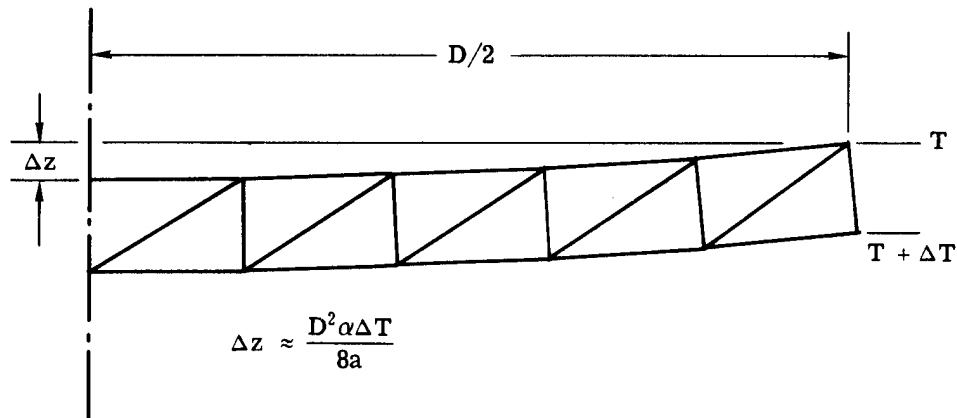
$$F = \sigma A$$

where  $A$  = cross-sectional area of the truss member. For the tubular members described in Section 4,  $A \approx 3.1 \times 10^{-4} \text{ m}^2$  (0.47 in.<sup>2</sup>), indicating a required force of only about  $\pm 220$  Newtons ( $\pm 47$  pounds), nicely within the design range of force actuators.

Using the equation in Fig. 24, this change, under a 100-degree temperature change, represents a sag ( $\Delta z$ ) variation, over the entire mirror, of about 0.2 mm, illustrating the very small dimensional changes which will occur when a low-expansion material is used. For materials

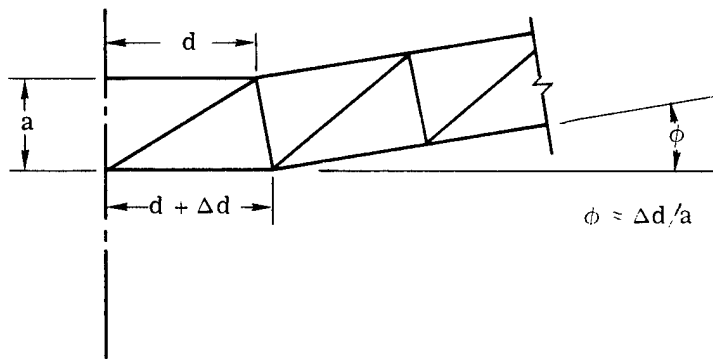


(a) Idealized truss

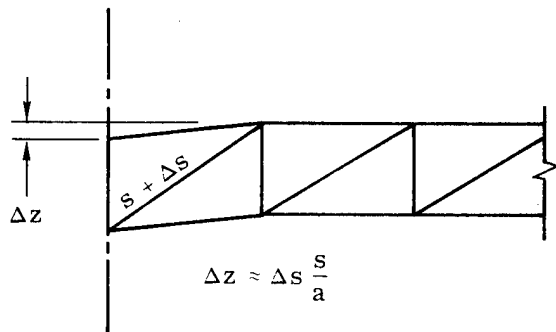


(b) Truss with axial thermal gradient

Fig. 24 — Thermal deformation of a truss



(a) Truss with rear displacement actuator



(b) Truss with diagonal displacement actuator

Fig. 25 — Active control concepts for supporting structure

having an  $\alpha$ -value approximately two orders of magnitude larger, such as aluminum or titanium, the length change of an element with  $\Delta T = \pm 100^\circ\text{C}$  would be  $\pm 1.5 \text{ mm}$  instead of  $15 \mu\text{m}$ , and the overall mirror sag would increase to about 20 mm. The use of parallel force actuator elements would not be effective by itself; an additional length changing element, such as a turnbuckle or other such screw positioning device, would have to be added.

The effective length of a truss member can also be changed by inserting a small block of material, with a large coefficient of thermal expansion, in line with the truss member. Active control of the temperature of the small block will then provide control of the overall member length. If we allow a  $100^\circ\text{C}$  control range to compensate for the  $30 \mu\text{m}$  length change in a graphite/epoxy truss, as described above, then a 30-mm-thick aluminum block would provide the needed control range. A temperature control to  $1^\circ\text{C}$  would provide a length adjustment control to  $0.3 \mu\text{m}$ . This indicates the feasibility of active thermal length control. Further work would establish the best compromise between heat loss, set by the maximum control range, and accuracy of temperature control, set by the required length change resolution.

It is concluded that as long as the truss is made of a low expansion material, such as graphite/epoxy, simple force or thermal approaches can be used for correction, with low stresses in the material or easily realized temperature changes in a short aluminum control block. We see no reason not to use graphite/epoxy as the truss material, and have not specifically considered any materials having a higher coefficient of thermal expansion.

If the gross truss deformations are removed, then the segment positioning actuators must compensate for only two, relatively small, sources of error—the thermal growth, and the initial manufacturing tolerances, in the attachment mechanism itself. If we assume that a positioning device, which may be a screw or a piezoelectric element, can have a resolution of one part in one thousand, and that the positioning tolerance is to be  $0.5 \text{ m}$ , then a range of  $0.5 \text{ mm}$  is available, more than enough to compensate for fabrication or thermal errors. The detailed design of such devices is not a part of this study. Possibilities include precision screws, differential screws, and a series of soft spring/stiff spring motion reducer concepts all easily capable of the full range of motion. Piezoelectric "creepers" can cover the full range, and simpler piezoelectric devices can cover the low end of the range.

If it should be desirable to compensate, at the segment attachments, for a truss which was grossly deformed after erection, there would be no difficulty in adding a coarse screw adjustment at each attachment point, to bring the segments within the final adjustment range. One design in Section 6.4 uses 75 hexagonal segments, each of which would require three fine adjustments and one optional coarse adjustment, for a total displacement actuator count of 225 to 300 actuators. With approximately one actuator in the truss for each attachment point, we can achieve wide-range redundant control of all segments in the 30-meter configuration with 375 actuators.

#### 4.2.5 Faceplate Bending Actuators

Additional actuators may be used between the rigid support points to control the local figure. Here the range that must be covered by the actuator is not the limiting factor in its performance. Instead, we must consider the residual figure error left after correction of a given figure error by a given number of actuators. Thus we must consider the types of error which can occur and the percentage correction obtained with different numbers of actuators. The major source of deformations will be thermal changes; an analysis of the deformation of the faceplates is given in Section 3, Figs. 10 and 11. These curves show that for a ULE or Cer-Vit faceplate, no figure control for thermal effects would be required. For aluminum faceplates, correction to 1 to 2 percent residual would be needed for a  $50$  to  $100^\circ\text{C}$  change.

The parametric analysis of Section 3.5 shows that a thin faceplate may have to be mounted on a supporting structure to satisfy dynamic requirements. The baseline concept, described in Section 6, satisfies this by including a 1.3-mm-thick glass faceplate on a 50-mm-thick graphite/epoxy structure; but this concept may increase the sensitivity of the mirror segments to axial temperature gradients or to uniform temperature changes. Gradients or changes occurring as the mirror changes from shadow to full sun exposure (see Fig. 12) may then require correction to 1 to 2 percent residual error. It can be seen that the range of correction, and thus, the number of actuators required, will depend critically on the match of thermal expansion between graphite/epoxy and glass, and on the transient thermal response of the system.

Typical examples of the control that could be achieved are given in Fig. 26. Percentages of correction achieved for focus changes will probably be between those for astigmatism and those for spherical aberration. The figure shows percent residual errors, calculated in a number of past efforts, and using a variety of actuator patterns. Two points, in squares, are for corrections applied by using forces between separated points on the mirror surface, described by R. M. Scott, "New Technique for Controlling Mirror Shapes", Optical Engineering 14:112, March-April, 1975. We see that only three actuators will remove most (85 to 97 percent) of the astigmatism; six single-pound actuators will leave a residual of less than 10 percent, and 80 actuators will leave very low residuals for gravity sag, astigmatism, and spherical aberration. The results have been calculated for a variety of mirror configurations, mostly 1.8-m (6-foot) diameter thin plates. Since the results are expressed in percent correction, they tend not to be influenced much by the mirror size or shape. Only if the thickness is very great so that shear effects predominates over bending, or very thin and deeply curved so that membrane forces are dominant, will significant variations be expected. The results will vary greatly with the distribution pattern of the actuators, however, and thus we have chosen not to draw a smooth curve of residual error versus number of actuators.

The results for 80 actuators assumed only 40 individual controls, with 40 actuators each operating on 2 points. Thus, there is some reason to move these points to the left, as shown by the dashed lines. The same is true for the corrections applied at 40 points, which assumed only 20 independent controls. In general, for a given number of independent controls, correction can be improved by spreading the actuator influence over several neighboring points. In system design, however, we have found it may be better to use one actuator for each control point in order to avoid the load-spreading structure. Each design will have its own compromise.

In other cases, the number of independent actuators may exceed the number of attachment points. One mirror used for an active control demonstration (ref 7) employed nine attachment points, with 27 independent controls. This gave control of axial position and slope in two directions at each point.

It is seen that in discussing the number of actuators, one must differentiate between:

1. The number of independent logical controls, each of which may drive one or more actuating devices
2. The number of actuating devices, which may be less than, equal to, or more than the number of actuated points
3. The number of actuated points (attachment points)
4. Self-reacting actuators which apply forces or moments between pairs of points on the faceplate which in some cases may be widely spread
5. Actuators reacting between the faceplate and the supporting structure.

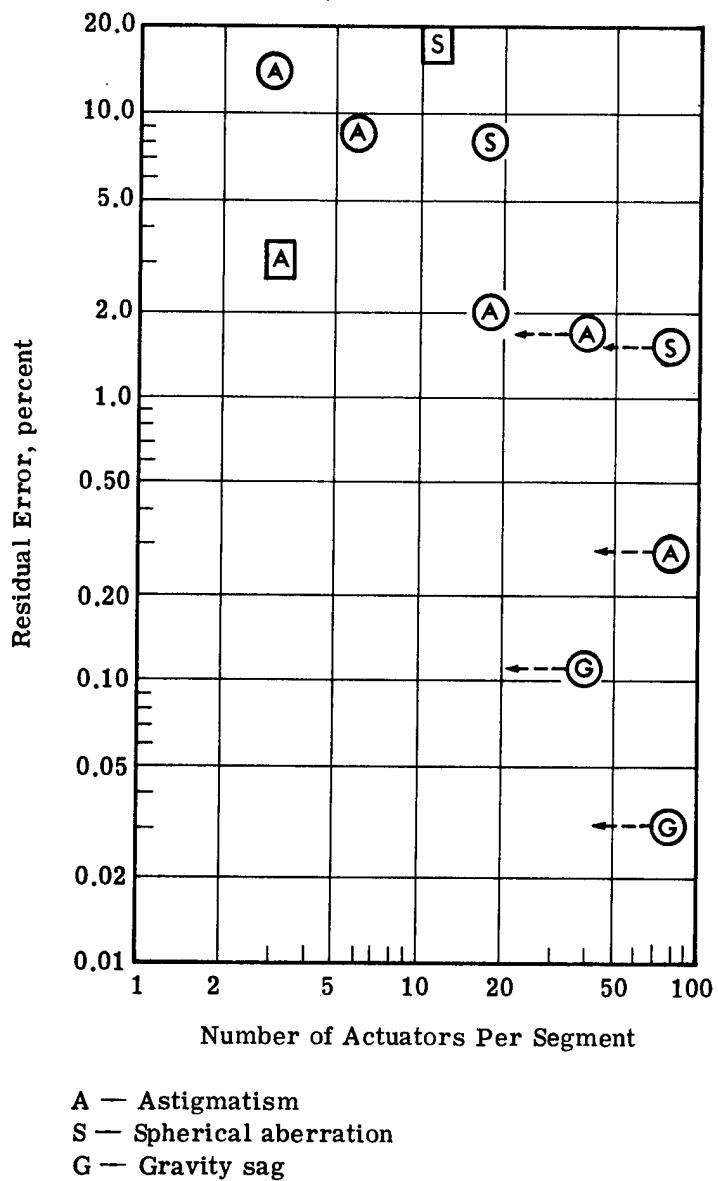


Fig. 26 — Residual error after correction of faceplate figure errors by actuators

The results obtained for 18 actuators were calculated for a novel configuration—the actuators were arranged only at the edge of the mirror, applying moments at the edge instead of forces. Relatively good control of astigmatism and spherical aberration was obtained (allowing refocus). Assuming that correction to 1 to 2 percent residual error is required for a 4-meter region, and that the actuator pattern could be optimized to give some improvement over the results of Fig. 26, we consider that 20 actuators is probably the maximum number required per segment.

Adding in all the segments and including truss and position actuators gives a total count of under 2,000 actuators, or about two per square meter of surface area. This would maintain a near-perfect figure for either a low expansion glass/graphite-epoxy composite structure, or a continuous metal mirror surface over a graphite/epoxy support structure. The figure would be obtained for an unshielded mirror, exposed to the high energy laser and to direct solar radiation at a varying aspect angle. The weight and cost of two actuators per square meter would probably be small compared to that for the mirror structure itself.

Two sets of numbers have now been generated for the actuator count: up to 300 for control of the support structure and mirror segment positioning; and up to 2,000 for control of local figure errors. It is shown above that the extent of control needed for local figure errors will depend on the detailed thermal characteristics of the mirror and system design. We conclude that the number of 2,000 should be considered as part of the baseline design, and that one goal of system design may be a reduction in the actuator count.

The use of piezoelectric moment actuators was described in Section 4.2.3, Fig. 23. An approximate calculation was made, using flat plate theory, to see if these devices arranged in rings could provide the shapes needed to correct a mirror. Fig. 23 shows the curve for refocused spherical aberration, used as a test case. Using a series of trial and error calculations, a fairly good match was obtained between the calculated mirror deformation and the shape set as a goal to be reached. It is probable that optimizing the forces with a least-square solution, and adjusting the radii at which the actuators were applied, would result in considerable further improvement. This approach may require a larger number of individual actuator elements, but they are simple and extremely light, and provide an interesting solution for control of a large thin faceplate.

#### 4.3 SENSING THE ERROR

Sensing the figure of the large mirror will require the design of specialized equipment, and the nature of the figure sensors will be affected by overall system design; but this is an area in which available technology is well developed. It is concluded that error sensing will not limit the feasibility of a large mirror. Real-time interferometers which provide a rapid readout of wave-front quality information have been built by Itek. A description of the concept and some test results are shown in the Appendix. Other sensors have been built and described by others (ref. 23 and 24). These sensors have more than adequate accuracy for the task and in many cases can have their range extended to cover large errors. Automatic autocollimators and other coarse alignment devices are also readily available. Many complex optical devices have operated reliably in space, including telescopes, cameras, spectrometers and other devices with elaborate electro-optical and mechanical operating sequences. An autocollimator which could successively scan over the regions or segments of a large mirror would not be complex, and a variable bandwidth white light interferometer could be used to equalize the path length between adjacent mirror segments. A strain gauge technique has also been proposed. We see little value, at this stage, in developing specific hardware concepts from the many competing possibilities available.

It is worth noting, however, some of the possible system configurations which could be used to incorporate a figure sensor source at or near the high-power receiver. One approach, probably

the simplest and most effective, is to use a source at the receiver on which the high-power beam is to be focused. An interferometer then measures this reverse beam as focused by the large primary mirror, and will provide for the proper focus setting and for figure control. System considerations become important here, since the returned reference beam must be separated from the outgoing high energy beam. By using a wavelength other than that of the high-power beam, problems of backscatter from mirror surfaces would be avoided, but separation of the beams is still necessary. A beam splitter in a 70-megawatt beam may be feasible, but probably would not be desirable. Time sharing, or operation of the sensor off axis, are then the most favorable approaches. Time sharing requires care; the high power beam cannot be turned off, since the thermal deformation of the mirror would make the figure measurement meaningless. The system could be defocused slightly, allowing the return beam to be brought to a focus inside the annular high power beam, with only a small change in flux density on the primary mirror. Another technique for separating the sensing and high-power beams would be to place the sensor off axis. Off-setting the aim point of the high-power beam would then allow a source on the potential receiver to be imaged onto the figure sensor. The method used would depend on the system design, including such factors as: the inner radius of the annular beam; the optical properties of the off-axis or defocused telescope; the ability to compensate for the off-axis or defocused aberrations in the figure sensor; the thermal time constant of the mirror and the uniformity and constancy of the beam; and the suitability of placing a source at the intended target.

The source need not be strong. We have analyzed the operation of an interferometer which would measure the wavefront to an accuracy of  $0.005 \mu\text{m}$  rms using a fifth magnitude star as a source, with a 30-millisecond measurement time per point. Measuring a  $60 \times 60$  grid of points (2,800 points within the circle) would then take less than 100 seconds. A 10-milliwatt source emitting in a 0.1 milliradian beam would provide the required signal source, indicating that there would be no source power or aiming problems if this approach were to be used.

A second approach is the use of a technique called "multi-dither", designed to optimize the high energy laser power delivered to a target, and widely reported in relation to high energy laser programs. In this technique, individual segments of a mirror are displaced periodically by small amounts, each segment identifiable by being oscillated at a different frequency; the energy received at the target is related to the phase of each displacement, and an appropriate correction signal is developed to indicate the desired direction of correction for that segment. The energy could be measured at the receiver, or a small corner cube could be used to reflect energy to a detector at the transmitter. The detector can be off axis, eliminating backscatter from transmitter surfaces. The principal problem here is in extending the technique to a very large number of measurement points, such as the 2,800 mentioned in the previous paragraph. The technique would probably not be applicable for this, but it may be useful for phasing the array of 75 large segments in the baseline design. Thereafter, the internal figure of each of the segments could perhaps be adjusted individually. A second problem is that the round trip propagation time of 0.3 second, for a range of 36 Mm, may create difficulties. Since the correction is based on the phase of the returned intensity modulation relative to the phase of each of the correcting elements, each operated at a discrete frequency and thus with no correlation between elements, the transit time must be known and properly compensated for if the proper phase relationships are to be measured.

#### 4.4 CONTROL LOGIC

Given a figure sensor which develops, in digital form, a set of measurements over the mirror surface, it is not difficult to conceive of a control logic which can provide the required commands to the control actuators. We assume, first, a sensor which measures wavefront (the first or third sensing concepts described above) and sets of actuators divided into three classes (faceplate bending, faceplate positioning, and truss control actuator) as described previously.

The control approach to be used will not be unique; many variations can be suggested. We present one approach in order to determine, very roughly, the computational requirements and the computer memory required.

Since there will be some redundancy in the control elements, one might start with a basic set, the truss control actuators. Knowing the deformation over the mirror surface (the influence function) which will result from a unit drive increment on each actuator, and given the measured surface error, the required actuator commands can be developed by a least squares solution. This will define the drive command for each actuator with the condition that the resulting rms figure error of the mirror surface is minimized. In general, if there are about twice as many measured values as control elements, a good solution will be found.

It can be shown that, for a given set of control elements and a given set of points at which the surface is evaluated, the computation process can be reduced to a matrix multiplication of the form:

$$[W] \times [P] = [F]$$

where W is the vector of N waveform measurements, P is a stored  $N \times M$  matrix, and F is the output vector of M actuator commands. P is generated in advance by knowing the measurement points and the nature of the actuator influence functions. If there were 75 truss control actuators and 200 measured points, the P matrix would require the storage of 15,000 values.

After the truss is controlled as well as possible, there will still be errors in the figure of the mirror. The next step would be to remeasure the error or to compute the residual after correcting with the truss control. After that, the position actuators would be set, using the error value measured at the location of each positioner, achieving accurate phasing between adjacent elements.

There may still be errors on the surface between position control actuators. These would be removed using faceplate bending actuators. Considering each segment or area separately, there would be influence functions corresponding to each force actuator. The solution for each force to be applied would then involve a matrix multiplication, as above. With up to 20 control elements per segment and up to 50 measured points, we would have 1,000 values to be stored for each of approximately 75 segments.

Adding up the storage requirements gives a need for about 100,000 words, more than the usual small 32K-word minicomputer, but a readily available amount of core storage for modest size machines. Processing time would involve the order of 100,000 multiplications and additions, but this would be processed within 10 seconds without any need for unusual speed.

#### 4.5 SUMMARY

Although it is not possible to analyze figure control capabilities without a detailed design of the primary mirror and the entire system, we have considered some of the basic parameters affecting the feasibility of control. The conclusion is that the needed control ranges are reasonable, that actuator concepts exist that could reasonably be developed as space-qualified hardware, and that sensing and control logic requirements can be met without new basic technology development. Much engineering remains to be done, and the number of components which may be needed is impressive, but reasonable in terms of the size of the mirror which will result. Total size and weight of the control elements will be relatively small.

## 5. STOW AND DEPLOYMENT CONCEPTS

### 5.1 DISCUSSION

In order to put the problem of stow and deployment of the 30-meter transmitter in perspective, it is instructive to consider the scaled relationship between the cross sectional area of the shuttle bay and the mirror as shown in Fig. 27. The area of the mirror is 56 times that of the storage area of the shuttle bay, indicating the significance of the packaging problem. Stow and deployment concepts must be formulated which efficiently use the allowable stow volume of approximately 226 cubic meters and provide, in orbit, a transmitter assembly capable of diffraction limited performance.

Technology for packaging the large mirror within the relatively small shuttle volume can be drawn from a review of studies associated with large antenna and solar collector concepts. At the initiation of this program, a state-of-the-art review was conducted. The scope of this review was very limited relative to the large number of documents on the general subject of expandable structures. For example, *Expandable Structures Design Handbook*, published in 1965 (ref. 8) provides an accumulated bibliography of approximately 1,200 documents. About 50 reports were reviewed for this program activity, with a bias toward understanding the technology associated with the inflatable class of structures. This preference was dictated by the favorable stow-to-deployment ratio which could be expected from these concepts.

Based on this limited review, assessment of applicable technology to the objective of this program can be made. Potential concepts can be identified by relating three generic parameters, i.e., type of reflecting surface, type of support structure for the reflecting surface, and the method used to deploy the mirror assembly. Each category is discussed in the following paragraphs.

### 5.2 DEPLOYMENT CONCEPTS

#### 5.2.1 Inflatable Structures

This concept group is characterized by the use of pressurization to deploy and expand the mirror structure to its desired shape. The use of fabrics, plastics and metal foils can provide very attractive candidate space structures because of their light weight and good potential stow-to-deploy volume ratio. The required general contour of the mirror may be maintained by several techniques such as pressure stabilization, chemical rigidization of the enclosure materials, injection of foams, or strain set of the structure.

Potential disadvantages because of the physical characteristics of the applicable materials are: (1) long and short term dimensional instability, (2) low stiffness properties, (3) nonuniformity of material properties, and (4) vulnerability to the operational environment, i.e., energy flux and micrometeorite penetration.

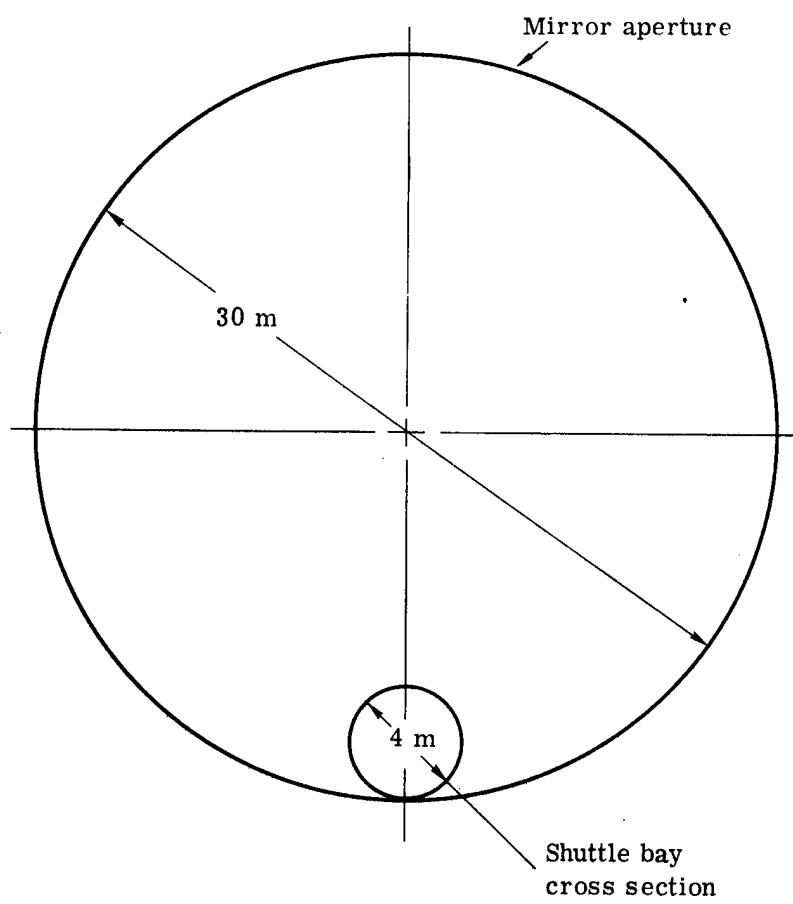


Fig. 27 — Shuttle bay-mirror area relationship

A possible concept for the 30-meter transmitter would be to utilize the technology from the ECHO and PAGEOS balloon satellite programs. These thin film structures were inflated to spheres of 30 meters in diameter. During the full-scale inflation test of the PAGEOS satellite, measurements showed that the polar and equatorial diameters were less than  $\pm 1/2$  percent ( $\pm 0.015$  m) from the design (ref. 9). Mathematical, manufacturing, and reliability techniques, which were developed, would be directly applicable.

The 30-meter reflecting aperture of the transmitter could be formed by aluminizing a portion of the inside surface of a balloon as indicated in Fig. 28. For a mirror focal ratio of 0.5 to 2, the required diameter of the spherical balloon for the proposed concept would be from 60 to 240 meters or 2 to 8 times larger than the referenced satellites.

This technique has the disadvantage that one side must be transparent. Mylar has poor transmission (50 percent) at the 10.6-micrometer wavelength, but has good optical properties otherwise. Polyethelene has good transmission (90 percent) but tends to have poor wavefront characteristics. Future research may expose other materials which have the necessary transmission and wavefront properties. The window problem could be eliminated by the concept of space rigidizing the reflective portion of the balloon and disposing of the front material.

A similar approach would be to attach two flat membrane elements to a peripheral inflated toroidal ring, Fig. 29. The mirror contour would be formed by differential pressure control of the ring and the area between the membrane surfaces. After deployment, the reflecting segment and toroidal ring could be rigidized to minimize the micrometeorite and window problems.

Probably the most promising concept within this category is the Airmat sandwich structure developed by Goodyear Aerospace Corporation. The structure is formed from two flexible membranes held a fixed distance apart, when under pressure, by a series of restraining cords called drop yarns. Stiffness and resistance to loads is derived by internal pressure or after pressurization, by chemical rigidizing.

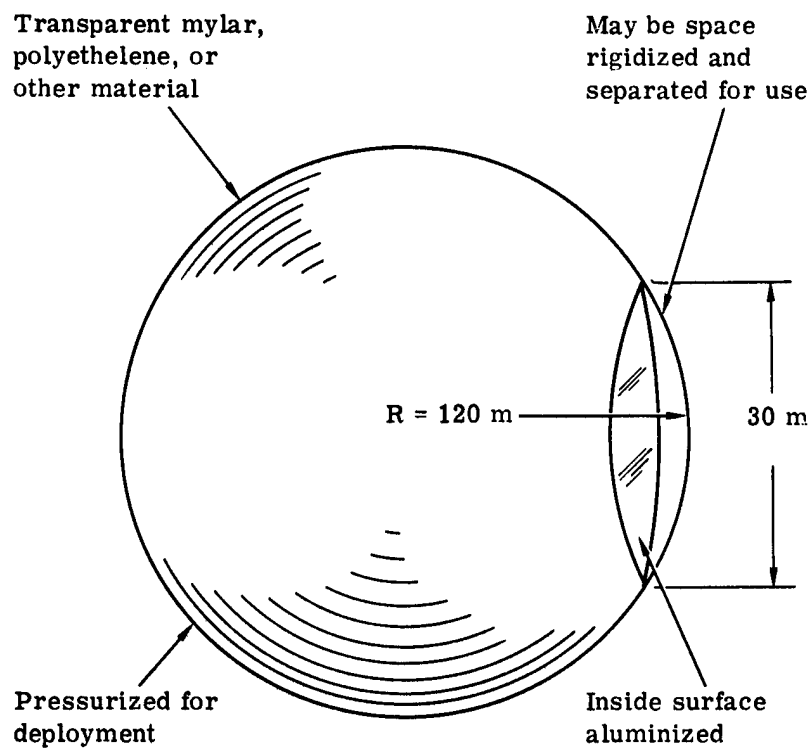
A number of reflectors have been fabricated using this concept, the largest unit, as far as it is known, being about 3 meters in diameter (ref. 10). It is felt that the major disadvantage of the approach, to date, is the use of woven fabrics, elastomers, and reflective film of high coefficient of thermal expansion. The use of these materials for the 30-meter transmitter would result in significant demands on the magnitude of correction to be accomplished by the active control system due to the thermal perturbations, or else a very good thermal control system must be used. A solution to this problem would be to investigate the use of graphite or DuPont's "Kevlar" fibers to form the base fabric material and selection of sealing and bonding materials to provide an effective low expansion assembly.

One of several possible configurations is shown in Fig. 30, a method for developing a parabolic surface. An inflated toroidal ring provides the major support to the parabola. The length of the individual drop yarns are designed to maintain the surface contour of the sealed fabric membranes when the assembly is pressurized. The relative rigidity of this type of structure would be greater than the balloon concepts. By changing the length of the drop yarns, active control of the surface could be effected.

### 5.2.2 Variable Geometry

These structures, as defined here, are those concepts in which rigid members are ground fabricated and assembled, launched in some sort of folded or collapsed configuration, and deployed in space. Included in this grouping would be those concepts in which the variable geometry is accomplished by utilizing the elastic memory properties of the structural materials.

This category of concepts would be of greater unit mass because of the materials used and deployment mechanisms. The mirror aperture would be limited by the ingenuity in use of the



Focal ratio (f/number) of the transmitter = 2

Fig. 28 — Balloon-mirror concept

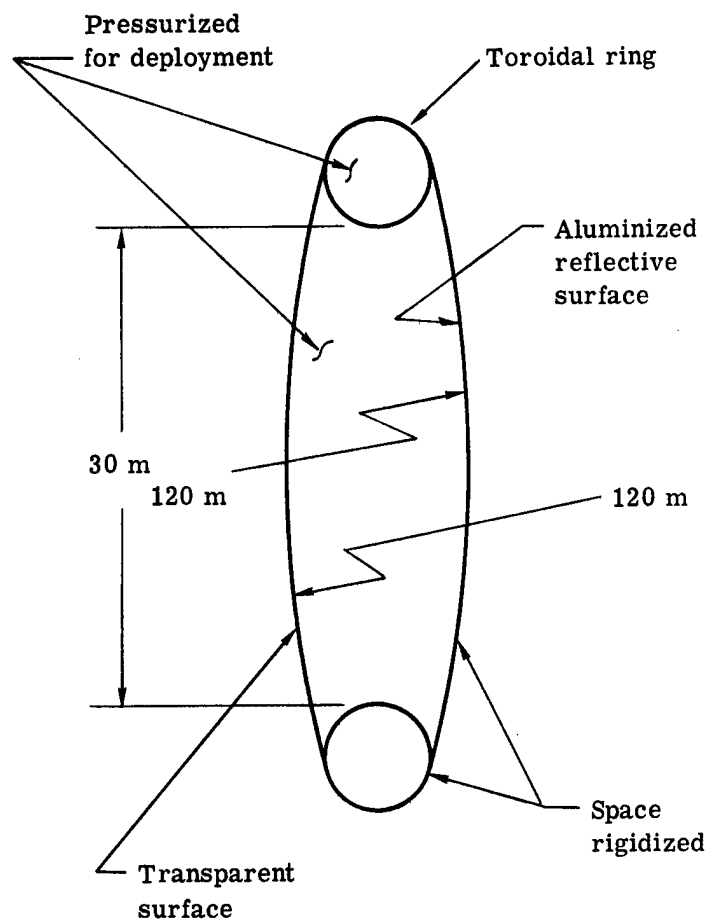


Fig. 29 — Toroidal balloon-mirror concept

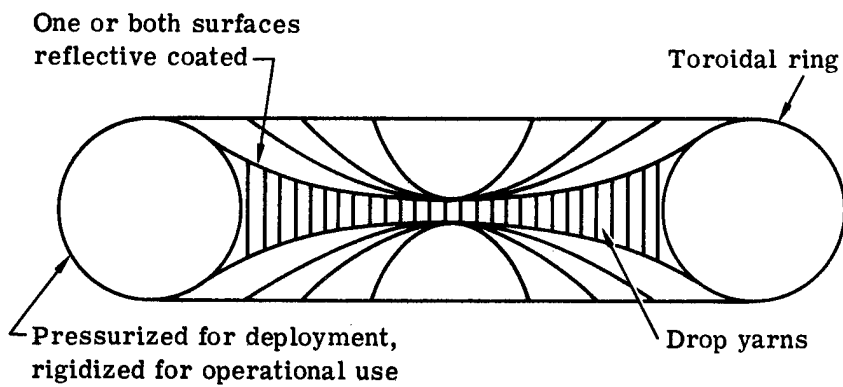


Fig. 30 — Double paraboloid inflatable mirror

allowable stow volume and design of the collapsed configuration. Mirror stiffness would probably be greater than for the inflatable structures. The variable geometry group of concepts, for the 30-meter aperture, are considered to be the least feasible at this time.

Within this class, the petal concept would have rigid segments of the mirror folding in towards the optical axis, contracting about the axis similar to a Chinese fan or sliding over each other like the technique used for photographic flash gun reflectors. The length of the package would be 15 meters or less which is compatible with the shuttle. However, if the total cross-sectional area of the shuttle bay could be utilized, the maximum allowable depth of a segment could only be 0.13 meter, an optimistic value.

An umbrella concept, in which a membrane reflective surface is supported taut between radial rib members, may be feasible if the number of ribs can be minimized. A 9-meter-diameter umbrella-shaped antenna reflector is being used on the NASA ATS-6 satellite. The design of a 15-meter deployable, graphite/epoxy rib antenna is discussed in ref. 11, along with fabrication and test results.

Radial control of the surface could be accomplished by active control of the rib structure. Tangential control of the surface would be a problem. If tangential control must also be provided by the ribs, rib spacing at the periphery may have to be on the order of 0.02 m for a total of 4,284 ribs in order to maintain diffraction limited performance.

Utilizing the elastic properties of materials is an intriguing concept for stow and deployment of large structures. Beryllium/copper, for example, could be formed into the desired general contour of the mirror, strained within its elastic limit for packaging and then sprung open upon command on orbit. The elastic properties of foam may also be used. Feasibility of this approach has been demonstrated (ref. 12).

The unique alloy, Nitinol, developed by the Naval Ordnance Laboratories offers a possibility for obtaining a continuous reflective surface using a rather stiff material (ref. 13). It is a nickel/titanium alloy which, when plastically deformed below its critical "memory" temperature will recover its original shape when heated above a critical restoration temperature. The base radius of the mirror would be set during the memory heat treat cycle by proper fixturing. The surface could then be final figured, coated, and strained by rolling or folding into a stow package. On orbit, the structure would be deployed and its original shape recovered by heating with solar and/or laser energy to a restoration temperature of less than 100 °C. Additional support to the reflecting surface could be provided by ribs or a deployable three dimensional truss.

### 5.2.3 Assembled Structures

This category includes the concepts in which the mirror members are partly ground fabricated and then assembled in space. The requirement of rather extensive extra-vehicular activities may be considered as the primary disadvantage. However, it is felt these concepts represent the most feasible and reliable approach to the deployment of a large aperture, diffraction limited mirror within the relative near future. Existing aerospace technology can be used to fabricate the various components of the mirror assembly; they are then stored in a convenient manner in the shuttle bay and assembled on orbit. If it is appropriate in order to obtain an acceptable mirror assembly, several shuttle flights could be considered.

## **5.3 SUPPORT CONCEPTS**

The three general classes of support structure for the reflective surface are identified as: self-supporting; discontinuous substructures; and continuous, three-dimensional substructures. Structural techniques having no supporting substructure are those in which the surface configura-

tion has sufficient structural rigidity to be self-supporting. Discontinuous substructures may be of the rib or petal type, for example, in which there is little or no stiffness continuity in the plane of the reflecting surface. Truss type structures or the Airmat concept, previously mentioned, are examples of structures having rigid interconnecting members arranged so as to produce a continuous three-dimensional load path.

#### 5.4 SURFACE CONCEPTS

Reflective surface concepts applicable for a diffraction limited mirror at 10.6 micrometers are grouped into the use of glass or glass/ceramic materials, metallic, or composite and membrane film surfaces. Coated glass/ceramic materials are considered the primary mirror material choices, desirable for their low coefficient of thermal expansion, but are fragile and present relatively poor volumetric stow potentials. Metallic surfaces such as aluminum, gold, or copper are considered to be advantageous since reflective coating may not be required. Coated composite material surfaces, for example, graphite/epoxy, present the potential for low thermal expansion, relatively high thermal conductivity and good stiffness-to-weight ratio. Membrane films, such as aluminized mylar, are attractive for their light weight and packagability. The major disadvantage may be the ability to obtain and maintain a low scatter surface of the proper general optical figure.

Reflective coatings for the mirror substrate is a topic that is only briefly addressed here. As an indication of the state of the art in coating technology, it is noted that Itek has been involved in an evaluation program in which silver and aluminum were produced by the Optical Systems Division and measured by Dr. Harold Bennett's group at the Naval Weapons Center (N.W.C.). These coatings were produced on superpolished fused silica and measurements of scatter as well as reflectance were obtained. Tables 4 through 6 present the measured data for specular reflectance at 0.6328 micrometer, 10.6 micrometers, and scatter in the visible spectrum, respectively. Samples B-43 and B-44 were silver coated at N.W.C. for surface roughness evaluation of the substrate. All others were coated at Itek and stored in either air or nitrogen. The films exhibit very good stability and all 10.6 reflectivities exceed 98 percent while silver approaches 99 percent after periods greater than one year.

Of the two coatings, aluminum can be produced more easily (no substrate heating is required). Itek has produced these coatings on elements 1.8 meters in diameter. Aluminum will yield infrared reflectance values slightly greater than 98 percent and will exhibit a solar absorptance of between 10 and 15 percent.

Silver must be heated (100 °C) in order to provide a durable protective overcoat. It is susceptible to sulfide formation and is, therefore, not as stable in the unprotected condition as aluminum. Silver will yield infrared reflectivities of 99 percent with solar absorption of about 6 to 10 percent.

Both of these coatings should be reviewed in light of tradeoff possibilities. One failsafe scheme could be considered which would suggest coating on station. The mirror may be coated prior to launch with the more durable aluminum coating. It would then be deployed into the 30-meter configuration. Finally, a silver coating could be deposited over the aluminum to provide the increased reflectance and lower loss. This option provides redundancy in that a good coating exists, while it holds out the potential for still better optical characteristics. Numerous questions will have to be resolved regarding cleanliness of the mirror, power to drive the vapor sources, concentration of contaminants in the vicinity of the mirror, etc. However, the potential for this scheme does exist.

Table 4 — Indicated Specular Reflectance Measured at 0.6328 Micrometer  
by N.W.C.

	A	B	C
B-43 (NWC, Ag, Air)	N/M	.9608	deteriorated
B-44 (NWC, Ag, N <sub>2</sub> )	N/M	.9809	.9790
B-42 (Ag, Protected, N <sub>2</sub> )	.9585	.9546	.9587
B-48 (Ag, Protected, Air)	.9557	.9514	.9552
B-52 (Au, Air)	.9269	.9116	.8804
B-51 (Au, N <sub>2</sub> )	.9274	.9093	.8945
B-46 (Al, SiO <sub>x</sub> , Air)	.8952	.8881	.8935
B-45 (Al, SiO <sub>x</sub> , N <sub>2</sub> )	.8960	.8990	.8958
B-47 (Au, SiO <sub>x</sub> , N <sub>2</sub> )	.8191	.8163	.8187
B-49 (Au, SiO <sub>x</sub> , Air)	.8164	.8143	.8175

A September 1973

B May 1974

C October 1974

**Table 5 — Indicated Specular Reflectance Measured by 10.6 Micrometers  
by N.W.C.**

	A	B	C
B-43 (NWC, Ag, Air)	N/M	.9868	N/M
B-44 (NWC, Ag, N <sub>2</sub> )	N/M	.9924	.9926
B-42 (Ag, Protected, N <sub>2</sub> )	.9899	.9902	.9898
B-48 (Ag, Protected, Air)	.9896	.9899	.9904
B-52 (Au, Air)	.9864	.9879	.9872
B-51 (Au, N <sub>2</sub> )	.9880	.9876	.9881
B-46 (Al, SiO <sub>X</sub> , Air)	.9837	.9826	.9825
B-45 (Al, SiO <sub>X</sub> , N <sub>2</sub> )	.9835	.9832	.9830
B-47 (Au, SiO <sub>X</sub> , N <sub>2</sub> )	.9886	.9890	.9886
B-49 (Au, SiO <sub>X</sub> , Air)	.9886	.9883	.9889

A      September 1973

B      May 1974

C      October 1974

Table 6 — Indicated Surface Roughness, Å

	A	B	C	D	E
B-43 (NWC, Ag, Air)	9.2	34.7	deteriorated	7.3	--
B-44 (NWC, Ag, N <sub>2</sub> )	10.6	18.2	19.4	2.1	22.4
B-42 (Ag, Protected, N <sub>2</sub> )	14.2	25.0	26.7	11.8	11.6
B-48 (Ag, Protected, Air)	14.5	19.8	17.6	9.6	18.6
B-52 (Au, Air)	13.1	19.7	27.2	8.6	15.9
B-51 (Au, N <sub>2</sub> )	15.3	18.5	19.0	11.7	16.0
B-46 (Al, SiO <sub>x</sub> , Air)	20.2	25.4	24.3	17.8	21.5
B-45 (Al, SiO <sub>x</sub> , N <sub>2</sub> )	21.0	24.0	28.1	18.3	19.2
B-47 (Au, SiO <sub>x</sub> , N <sub>2</sub> )	22.8	24.1	19.3	45.3	26.0
B-49 (Au, SiO <sub>x</sub> , Air)	25.0	27.7	26.6	42.0	45.2

A measured by N.W.C., 5461 Å      September 1973 (Coblentz Sphere)  
 B measured by N.W.C., 5461 Å      May 1974  
 C measured by N.W.C., 5461 Å      October 1974  
 D measured by Itek 6328 Å      December 1973 (Goniophotometer, Numerical Integration)  
 E measured by Itek 6328 Å      June 1974

## 6. 30-METER MIRROR CONCEPTS

### 6.1 DISCUSSION

To show the feasibility of deploying a 30-meter, diffraction limited mirror, three concepts are exhibited in this section. These concepts encompass the deployment categories of inflatable, variable geometry, and assembled in space structures. Each concept is based on existing technology which, under further development, could be integrated into a viable program for the implementation of a large aperture transmitter in space.

Whatever the concept, the philosophy of material selection will be critical. The principal sources of distortion in the mirror figure during operation will be from thermal effects and vibration inputs.

The effect of the dynamic environment can be minimized by the use of relatively lightweight, stiff materials and good design practice. The design goal should be to provide a mirror configuration in which the figure anomalies resulting from the dynamics of the system are within tolerable limits without high frequency, active figure control.

Mean operating temperature of the mirror may differ significantly from the temperature at which the mirror was figured. This results in two influences, a focus change and distortion from anisotropic behavior of the coefficient of expansion, even though the mirror is isothermal. Thus, the mirror substrate material and its supporting structure must be homogeneous and isotropic.

A more important thermal effect, however, comes from the presence of thermal gradients. Minimization of the distortion due to thermal gradients can be approached in three ways:

1. Material selection: use of materials which exhibit near zero expansion at the mirror operating temperature
2. Thermal isolation
3. Active optics: use of an auxiliary control system to restore the mirror figure.

The technology for thermal isolation is available; however, for the 30-meter system, the size and complexity of this auxiliary system may not be desirable. Active optical control is a viable solution, but the size, weight and complexity of this subsystem is a direct function of the magnitudes and type of aberrations which have to be corrected. Thus, from a systems standpoint, it is desirable to select for a design concept those materials which exhibit the least degrading properties in the operational environment.

### 6.2 30-METER INFLATABLE CONCEPT

This concept is based on the Airmat sandwich structure technology developed by Goodyear Aerospace Corporation. It consists of two flexible fabric membranes held a fixed distance apart,

when under pressure, by a series of interconnecting threads called drop yarns, see Fig. 31. The main elements of this composite structure are: (1) the reflective surface of metallized film, (2) an anti-markoff coat on the back side of the film to prevent show-through of the adjacent material texture, (3) a sealed fabric sandwich structure, and (4) a bonding layer for joining the two sub-assemblies.

As shown in Fig. 32, the inflatable structure would be made up of 24 preshaped gores. The mirror contour would be achieved by weaving the gores into a specific curvature (ref. 14). The maximum width of the gores would be 6.1 meters, which is consistent with existing facilities (ref. 15).

Several modes of folding the structure can be used to package the mirror structure for stowing into the shuttle bay. One technique is described in ref. 10 and shown in Fig. 33. The outer periphery of the mirror would be folded inward towards the center hub by a series of tucks. Additional tucks are made in the half-folded structure such that the assembly is formed into a cylindrical shape. In order to form the stow package, cuts extending through the reflecting surface and backing coat are made along the fold lines. Thus, the fabric membrane of the Airmat structure acts as the hinge during packaging. Using this technique for the 30-meter mirror, a minimum stow package envelope of 7 to 8 meters long and 4 meters in diameter could be formed, thus utilizing only 44 percent of the shuttle bay length.

A possible technique which would eliminate the requirement for tight folds and cut lines, would be to utilize the total allowable volume of the shuttle. The periphery of the assembly would be folded in towards the center hub along 72 fold lines. Gentle fold radii of about 0.175 and 0.075 meter could be formed by auxiliary formers which would have to be discarded after deployment. Tuck width at the mirror periphery would be about 1.3 meters. Assuming a 30-meter diameter, 3 meters in depth, the stow envelope would be about 16 meters long and 4 meters in diameter.

Deployment is accomplished by pressurization of the assembly. A 3-meter diameter Airmat structure was deployed with a pressure of 0.8 kN/m<sup>2</sup> (ref. 10). Smaller, 0.6-meter-diameter solar collectors have been deployed with pressures up to 3.4 kN/m<sup>2</sup> (ref. 16). Assuming that the deployment force is a function of circumferential area, that is circumference times overall depth, it is concluded that a pressure of about .08 kN/m<sup>2</sup> would be required for the proposed 30-meter configuration.

After deployment, the general contour of the mirror could be maintained by internal pressurization. This approach does not seem desirable because of the hazard of meteoroid penetration. The preferred approach would be to rigidize the structure immediately after deployment. Several chemical techniques have been developed which will rigidize films or impregnated fabrics. The rigidizing processes can be generalized into plasticizer boil-off (ref. 17), ultraviolet and infrared cured plastic resins (ref. 18), and gas catalysis curing techniques (ref. 16, 19). Another associated technique would be to activate plastic foam reactants to fill the interior envelope of the Airmat structure and solidify to rigidize the assembly (ref. 20).

Current fabrication philosophy of the Airmat structure utilizes high coefficient of thermal expansion elastomers, adhesive, and fabric materials. For example, the thermal expansion of rigidized fiber glass has been measured to be  $7.2(10^{-6})$  strain/°C (ref. 21). The implications of this expansion value can be seen by considering the sag of the 30-meter mirror as the result of a uniform temperature change. It may be expected that the base level temperature change of the mirror could be about 100 °C. This would result in a sag change of 66 waves over the 30-meter aperture, a significant magnitude to correct for.

Perhaps future developments using graphite or "Kevlar" fibers for the woven fabric and discrete selection of sealing, bonding, and rigidizing materials could provide an effective thermal expansion of at least an order of magnitude less. The alternate solution to the thermal distortion of the mirror, if high expansion materials are used, is to provide active thermal control of the mirror to less than 1 °C.

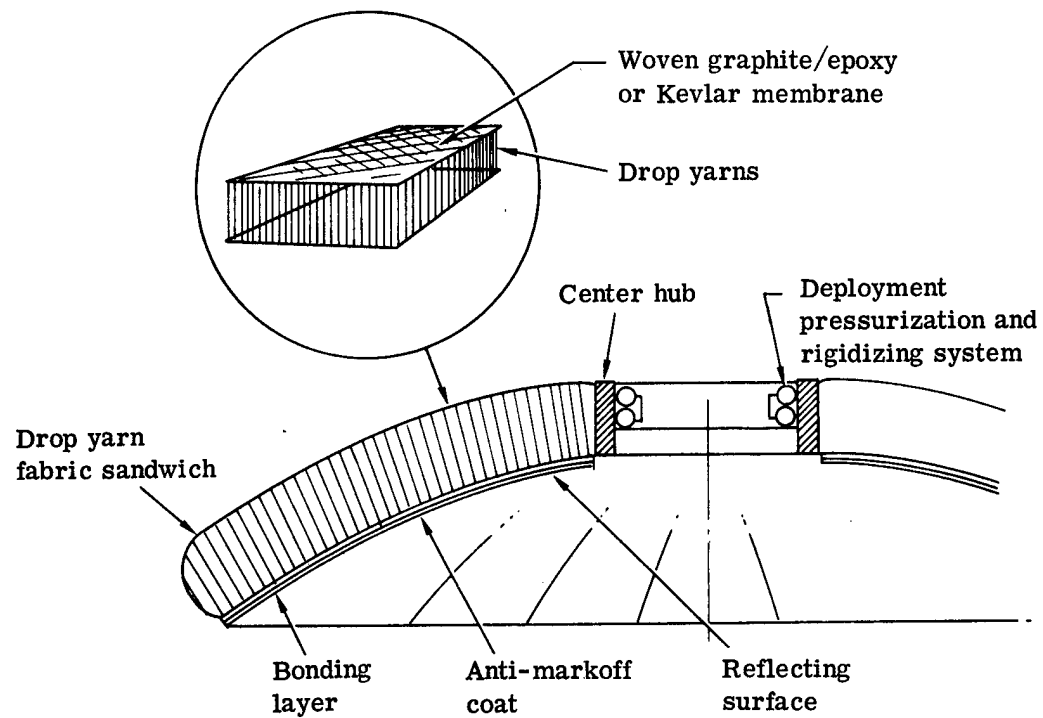


Fig. 31 — Inflatable deployment concept

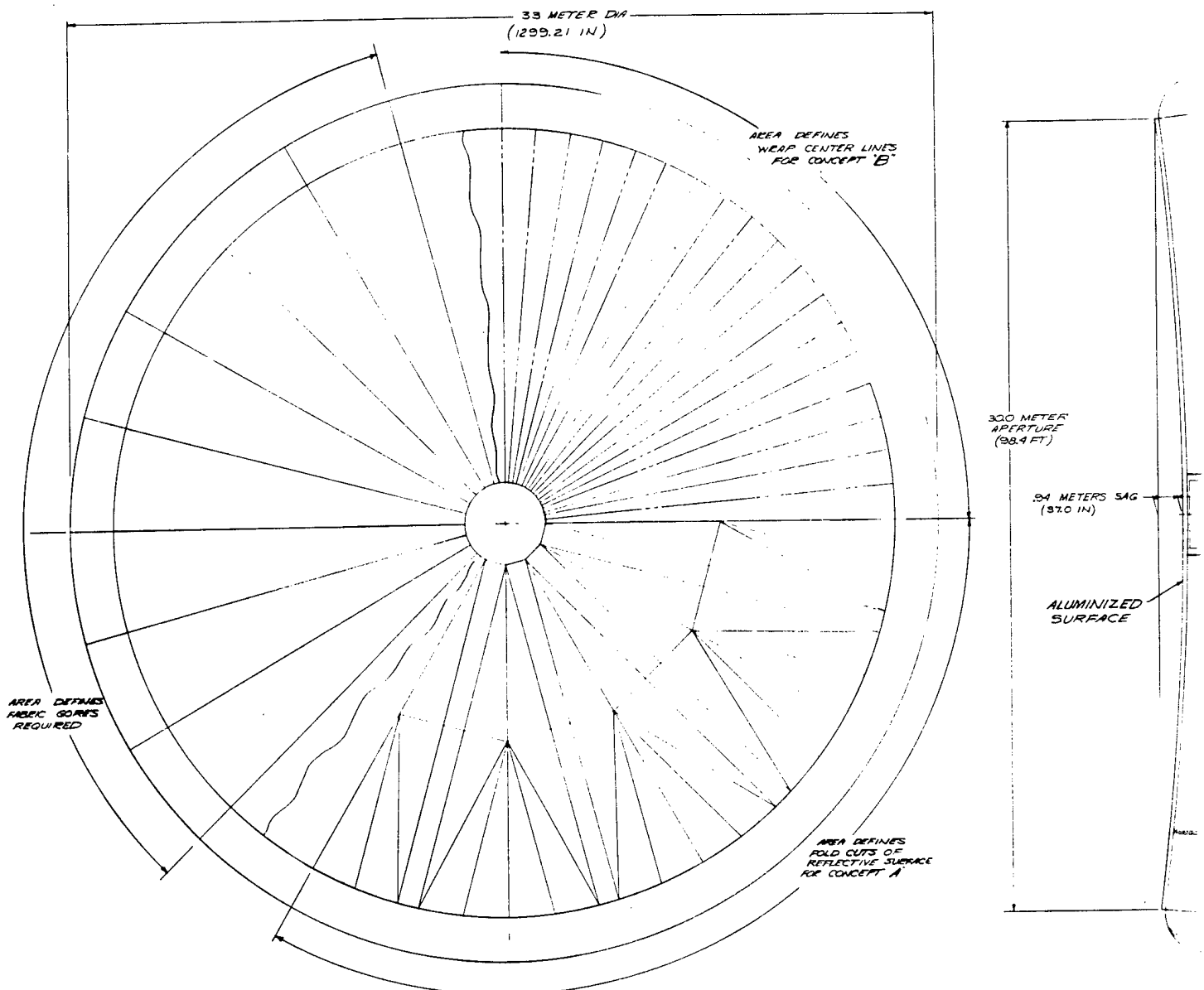


Fig. 32 — 30-meter

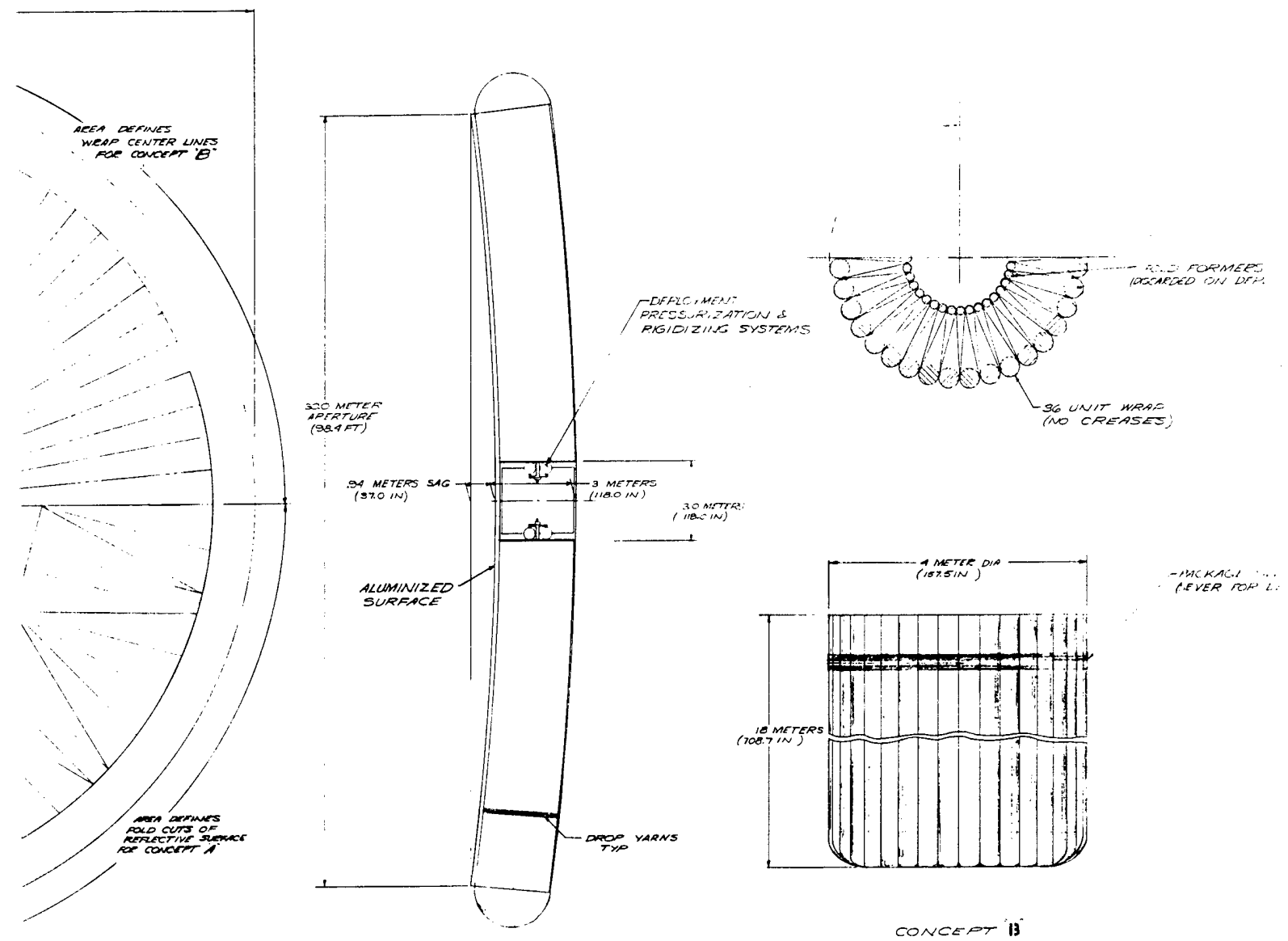
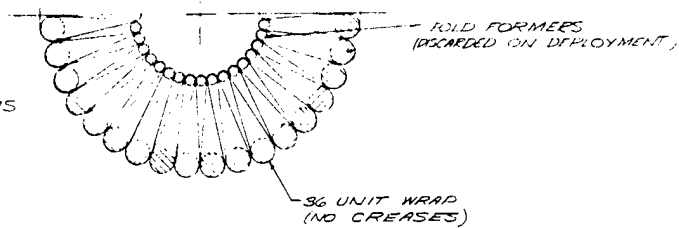


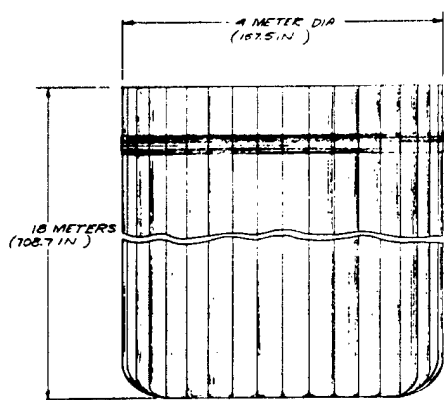
Fig. 32 — 30-meter inflated mirror concept

DEPLOYMENT  
PRESSURIZATION &  
PIGIZING SYSTEMS



FRS  
1)

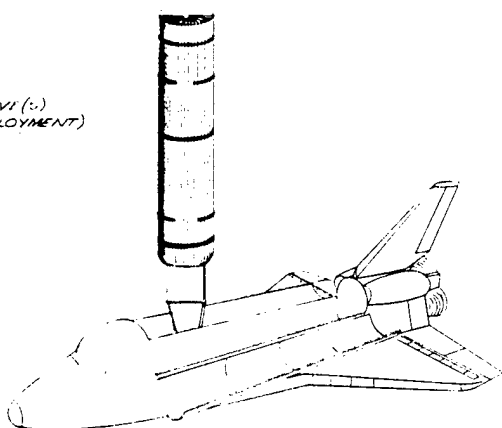
3.0 METER  
(118.1IN)



YARNS

CONCEPT 13

PACKAGING (LEVI (2))  
LEVER FOR DEPLOYMENT

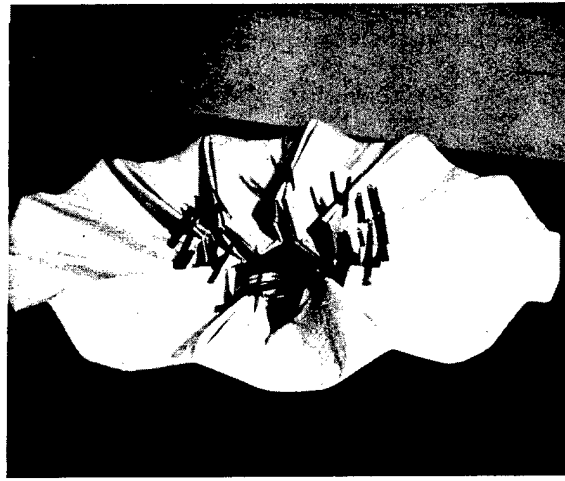


SHUTTLE DEPLOYMENT OF MIRROR

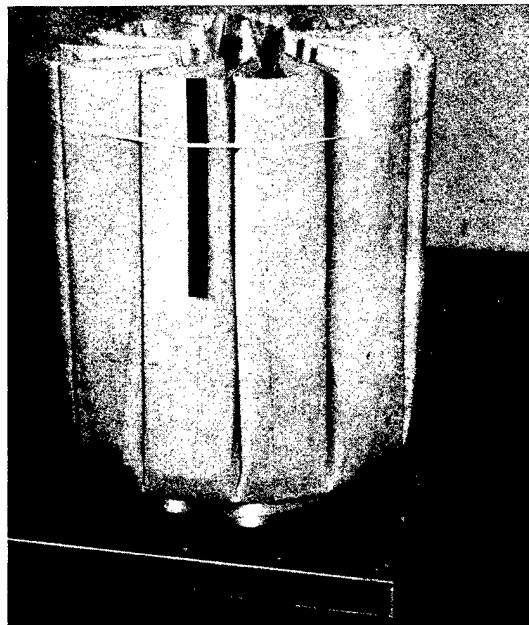
③



(a) Folding started



(b) Partially folded



(c) Folded mirror (side view)

Fig. 33 — Airmat folding sequence (Ref 10)

Active figure control for this concept may be effected by changing the length of the drop yarns or perhaps by the use of thermal "patch heater" actuators. This is an area which will require further tradeoff studies.

Utilizing the data from ref. 17, it is estimated that the launched weight will be on the order of 4,000 kg, well under the allowable weight of the shuttle.

### 6.3 30-METER VARIABLE GEOMETRY CONCEPT

For the variable geometry concept, the elastic memory properties of the alloy Nitinol presents a feasible means for producing a continuous reflecting surface with a material whose stiffness is comparable to aluminum.

Test data on Nitinol wire indicates recovery as high as 100 percent provided the strain from the memory shape did not exceed 8 percent. If we consider the possibility of a folded or rolled continuous reflecting surface, based on a simple strip analogy, the allowable radius is shown in Fig. 34. The small allowable radius is somewhat surprising, but if real, worth further investigation.

Density of the material is quite high,  $6.45 \text{ g/cm}^3$ , which would limit the substrate thickness to about 3 millimeters for the 30-meter application. Thermal coefficient of expansion is  $10.4 \text{ strain/}^{\circ}\text{C}$ , which would have significant implication on the design of the active figure control and thermal protection of the mirror satellite. The specific damping capacity of the Nitinol alloy, the percentage of vibration energy absorbed per cycle, is about 25 percent or three times that of gray cast iron. This property may be important depending on the dynamic input to the mirror structure during operation. Magnetic permeability is less than 1.002, whether the disturbance of the magnetic moment on the transmitter-satellite is significant will depend on the criteria set for the pointing control system.

There are several fundamental questions which should be answered in order to qualify the potential of this material:

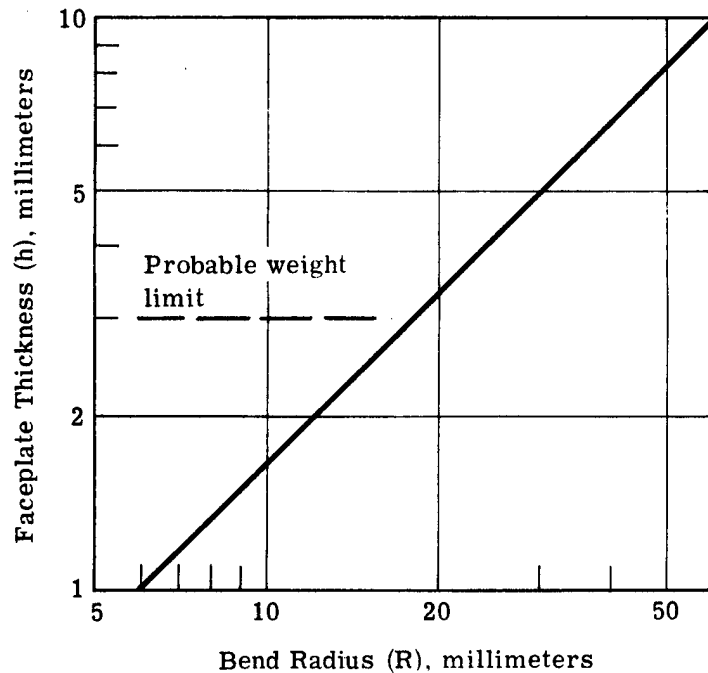
1. How good is the "memory" recovery in terms of the optical requirements?
2. Since the alloy is 57 percent (by weight) nickel, can the surface be optically polished directly; if not, can it be coated?
3. What are the strain limits for biaxial strain? What are the edge effects?

Fig. 35 shows the proposed concept. One possible configuration consists of 36 ribs, attached to the Nitinol substrate, to provide additional support to the reflecting surface. These ribs would also assist in forming the folds for packaging. Depth of the rib structure can probably be no greater than 0.5 meter. The force required to rotate and lock the ribs into their final position is provided by the Nitinol substrate as it is forced to return to its initial shape when heated to its restoration temperature.

An alternate support configuration would be to use the expandable truss concept. Some means would have to be devised to attach the Nitinol faceplate to the truss, after deployment. The truss, however, would provide a stiffer support to the reflecting surface.

It is proposed that piezoelectric actuators could be used for the active figure control of the Nitinol faceplate. Additional actuators would be incorporated into the rib or truss support structure to provide overall contour control of the mirror assembly.

It is estimated that the stowed weight of this concept would be 20,000 kg, about 75 percent of the allowable payload weight of the Space Shuttle.



$$\text{Strain } (\epsilon) = h/2R$$

$$\epsilon = 8\%$$

Fig. 34 — Nitinol plate thickness versus bend radius

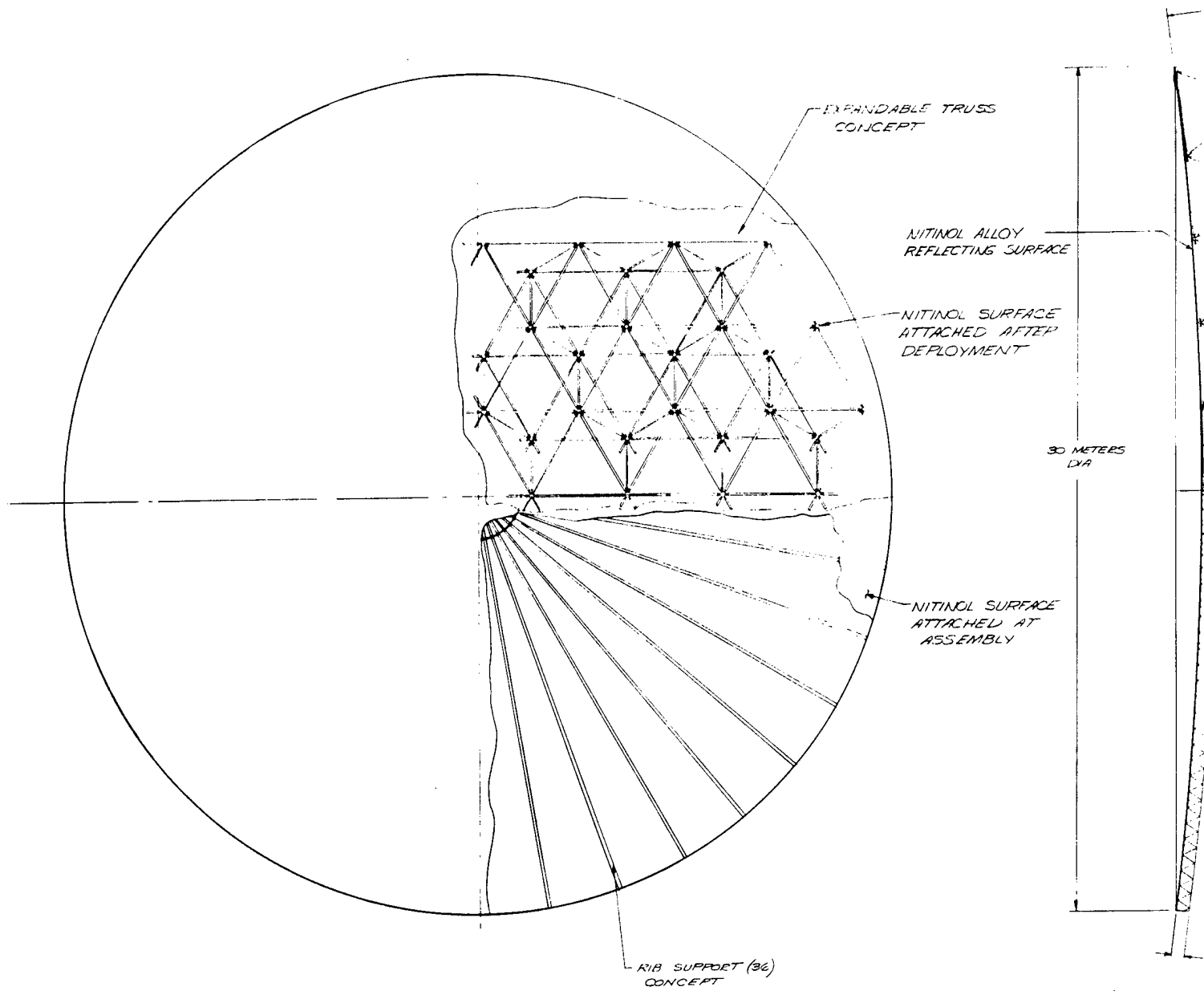


Fig. 35 — 30-meter va

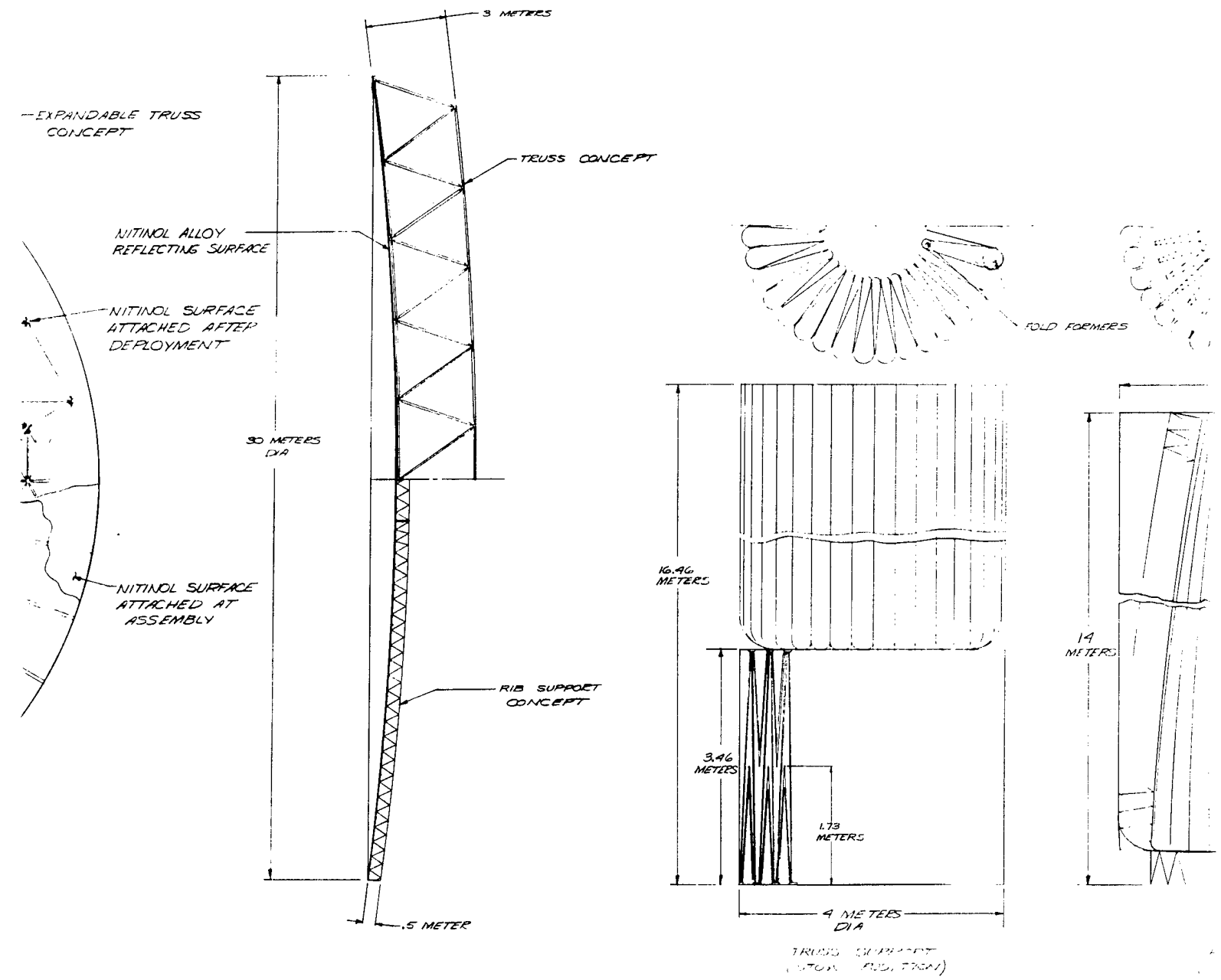
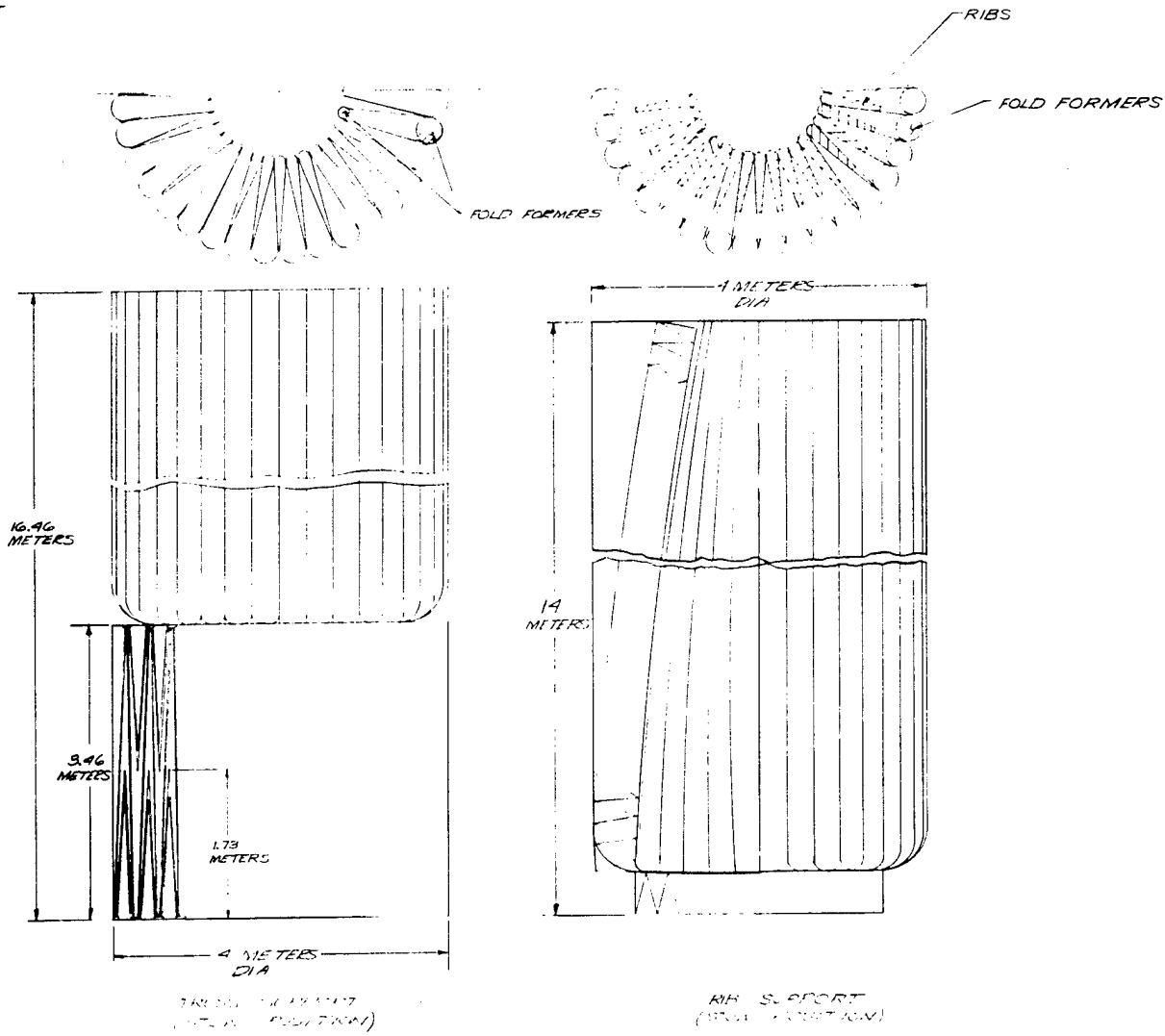


Fig. 35 — 30-meter variable geometry concept

USS CONCEPT



ry concept

#### 6.4 ASSEMBLED IN SPACE CONCEPT

This configuration is based on the concepts of partial assembly in orbit, low thermal expansion glass reflecting surface, and a truss utilizing the potential of graphite/epoxy to obtain low expansion characteristics by proper lay-up of the matrix plies. The expandable truss and individual segments of the mirror aperture are stowed separately in the shuttle bay. After deployment of the truss, the mirror segments are assembled to the truss by EVA operations.

Segmented panels of triangular and hexagonal format were considered. Both configurations were sized to fit within a 4-meter-diameter envelope compatible with the shuttle bay plus allowance for stowage support structure. The triangular segments approach provided complete coverage of the required aperture using a total of 150 segments. The triangular format does not utilize efficiently the allowable stow volume of the shuttle, nor is it a particularly good configuration from an optical fabrication standpoint. The hexagonal segment concept minimizes the preceding disadvantages.

Referring to Fig. 36, 75 hexagonal segments compose the reflecting surface. The maximum diametrical dimension of the transmitter would be 34.6 meters. Each segment consists of a 1.3-millimeter-thick reflecting surface of low expansion fused silica or Cer-Vit bonded to an isogrid graphite/epoxy back-up structure. The thin bond line could follow the geometric pattern of the isogrid structure or be effected locally as shown. Spacing of the attachment areas must be 100 millimeters or less, so that the surface quality can be proven by optical testing in the 1-g gravity environment.

The maximum diametrical dimension of the hexagonal segments is 4 meters, thus allowing sufficient stow structure within the shuttle bay. Consideration of the required space envelope for the support truss resulted in an allowable depth of 150 millimeters for each of the panels. Figure control actuators would be an integral part of these panel assemblies, thus allowing ground based checkout and operational verification of performance.

It is felt that three position actuators for each panel will be required for coarse alignment of the segments. These actuators would be incorporated as part of the expandable truss assembly. A bayonet type "quick" connect would be provided on the end of the position actuator for securing the panels to the truss structure.

The concept of bonding the reflective surface to the graphite/epoxy structure is predicated on matched coefficient of thermal expansion. This approach will require further technical evaluation. However, IR&D activities by Itek and Convair Aerospace Division on ULE/graphite-epoxy mirror substrates of 0.2 to 0.3 meters in diameter has indicated the feasibility of the concept.

The 0.2-meter diameter substrates consisted of a disk stiffened by radial ribs and a peripheral ring. A 0.006-meter-thick sheet of ULE was bonded to the graphite/epoxy structure over the total interface area. The goal of this program was to assess the feasibility of optically figuring the ULE faceplate and to determine the effect of temperature and humidity on the mirror blank.

A reasonably good surface quality of 0.04 wave rms at 6328 Å was attained. An interferogram of the surface, Fig. 37, was produced using an unequal path, Twyman-Green interferometer. The contour plot of the surface errors results from a computer evaluation of the interferogram.

It is known that the graphite/epoxy material is hygroscopic. The effect of humidity on a flat mirror sample is shown in Fig. 38. The major difference in surface figure is 1.0 wave (at 6328 Å) of astigmatism. This astigmatic error is equivalent to a strain differential of only  $3 \times 10^{-7}$ . It is concluded that the graphite/epoxy material must be sealed to eliminate this detrimental characteristic.

Fig. 39 shows the effect of a soak temperature change of 2.7 °C on a third sample. The difference of 0.09 wave rms (6328 Å) over this temperature range dictated a reevaluation of the approach to bonding the ULE to the supporting structure. This reassessment has resulted in a second generation concept as shown in Fig. 40. In this figure, the back structure is being viewed through the clear ULE faceplate. The diameter of the composite mirror blank is 0.3 meter, with a radius of curvature of 1.22 meters. In this configuration, the faceplate is 0.003 meter thick and is bonded to the back-up structure along each radial and tangential rib line. The goal of this concept was to decrease the bond area in order to minimize the strain effect on the optical surface due to the relative large thermal expansion of the adhesive.

Evaluation of this concept continues. A coating has been developed which solves the hydroscopic problems. McDonnell Douglas Corporation has recently disclosed the development of a family of adhesives that are tailorable across a broad spectrum of desired characteristics. A major point of interest being that bond lines of only a few molecules thick are feasible. Thus, the potential exists to virtually eliminate the influence of the adhesive interface.

The truss configuration is based on the concept first proposed by the Convair Division of General Dynamics (ref. 22). It is made up of rigid graphite/epoxy tubular members and spring flexure joints to provide the folding capability. Because of its foldable members, the truss is capable of being stowed in a relatively small volume of 4 meters diameter by 7 meters long. The configuration of folding the fore and aft truss members outward away from the nonfolding diagonal members was selected in order to maximize the cross-sectional dimensions and, hence, the stiffness of the truss members. Maximum allowable diameter of the truss tube members, assuming a 4-meter-diameter stow package, is about 75 millimeters. Each member is 3.46 meters long. The wall thickness of the graphite/epoxy tubes is 1.3 millimeters, representing a balance ply lay-up for a low effective coefficient of thermal expansion.

Weight of the mirror assembly is estimated to be 10,251 kg. The natural frequency of this large structure was calculated to be 20 Hz. However, it is felt that this is optimistic because of the assumptions made, and that a more refined analysis may show a natural frequency of an order of magnitude less.

A disadvantage of this concept is the requirement for extravehicular activities. The physical limitations of an astronaut when operating in the orbital environment is an important factor in justifying the feasibility of assembling the large mirror segments to the truss structure. An astronaut's ability to perform EVA tasks has been demonstrated on recent space programs and continued advancement in capability is to be expected.

## 6.5 CONCEPT EVALUATION

The concepts for the 30-meter transmitter have been evaluated as to the relative merits of each. The rating matrix is shown in Table 7. A simple ranking scheme is used to identify what is felt to be the relative merits of each concept for the nine performance parameters considered.

Based upon the results shown, the assembled in space concept would be the preferred approach. Each concept presented was based on current state-of-the-art technology. Additional development within these technology areas would be required, however, before a diffraction-limited 30-meter mirror could be placed in orbit. If there is a requirement for technology beyond the current state of the art, it is in the area of developing larger material production equipment and facilities compatible with the needs of the large mirror assembly.

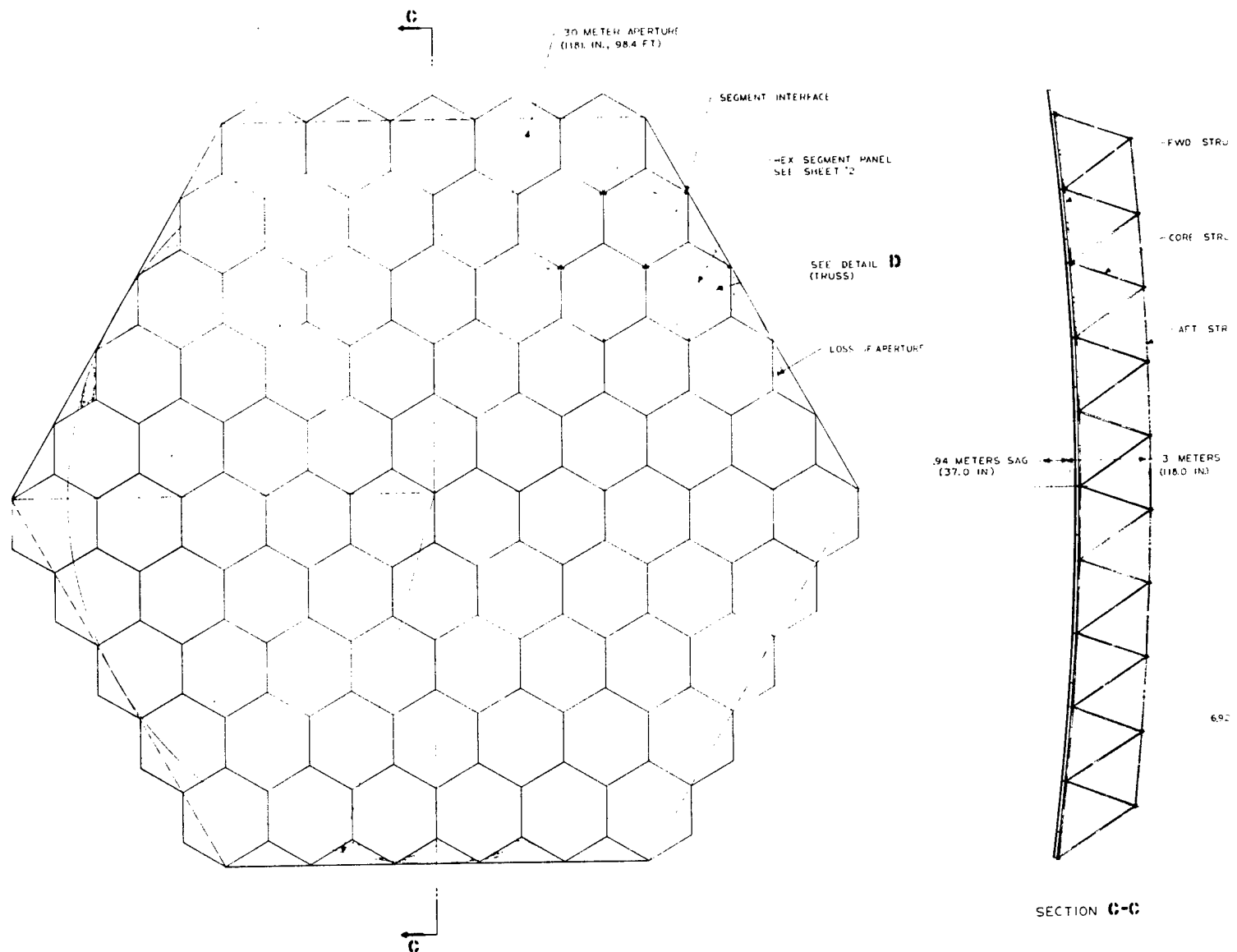


Fig. 36 — 30-meter ass

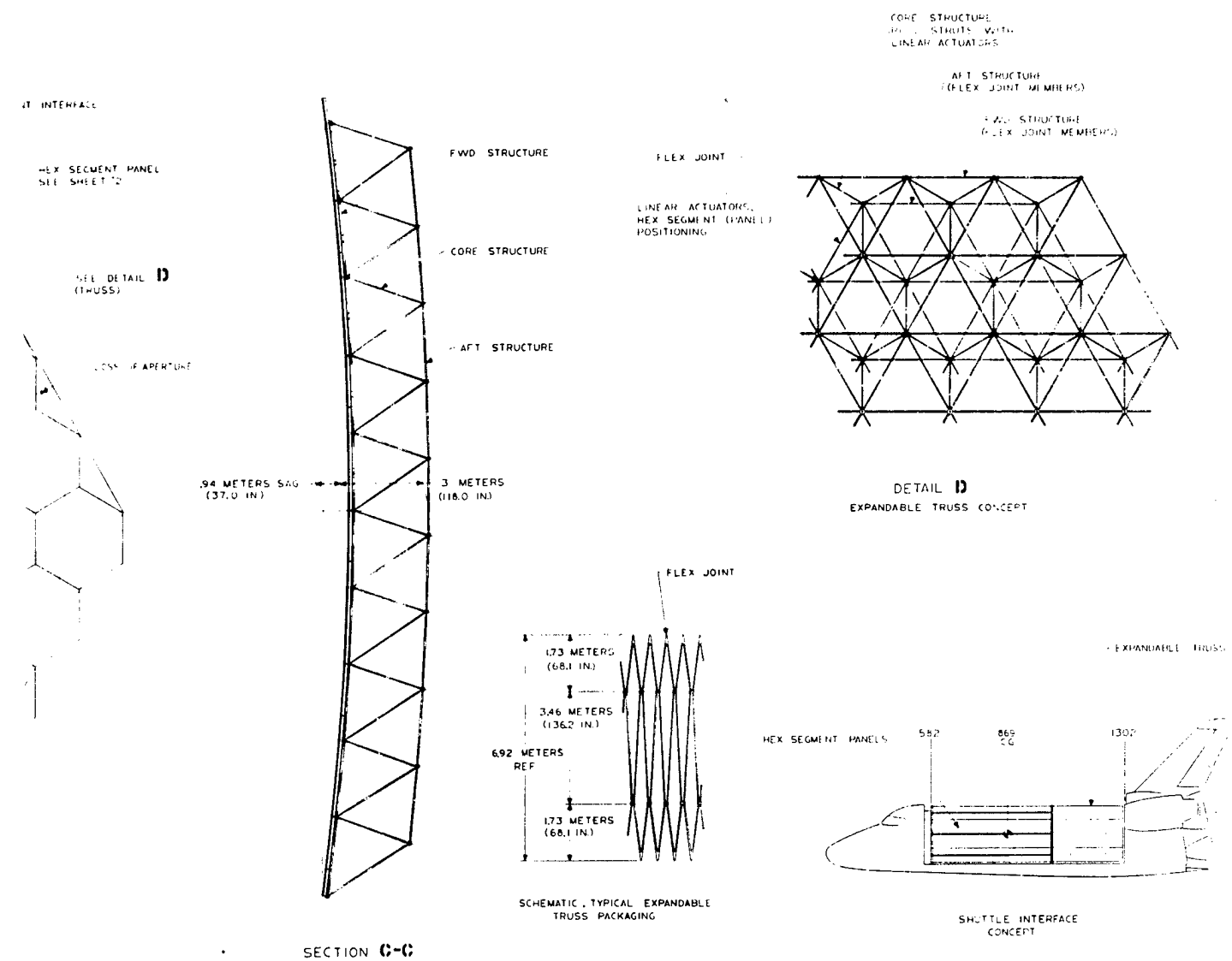


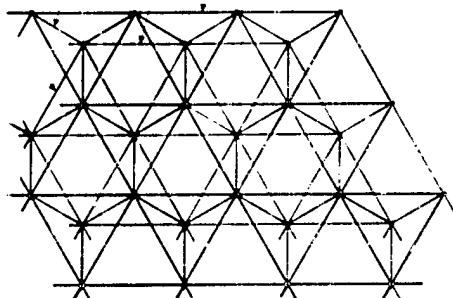
Fig. 36 — 30-meter assembled in space concept

CORE STRUCTURE  
(MMG STRUTS WITH  
LINEAR ACTUATORS)

AFT STRUCTURE  
(FLEX JOINT MEMBERS)

FWD STRUCTURE  
(FLEX JOINT MEMBERS)

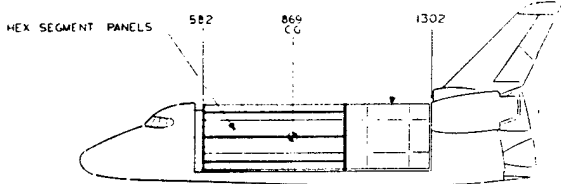
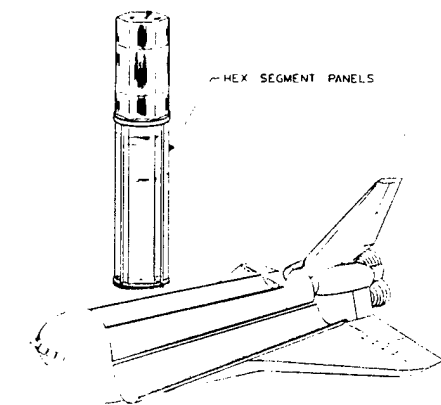
TONS.  
(KNEE)



DETAIL D  
EXPANDABLE TRUSS CONCEPT

EXPANDABLE TRUSS

HEX SEGMENT PANELS



SHUTTLE INTERFACE  
CONCEPT

SHUTTLE DEPLOYMENT OF MIRROR

concept

③

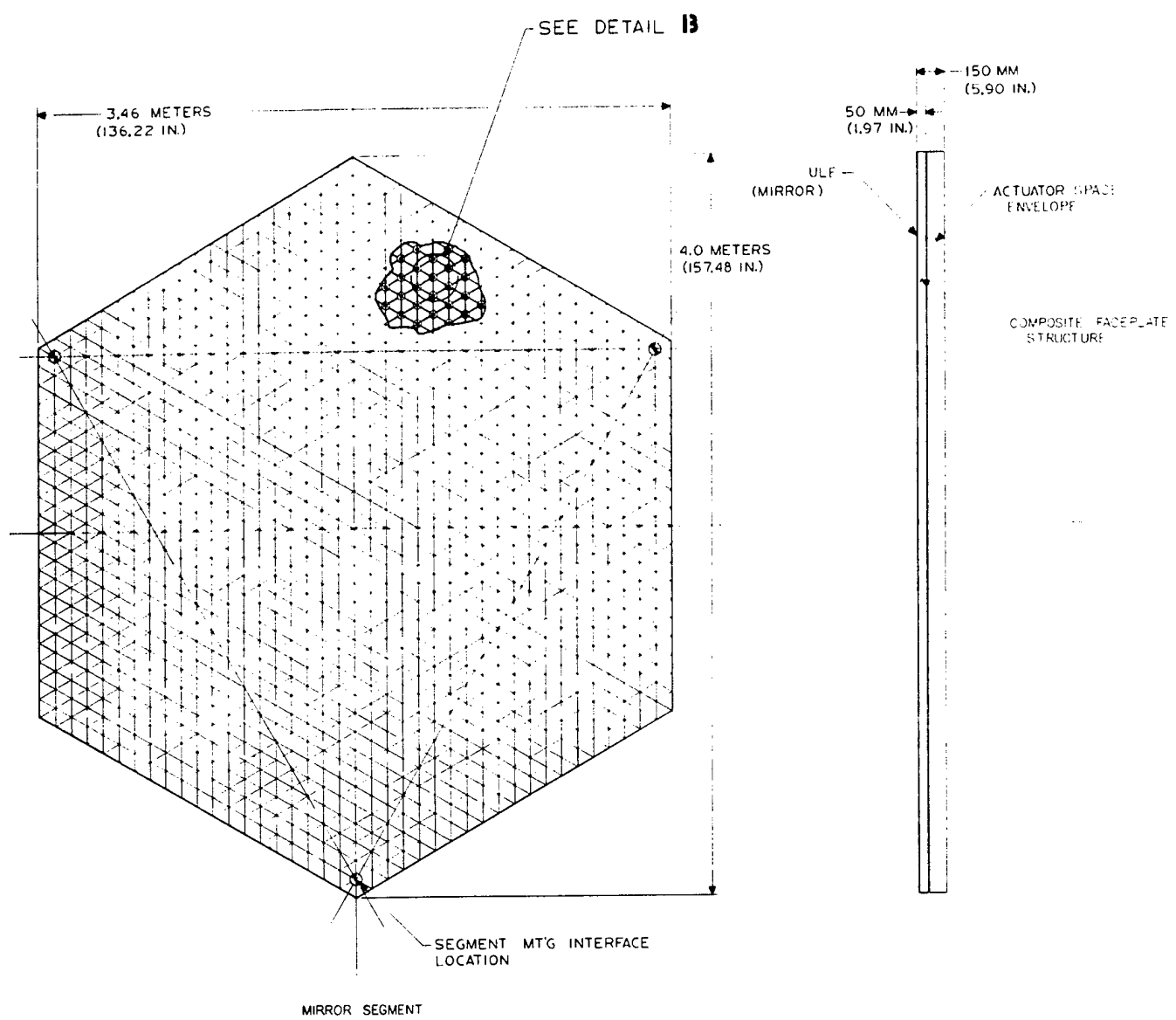


Fig. 36 — 30-meter assem

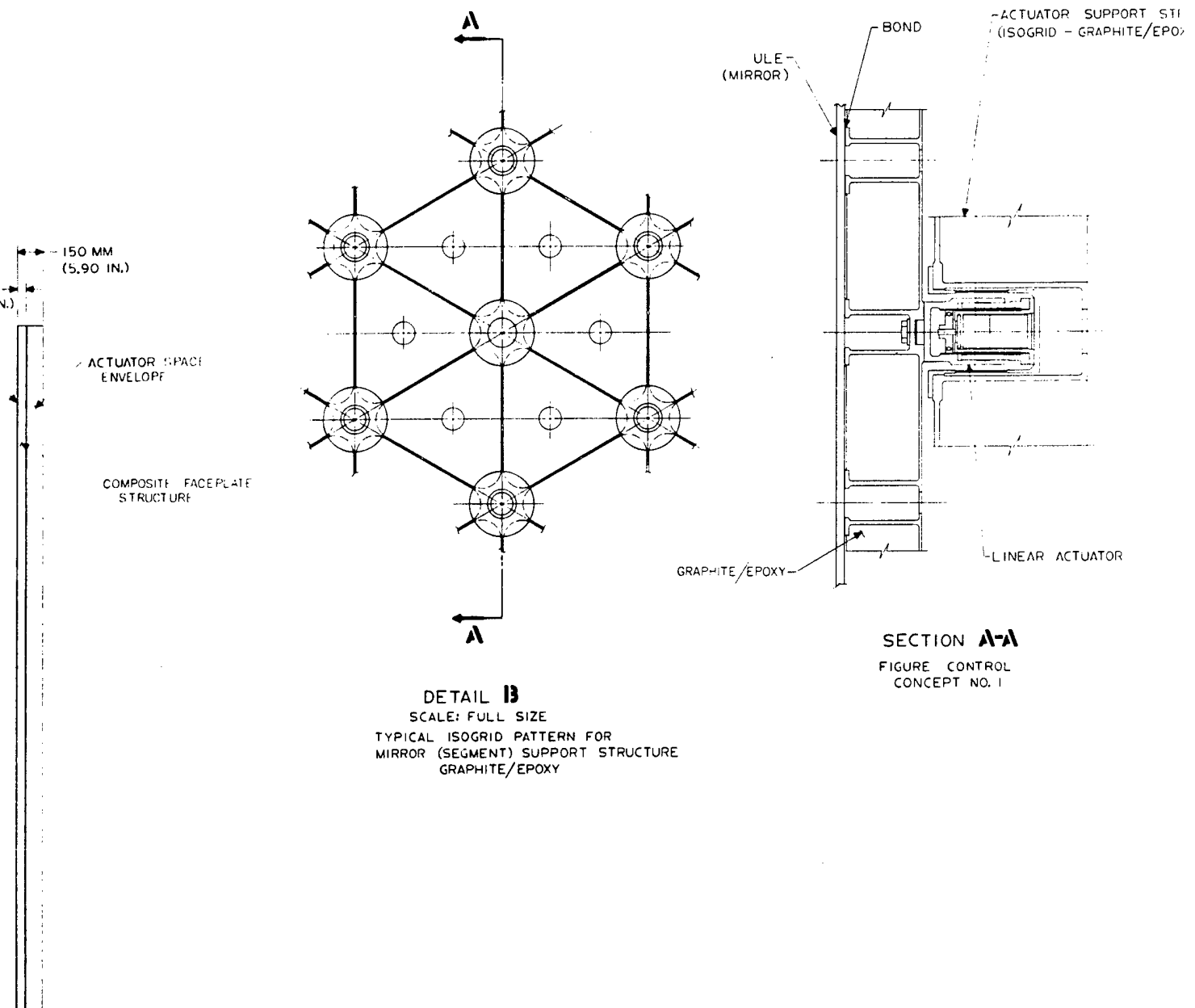
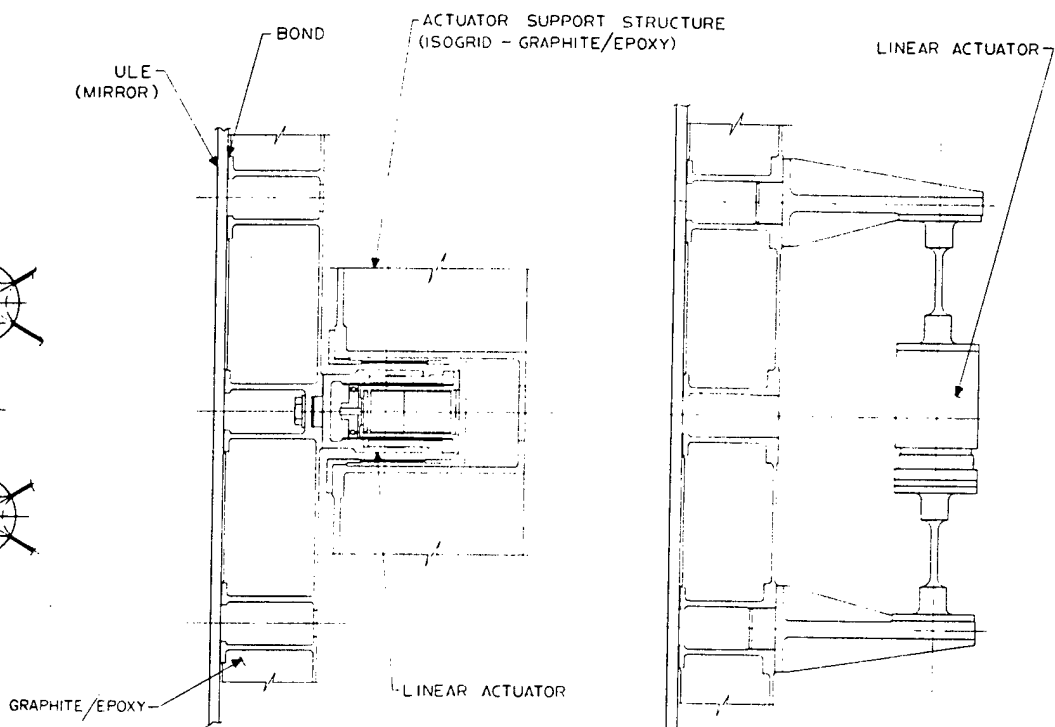
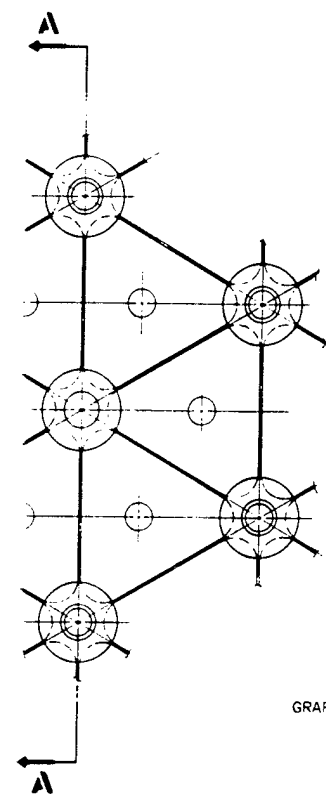
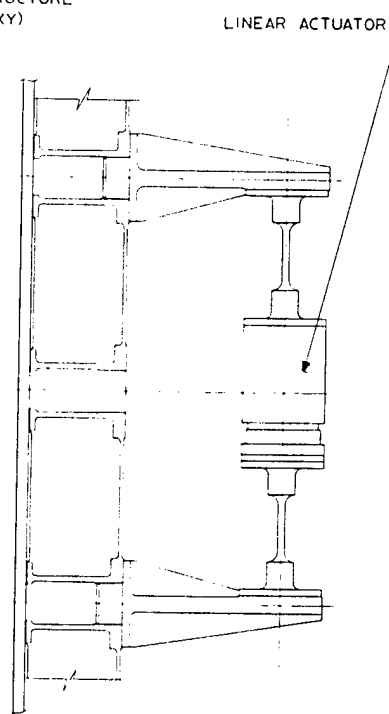


Fig. 36 — 30-meter assembled in space concept (Cont.)



SECTION A-A

FIGURE CONTROL  
CONCEPT NO. 1



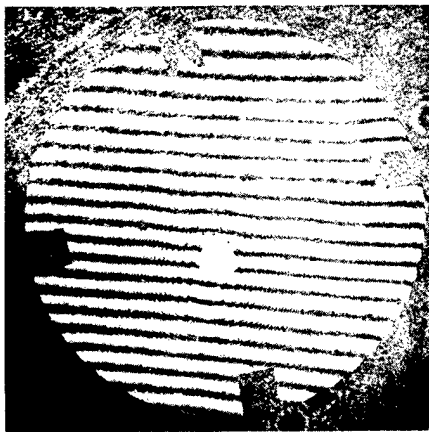
SECTION A-A

FIGURE CONTROL  
CONCEPT NO. 2

TAIL B

FULL SIZE  
ISOGRID PATTERN FOR  
SEGMENT SUPPORT STRUCTURE  
GRAPHITE/EPOXY

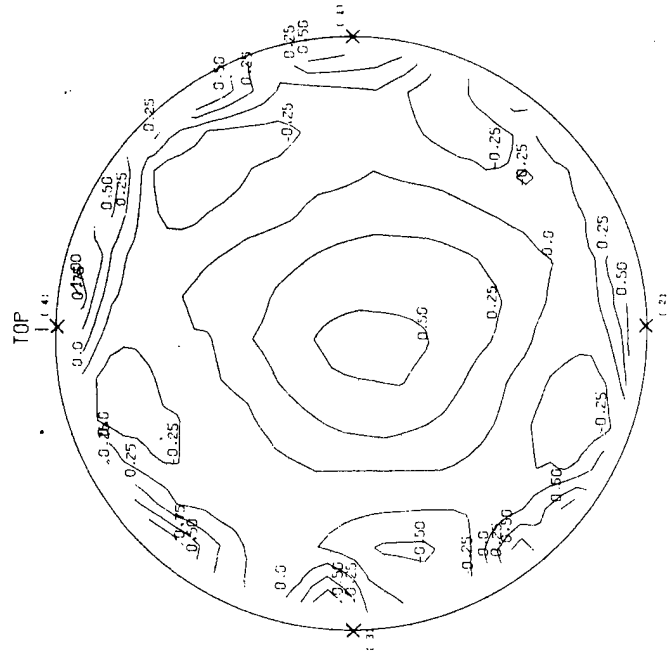
concept (Cont.)



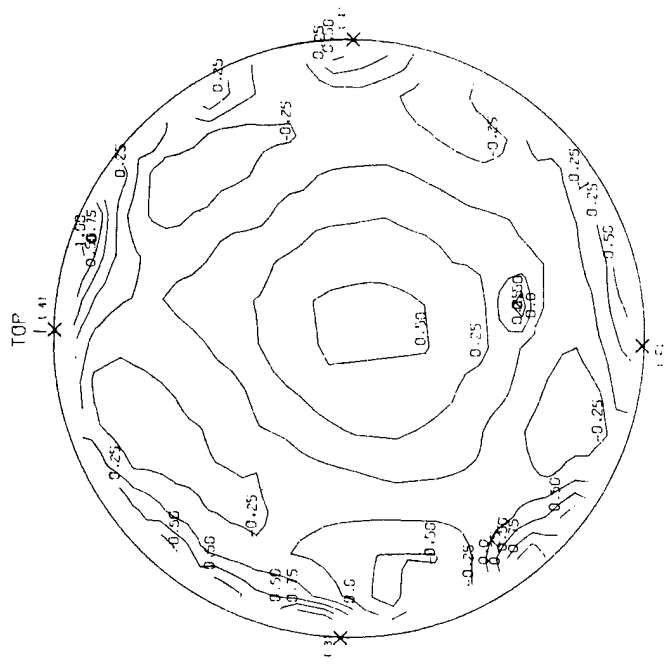
RMS SURFACE ERROR = 0.04λ

Fig. 37 — Surface obtained for graphite-epoxy/ULE sphere

9 Feb. 1973



23 Feb. 1973



1.3 waves astigmatism  
0.31 wave residual rms

2.3 waves astigmatism  
0.32 wave residual rms

$3 \times 10^{-7}$  strain, astigmatic

Fig. 38 — Effect of humidity on composite integral laminated flat

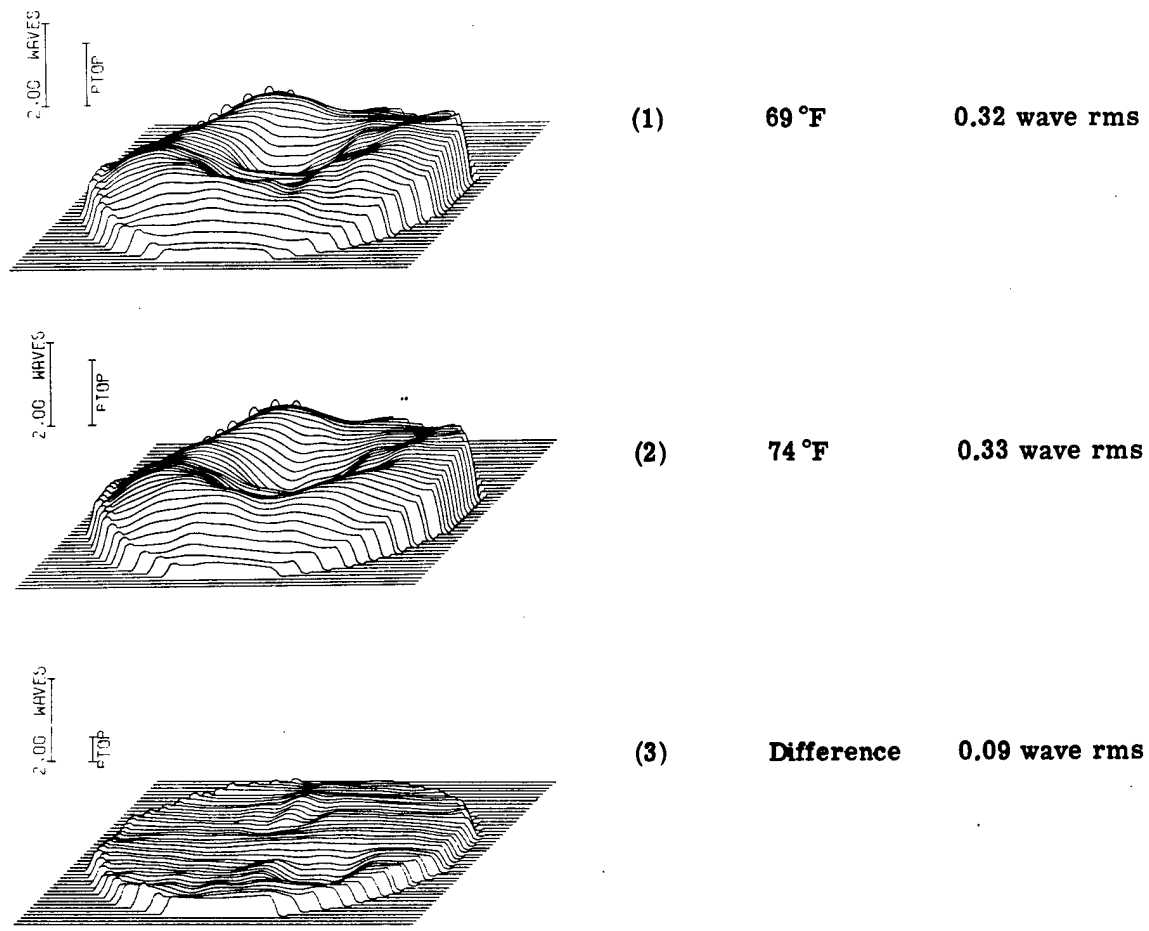
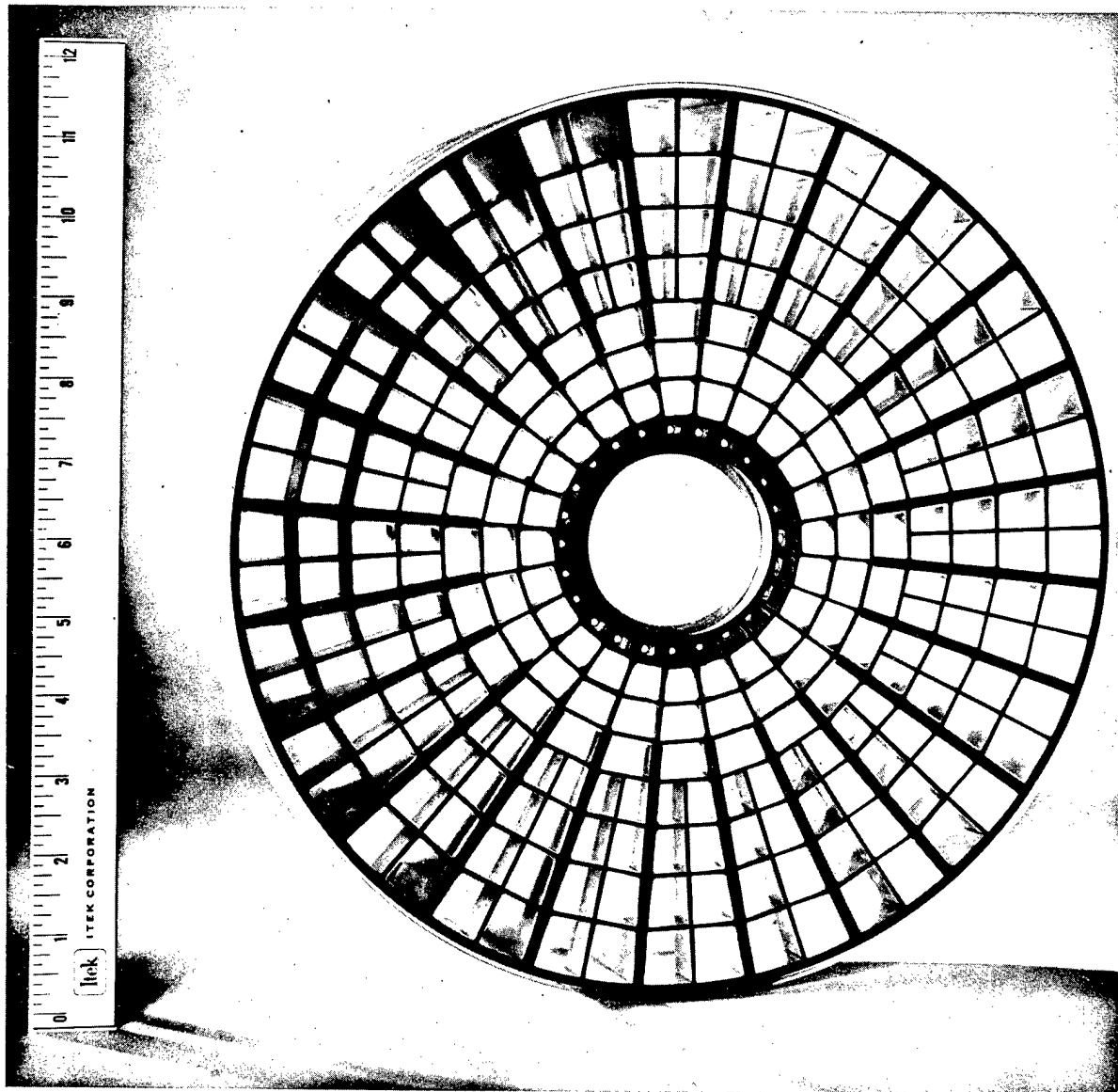


Fig. 39 — Effect of temperature on composite blank



20,454

Fig. 40 — Graphite-epoxy mirror developed under IR&D by Convair Aerospace and Itek Corporation (view looking through ULE faceplate)

Table 7 — Evaluation Matrix, 30-Meter Mirror Concepts

	Inflated	Variable Geometry	Assembled in Space
Diffraction limited performance	1	2	3
Stow packaging	3	1	2
Overall reliability	1	2	3
Ease of maintenance	1	2	3
Weight	3	1	2
Ease of fabrication	2	1	3
Simplicity of design	3	2	1
Development time	2	1	3
Cost	<u>3</u>	<u>1</u>	<u>2</u>
Total Score	19	13	22

Ranking: Good = 3, Fair = 2, Poor = 1

## 7. CONCLUSIONS AND RECOMMENDATIONS

### 7.1 CONCLUSIONS

Feasible concepts for implementing a 30-meter diffraction limited laser transmitter in space are presented. The following conclusions have been made:

1. The assembled-in-space concept, representative of a segmented mirror configuration, appears to be the more practical approach. The major disadvantage of this concept is the requirement for extravehicular activity by astronauts to assemble the mirror structure.
2. Continuous reflecting surfaces can be effected by the inflatable and variable geometry deployment concepts.
3. The inflatable Airmat concept requires additional development, within the existing state-of-the-art technology, to incorporate the use of low thermal expansion materials.
4. The strain properties of the alloy, Nitinol, presents a unique possibility for deploying a variable geometry mirror utilizing a stiff, high Young's modulus, material. Additional understanding of the strain properties of the material is required.
5. Low coefficient of thermal expansion materials should be selected for the mirror structure in order to minimize complexity of the thermal and active figure control systems.
6. Actuator concepts exist, for the active figure control system, which can be developed into space-qualified hardware. The sensing and control logic requirements can be met without new basic technology development.

### 7.2 RECOMMENDATIONS

Based on experience and the results obtained in the present work, the following additional investigations are recommended:

1. Formulation of a detailed thermal/structural math model of one or more of the proposed concepts in order to define the influence functions for simulated operational load. This data would be used to evaluate the range, percentage of correction, and type of actuator required to effect active surface control.
2. Investigate the use of graphite and/or Kevlar fibers in forming the fabric for the Airmat structure; including the selection of scaling, bonding and rigidizing materials to provide an effective low thermal expansion assembly. Fabricate 0.5-meter-diameter Airmat samples to demonstrate deployment, rigidizing, and thermal characteristics.
3. Perform tests on small samples of the Nitinol alloy to qualify the potentials of this material for use in the laser-transmitter. The following questions should be answered:

- a. What are the strain limits for a biaxial strain condition?
- b. What are the edge effects on the strain limits?
- c. How good is the "memory" recovery in terms of the optical requirements?
- d. Can the material be optically polished, can it be coated?

## 8. REFERENCES

1. Yaffee, M. L., Lasers Investigation for Space Propulsion, Av. Week & Space Tech., pp. 47-54 (21 Apr 1975).
2. Space Shuttle System Payload Accommodations, Level II Program Definition and Requirement, JSC 07700, Volume XIV, Rev. C, July 1974.
3. Wetherall, W. B., and Rimmer, M. P., General Analysis of Aplanatic Cassegrain, Gregorian, and Schwarzschild Telescopes, *Appl. Opt.*, 11(12):2817 (Dec 1972).
4. American Institute of Physics Handbook, 3rd ed., Sec. 6, Optics, McGraw-Hill Book Company, Inc., New York, 1972, p. 157.
5. Koller, L., "Ultraviolet Radiation," 2nd ed., Sec. 4, Solar Radiation, John Wiley & Sons, New York, 1965, pp. 107-9.
6. Timoshenko, S., "Theory of Plates and Shells," 2nd ed., McGraw-Hill Book Company, Inc., New York, 1959, p. 249.
7. Large Diameter Active Mirror with Holographic Figure Sensing, Final Report, Optical Sciences Center, University of Arizona, Tucson, Arizona, 85721, SAMSO TR-75-17, Oct 1974.
8. "Expandable Structures Design Handbook," Technical Documentary Report No. RTD-TDR-63-4275 (AD468345), Lockheed-California Company, June 1965.
9. Stenlund, S. J., 3rd Expandable and Modular Structures Conference, Pageos Fabrication Accuracy and Reliability, AFAPL-TR-68-17 (AD668181), Apr 1968, p. 181.
10. McKillip, W., et al., 3rd Aerospace Expandable and Modular Structures Conference, Gas-Cured Urethane Resin Systems for Space Structures, AFAPL-TR-68-17 (AD668181), Apr 1968, p. 89.
11. Randolph, R. E., and Sullivan, M.R., Curved, Tapered, Circular Cross Section Graphite/Epoxy Antenna Ribs, Report received from: Harris Corporation, Electronic Systems Division, Melbourne, Florida.
12. Jurich, L., and Hose, R. L., Applications Study of Expandable Space Structures, AFAPL-TR-70-45 (AD879707), Nov 1970.
13. Wagner, H. J., and Jackson, C. M., What You Can Do With That 'Memory' Allow, *Mat. Eng.*, pp. 28-31 (Oct 1969).
14. Harris, J. T., 3rd Aerospace Expandable and Modular Structures Conference, Development of Compound Curvature Airmat, AFAPL-TR-68-17 (AD668181), p. 105, Apr 1968.
15. Forbes, F. W., Expandable Structures for Space Applications, AF Aero Propulsion Laboratory, AD607541 (July 1964).
16. Rochon, R., et al., Aerospace Expandable Structures and Maintenance Support Devices, AFAPL-TR-65-40 (AD471333), Vol. I, July 1965.
17. Russell, I. W., and Hansen, N. S., The Application of a Gelatin Resin System to Aerospace Expandable Sandwich Structures, AFAPL-TR-65-84 (AD476133), Oct 1965.
18. Schwartz, S., Jones, R., and Keller, L., Ultraviolet and Heat Rigidization of Inflatable Space Structures, Air Force Expandable Structures Conference, Oct 1963.

19. McKillip, W. J., et al., Vapor Rigidized Expandable Solar Collectors and Aerospace Cylinders, AFAPL-TR-66-149 (AD819174), May 1967.
20. Swanson, P., Solar Reflector Foaming Technology Development, AFAPL-TR-64-128 (AD609223), Dec 1964.
21. Southerian, R. E., Space Environment Effects on Expandable Structures Materials, ARO, Inc., AEDC-TR-67-57 (AD811678), Apr 1967.
22. Expandable Truss Antenna Growth Characteristics, General Dynamics, Convair Aerospace Division, GDC DCL-69-001, Mar 1969.
23. Golden, L. J., Dynamic Hartmann Test, *Appl. Opt.*, 14(10):2391 (Oct 1975).
24. Peters, W. N., Arnold, R. A., and Gowrinathan, S., Stellar Interferometer for Figure Sensing of Orbiting Astronomical Telescope, *Appl. Opt.*, 13(8):1785 (Aug 1974).

Appendix  
REAL-TIME, LATERAL-SHEARING INTERFEROMETER

### 1. PRINCIPLE OF SHEARING INTERFEROMETRY

Interferograms are always produced by combining two coherent wavefronts. In regions over which the two waves are in phase, a bright area appears; where the two waves are 1/2 wavelength out of phase, they tend to cancel, and this destructive interference results in a dark area. The resulting pattern, an interferogram, then has dark and light bands alternating as the difference between the two wavefronts changes by 1/2 wavelength. It is a contour map with the bright lines a contour interval of 1 wavelength of light.

If a coherent source of light such as a laser is available, then an interferometer can be made in which one of the wavefronts is a reference wave of known plane or spherical shape. The other wavefront is obtained by passing light through the lens or optical system being tested. The two wavefronts are combined, and the result is a map of the system wavefront errors relative to a known plane or spherical wave.

If a laser is not available, shearing interferometry can be used, and a wavefront is interfered with itself. A traditional form of shearing interferometry is illustrated in Fig. 41. Light from a distant point source enters the optical system to be tested and is focused to an image. Here a field lens is placed; the field lens projects an image of the system entrance pupil onto the interference plane. In a telescope, the entrance pupil is usually the primary mirror. Between the field lens and the interference plane we may place beam splitters and mirrors which result in two images of the pupil being formed.\* One of the mirrors is then tilted slightly so that the two images are not coincident but rather are separated, or sheared as it is called, by a small amount. Interference is then obtained between these two sheared wavefronts. The interferogram is then a contour map of a surface which is the difference between the wavefront at pairs of points separated by the shear distance,  $L$ . Thus if  $Z(x, y)$  describes the incident wavefront, then the shearing interferogram maps out a surface given by

$$\Delta Z(x, y) = Z(x, y) - Z(x - L, y)$$

assuming that the shear is in the  $x$  direction. It is instructive to consider what happens for simple forms of  $Z(x, y)$  as indicated in Table 8.

---

\* Those familiar with interferometers will recognize this as a Mach-Zehnder interferometer. This configuration for a shearing interferometer was originally discussed by Bates, Proc. Phys. Soc., 59:940 (1947), and is also shown in "Principles of Optics" by Born and Wolf, Macmillan, 1959, p. 314.

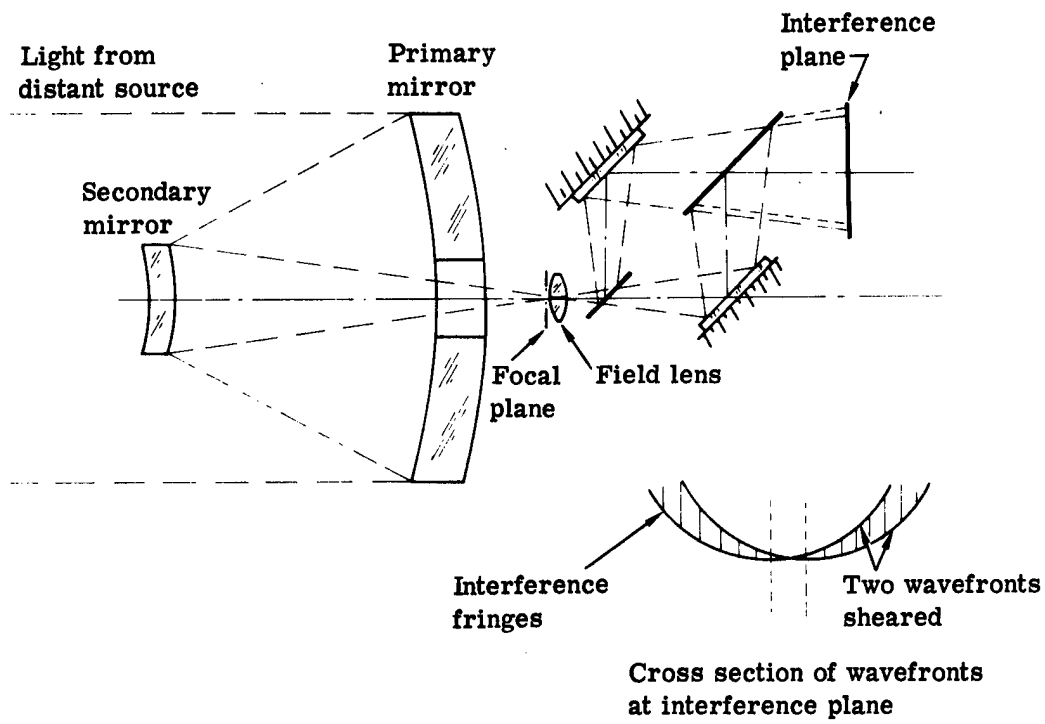


Fig. 41 — Lateral shearing interferometer

Table 8 — Fringe Patterns for Simple Forms of  $Z(x, y)$  in Lateral Shear

Equation for Surface $Z(x, y)$	Type of Aberration	$\Delta Z(x, y)$	Fringe Pattern
$Z(x, y) = \text{constant}$	Phase error	0	No fringes
$Z(x, y) = Kx$	Tip	$KL$	No fringes
$Z(x, y) = K(x^2 + y^2)$	Defocus	$2KxL - KL^2$	Uniformly spaced
$Z(x, y) = Kx^2$	Astigmatism	$2KxL - KL^2$	straight lines

## 2. INTERFEROGRAM MEASUREMENT

The major problem with interferometry is often one of measuring the interferogram to determine the fringe locations. This is commonly done by scanning an interferogram after recording on a photograph. Real-time scanning from a TV display can be used; but scanning to find locations is not easily done, particularly near the edge of the aperture. It has been found, however, that a process similar to scanning can be achieved by allowing the star image to move across the focal plane.

The first point to be seen is that with the configuration of Fig. 1, an interference pattern is obtained regardless of where in the focal plane the point source is imaged, so long as it is within the limits of the field lens.

Second, if the source is off axis, this results in a wavefront "tip." Referring to Table 1, we have  $Z(x, y) = Z_0(x, y) + \theta x$ , where  $\theta$  is the tip angle and  $Z_0(x, y)$  is the wavefront coming through the system when the source is on axis. Then the interferogram represents the surface

$$\Delta Z(x, y) = Z_0(x, y) - Z_0(x - L, y) + \theta L = \Delta Z_0(x, y) + \theta L$$

If  $\theta$  is changing with time at the rate  $\dot{\theta} = d\theta/dt$ , and if over a measurement period  $Z_0(x, y)$  is constant, then

$$\Delta Z(x, y) = \Delta Z_0(x, y) + \dot{\theta} L t$$

which shows that each point in the interferogram is modulated with a period  $t_0 = \lambda/\dot{\theta} L$ , where  $\lambda$  is the wavelength of light being used. The measured surface  $\Delta Z_0(x, y)$  will then be observed directly as phase variations on the modulated signal. Phase measurements can then be made fairly easily with an rms error of less than 0.01 wavelength.

An additional fact should be noted. Table 1 shows that astigmatism in the direction of shear is not identifiable, since it gives the same result as defocus. The addition of a second interferometer with shear in the  $y$  direction will remove this indeterminacy. It is necessary, of course, that the position of the two interferometers remain fixed so that the defocus term is identical for both.

The interferometer can be designed as a compact package; care must be taken in design so that the spatial relationship between the two parts is maintained. As proposed for use with a large telescope, the interferometer would be oriented so that star motion is at approximately 45 degrees to the shear directions.

## 3. GRATING-SHEARING INTERFEROMETER

Although the Mach-Zehnder configuration shown above produces a sheared-wavefront interference pattern, the same effect can be achieved much more simply by the use of diffraction gratings. The basic principles of the interferometer can be seen in Fig. 42. Two diffraction gratings having slightly different line spacings are placed near the focal plane of the telescope. For any given wavelength of light, this produces two diffracted cones of rays at two slightly different angles. The diffraction angle is chosen large enough to keep the zero-order undiffracted rays separate. The amount of shear is determined by the angular difference between the two diffracted beams. Interference takes place in the region of overlap of the two beams. It can be shown that each point in the pattern represents the wavefront difference between two points in the incident wavefront separated by the shear distance. It can also be shown that astigmatism cannot be measured with a single fixed shearing pattern. Thus, we use two sets of gratings, at right angles to each other, producing interference patterns sheared at right angles.

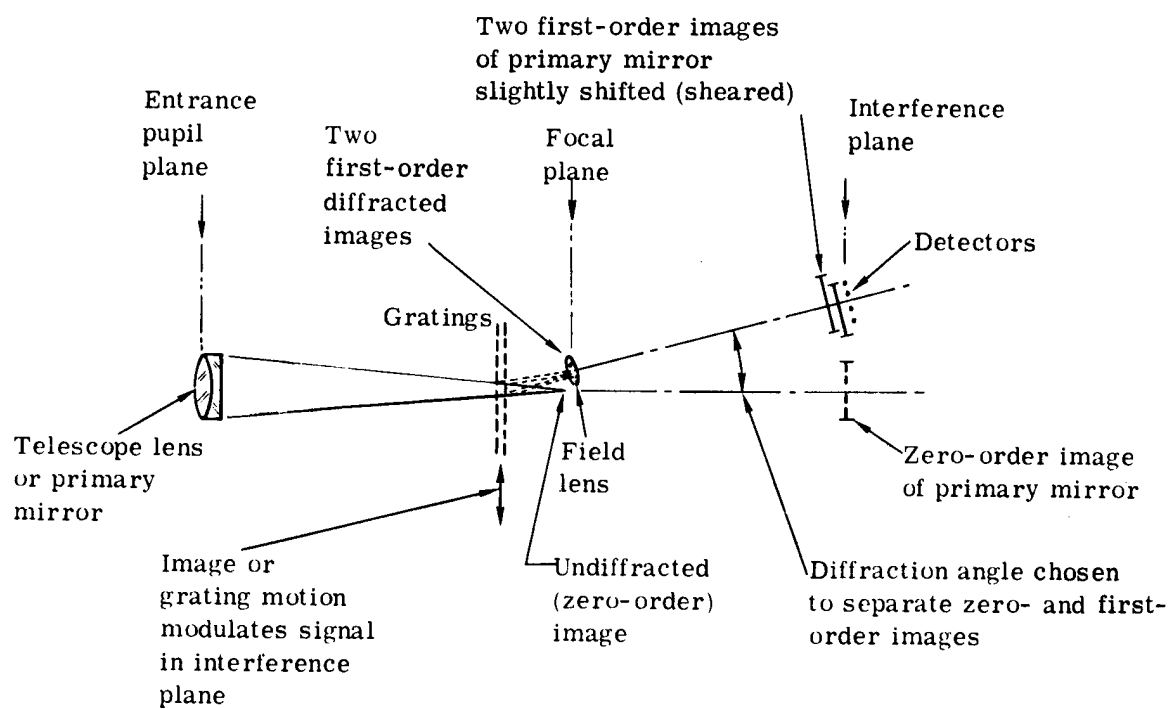


Fig. 42 — Lateral shearing grating interferometer

In our existing interferometer we use two grating plates, each containing two sets of holographically recorded fringes at right angles. The two grating plates have line spacings of about 310 and 330 lines per millimeter, giving a shear equal to about one-seventh of the pupil diameter. This is designed to be consistent with the spacing of measured points, as described below.

#### 4. MODULATOR

It is shown in Section 1 that the interference pattern will be modulated if there is relative motion between the image and the grating. If the image moves across the field of view, this is equivalent to a tilting wavefront, which produces a constantly changing optical path difference at any point in a shearing interference pattern. The constantly changing optical path implies that the pattern is modulated. If some defocus is introduced so that the sheared patterns show a series of straight, parallel fringes, then tilting the wavefront causes the fringes to move across the interference plane. Modulation will occur, however, even if there is no defocus and thus no fringes are seen. The entire pattern will then alternate between light and dark.

When the image is stationary but the grating is moving, the reason for the modulation is difficult to understand intuitively. It can best be seen by noting that a moving grating causes a Doppler shift in the diffracted light, just as scattered light from a moving target is shifted.\* The frequency change is

$$f = v/a$$

where  $v$  is the velocity of the grating and  $a$  is the line spacing of the grating. We use  $1/a$  about 310 lines per millimeter and generate a 3 kHz modulation by a constant velocity of about 10 millimeters per second normal to the grating lines.

The modulator drive we have built is shown in Fig. 43. The loudspeaker-type electromagnetic drive provides a motion of  $\pm 1$  millimeter, limited by the diaphragms, which provide a flexure support for the shaft. The grating is moved at 14 millimeters per second at 45 degrees to the two grating axes. This gives a modulation rate of 3 kHz. We have measured departure of the motion from a straight line to be less than 2 micrometers. This will cause less than 1/600 wavelength peak-to-peak focus error.

In operation, the grating is driven so as to obtain a single excursion at a constant velocity over as much of its range as possible. Tests have shown that a constant modulation frequency is obtained over about 50 milliseconds, giving about 150 uniformly modulated cycles in the interference plane. All phase measurements are made in parallel, using from 1 to 100 modulation cycles, depending on the amount of averaging desired. The measurement could be repeated at least 10 times per second if needed, but a single drive of the grating provides a complete wavefront measurement.

#### 5. PHASE MEASUREMENT

The technique for phase measurement in the existing interferometer is shown in Fig. 44. In this case an array of 28 detectors is used in each of the two interference patterns with one being selected as the reference channel. After appropriate filtering, zero-crossing detectors are used for each channel and only positive-going zero crossings result in pulses. The zero crossing of the reference then turns on a gate for each channel; the zero crossing in each other channel then turns off the gate. The "on" time is measured by counting clock pulses coming at a rate of 100 per cycle.

---

\*This is described by W. H. Stevenson in Optical Frequency Shifting by Means of Rotating Diffraction Grating, *Appl. Opt.*, 9:649 (Mar 1970).

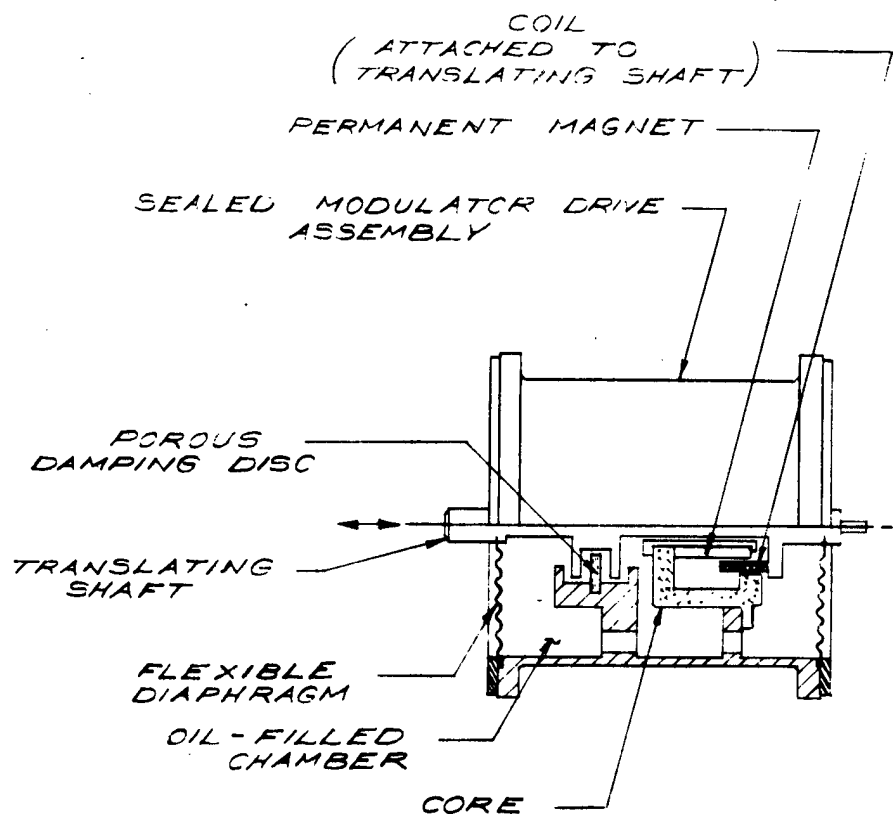


Fig. 43 — Modulator drive

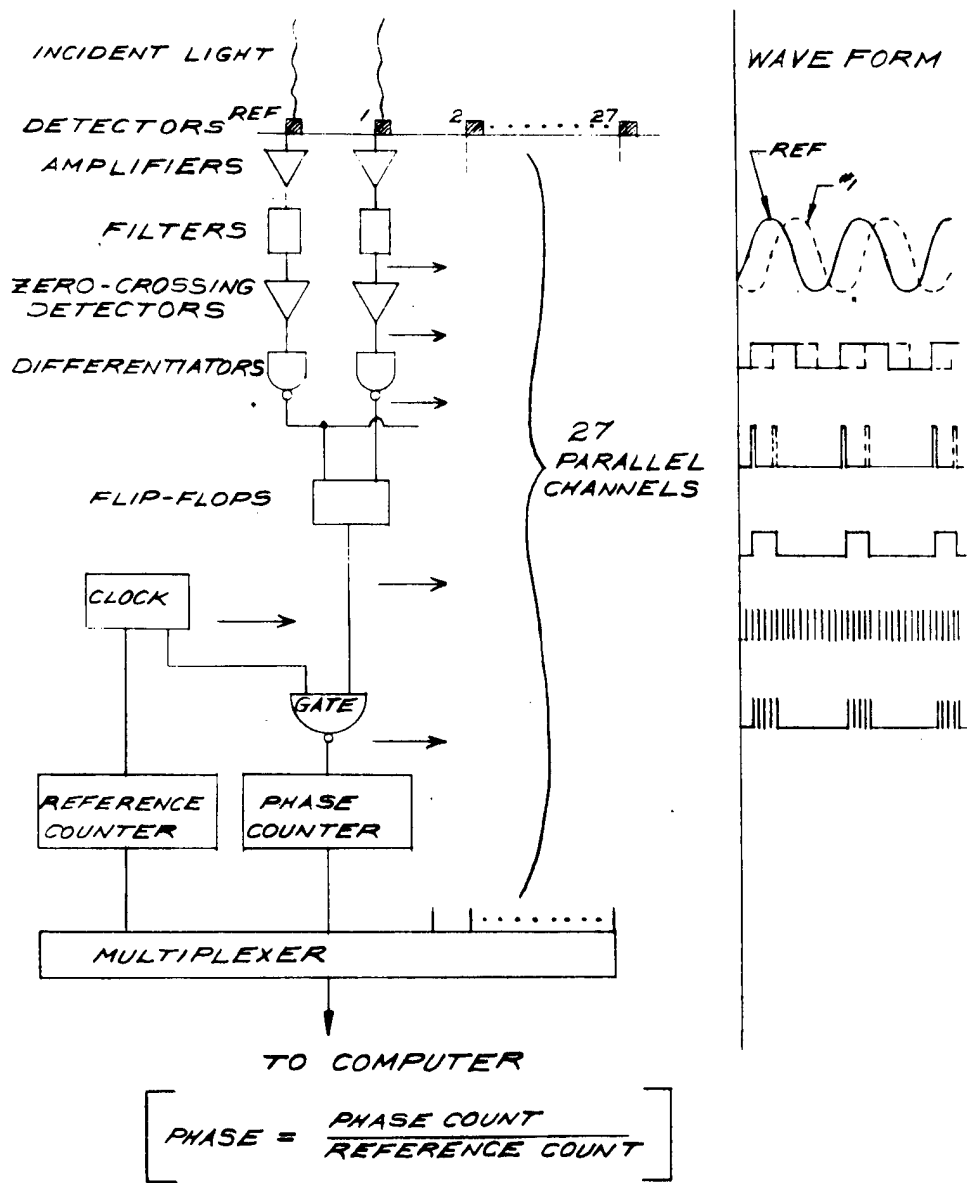


Fig. 44 — Electronics and control system block diagram

The phase error in each channel is then the number of counted pulses divided by the total number as measured by the always-on reference counter. With this technique, a digital phase value convenient for interfacing with the computer is obtained directly.

Other interferometers have also been built for use with a real-time atmospheric correction system. In this case, a substantial improvement has been made by using an oscillator in a phase-locked loop to replace the simple zero-crossing detector. This has the advantage that a brief noise pulse or dropout of signal does not introduce a large count error, and is particularly ideal when rapid phase measurements are to be made. The phase detector is also completely independent of signal amplitude so long as the signal-to-noise ratio is adequate.

The 56 measured phase values, stored in 56 separate counters in the phase detecting electronics, are then multiplexed for serial transmission to a small computer used for data analysis.

## 6. DATA ANALYSIS

The object of the data analysis is to convert the phase measurements made in the shearing interference patterns into incident wavefront information, and then to analyze the wavefront in terms of conveniently descriptive quantities such as rms error and optical aberration coefficients.

Phase values are determined in the interference plane. These represent the optical path difference between points on the wavefront and other points on the same wavefront separated by the shear distance. Each measurement is then a wavefront difference. The problem is to derive the incident wavefront shape from the measurements of wavefront difference from point to point.

For the simplest approach to data reduction, the detectors are separated by a space equal to the shear distance. This is illustrated in Fig. 45. The mirror is shown with a grid representing a shear distance of 1/7 of the mirror diameter. The grid intersections represent points at which the wavefront is to be evaluated. This results in a set of 36 evaluated points. A smaller shear value would give a finer grid and thus a greater number of points; a larger shear would give fewer points. Both x-shear and y-shear patterns are used. Each measurement in the interferometer gives a difference in wavefront between two points separated by the shear distance. Thus the measurements are represented by arrows connecting adjacent points. It is not necessary to make all connections, but each point to be determined must have at least one connection. For the 36-point grid, as shown, there are a total of 56 possible connections. (The interferometer was constructed with the center point not used, simulating operation with a Cassegrain telescope having a central obscuration.)

### 6.1 Least-Squares Solution

The use of shearing interferometry for precision measurement is made possible by proper analysis of the data. It is shown here that the resulting data are at least as accurate as those obtained by a conventional Twyman-Green type of interferometer. In fact, the common path characteristic of the shearing interferometer will permit more accurate use in real environments by decreasing the sensitivity of the instrument to ambient vibrations.

Given the grid and the measured shear values, the wavefront values are reconstructed by a least squares minimization approach. In this approach we find a value for each of the points on the reconstructed wavefront. Let  $W_{i,j}$  describe the points on the wavefront, where  $i$  and  $j$  are the row and column number of the wavefront points. The measured values will then correspond to  $W_{i,j} - W_{i+1,j}$  and other combinations where  $i$  or  $j$  differ by 1. It is then possible to write all the shear measurements (56 in this case) in terms of the 36 values of  $W_{i,j}$ . The equations, of course, are linear, so that a least squares solution can be written for the  $W_{i,j}$  values. The analysis operates so as to minimize the mean square error between the shear measurements and the values that would be calculated by the differences between adjacent  $W_{i,j}$  values. The effects of measurement

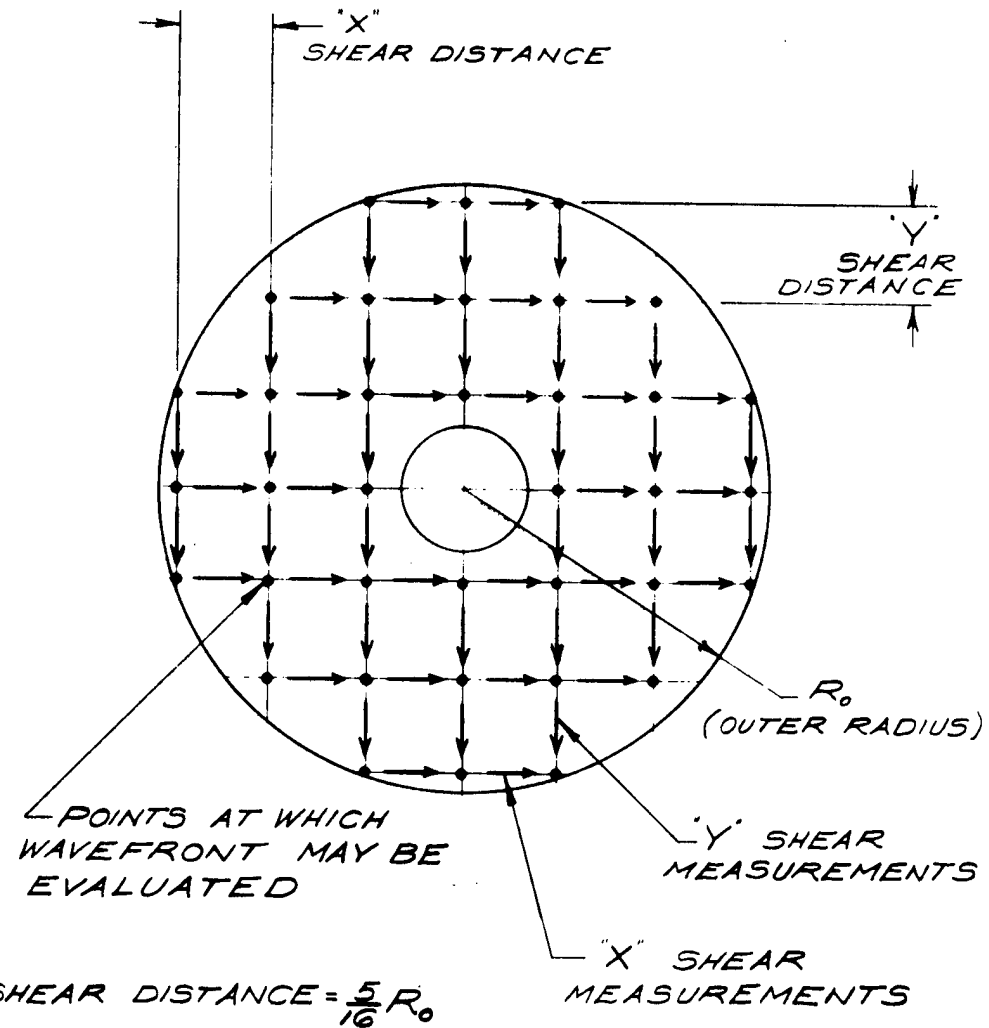


Fig. 45 — Shearing interferometer measuring grid (36 points, 56 measurements)

error have been examined using an analysis as illustrated in Fig. 46. Assuming an input surface, random errors are introduced to give simulated real measured data. The wavefront is then reconstructed as it would be in the signal processing section of the real interferometer, using the analysis technique described above. The reconstructed surface is then evaluated in terms of its rms error from the original input surface. Since the entire analysis is linear, up to the computing of the rms error, the error propagation effects can be seen by considering a perfect input surface and determining the rms error of the output surface.

One thousand sets of random data were taken, and the results were evaluated. The results are very favorable. One case considered was the 36-point grid shown, using 56 measured shear values. For an rms measurement error of 0.01 wavelength for each measured shear value, the resulting rms surface error will be less than 0.008 wavelength for 90 percent of the measurements. In 1,000 simulated random surface measurements, the maximum rms surface error was only 0.01 wavelength. The significance of this is that errors are not cumulative as in usual procedures for analyzing shearing interferograms.

Other grids were investigated with comparable results, as shown in Table 9, for different values of shear. The shear is expressed as a fraction of a unit radius. The table gives the resulting rms surface error determined in the 1,000 random error runs for each case. The first column gives the rms surface error that includes 90 percent of the runs; the second column indicates the worst case rms value.

Wavefront values are easily calculated in a small computer. Although the least squares solution requires a matrix inversion, this need be done only once, in a separate computer, and the inverted matrix stored in the small computer to be used. The data analysis operation then consists basically of multiplying the 56-value vector of measured data by a 56 by 36 stored matrix to give the 36 wavefront values. For our original interferometer, we performed all analyses and control within the limits of a 4K, 16-bit word memory.

## 6.2 Solving for Polynomial Coefficients

When the shear equals the sample spacing, the data analysis is exact—i.e., no interpolation or other assumptions are required. As the shear is reduced, some form of interpolation is necessary. In the simplest form, the measured values could be scaled up by the ratio of sample spacing-to-shear distance (linear interpolation). Other interpolations could also be made. However, a more useful approach is to use a polynomial fit to the data.

The most useful polynomials for analysis of optical data are usually the circle polynomials of Zernike. These are orthonormal over a unit circle and can easily be orthonormalized for use over a discrete set of points. Any set of orthonormal functions could be used, but we have found no advantage in departing from the Zernike polynomials. The 36 polynomials through the seventh power of the radius are given in Table 10.

The important aspect of solving for a wavefront or of fitting orthonormal polynomials to measured data is that all effects are linear and independent. As a result, it can be shown that if there are M measured points and N polynomial terms or wavefront points to be determined, it is necessary only to multiply the vector of M values by a previously generated M by N matrix, stored in the analysis computer, to determine the N values. Only one matrix multiplication is needed for any output. By storing several matrices on tape, any desired output may be obtained upon command. We can express the procedure as:

$$[W] \times [P] = [F]$$

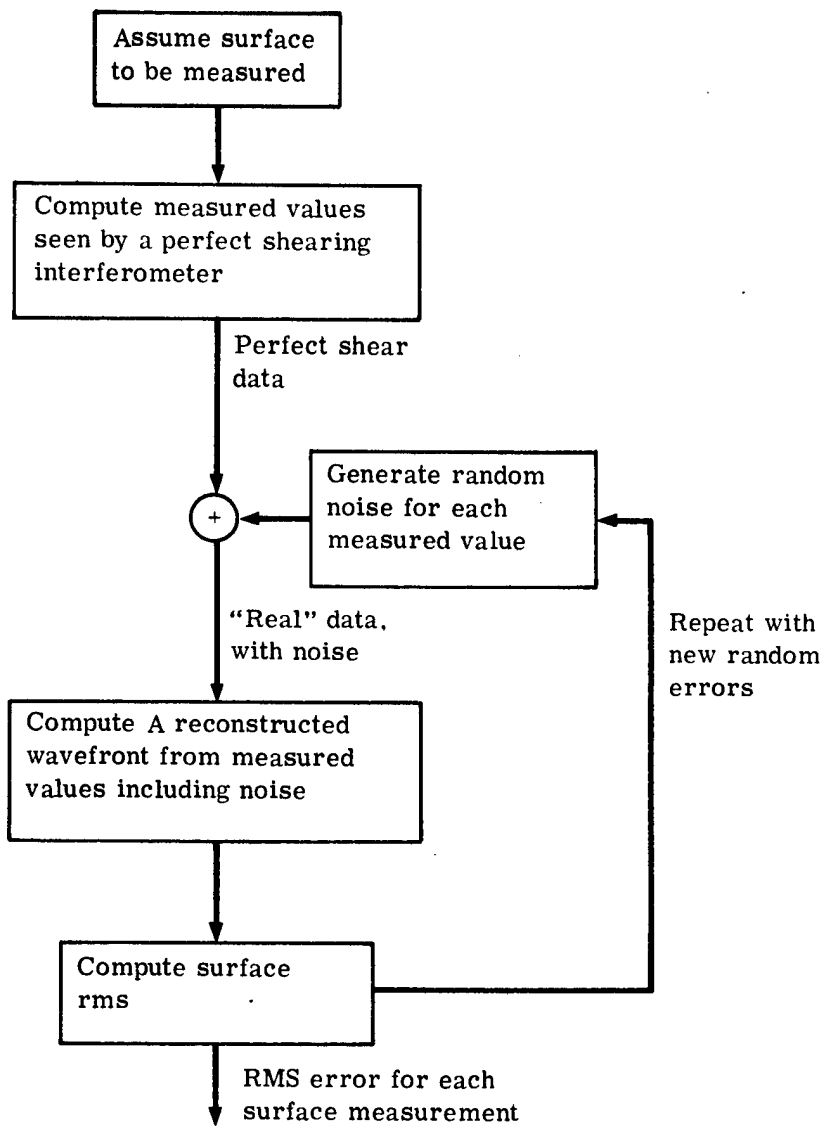


Fig. 46 — Procedure for determining effects of measurement error

Table 9 — Reconstructed Wavefront Errors for 0.01 Wavelength RMS Shear Measurement Error

Shear	Number of Wavefront Points Determined	Number of Shear Values Measured	Reconstructed Wave 90% RMS Error	Peak RMS Error in 1,000 Runs
0.375	20	28	0.008	0.011
0.375	24	36	0.008	0.012
0.3125	36	56	0.008	0.010
0.300	37	60	0.008	0.010
0.250	48	76	0.008	0.011

Table 10 — Zernike Circle Polynomials (through order 7)

Equation, $z =$	Name of Equivalent Optical Aberration
1	Phase
$\rho \cos \theta$	Tip
$\rho \sin \theta$	Tilt
$2\rho^2 - 1$	Defocus
$\rho^2 \cos 2\theta$	Astigmatism, axes at 0, 90 degrees
$\rho^2 \sin 2\theta$	Astigmatism, axes at 45, 135 degrees
$(3\rho^3 - 2\rho) \cos \theta$	Coma, axis at 0 degree
$(3\rho^3 - 2\rho) \sin \theta$	Coma, axis at 90 degrees
$\rho^3 \cos 3\theta$	
$\rho^3 \sin 3\theta$	
$6\rho^4 - 6\rho^2 + 1$	Spherical aberration
$(4\rho^4 - 3\rho^2) \begin{Bmatrix} \cos 2\theta \\ \sin 2\theta \end{Bmatrix}$	
$\rho^4 \begin{Bmatrix} \cos 4\theta \\ \sin 4\theta \end{Bmatrix}$	
$(10\rho^5 - 12\rho^3 + 3\rho) \begin{Bmatrix} \cos \theta \\ \sin \theta \end{Bmatrix}$	
$(5\rho^5 - 4\rho^3) \begin{Bmatrix} \cos 3\theta \\ \sin 3\theta \end{Bmatrix}$	
$\rho^5 \begin{Bmatrix} \cos 5\theta \\ \sin 5\theta \end{Bmatrix}$	
$20\rho^6 - 30\rho^4 + 12\rho^2 - 1$	
$(15\rho^6 - 20\rho^4 + 6\rho^2) \begin{Bmatrix} \cos 2\theta \\ \sin 2\theta \end{Bmatrix}$	
$(6\rho^6 - 5\rho^4) \begin{Bmatrix} \cos 4\theta \\ \sin 4\theta \end{Bmatrix}$	
$\rho^6 \begin{Bmatrix} \cos 6\theta \\ \sin 6\theta \end{Bmatrix}$	
$(35\rho^7 - 60\rho^5 + 30\rho^3 - 4\rho) \begin{Bmatrix} \cos \theta \\ \sin \theta \end{Bmatrix}$	
$(21\rho^7 - 30\rho^5 + 10\rho^3) \begin{Bmatrix} \cos 3\theta \\ \sin 3\theta \end{Bmatrix}$	
$(7\rho^7 - 6\rho^5) \begin{Bmatrix} \cos 5\theta \\ \sin 5\theta \end{Bmatrix}$	
$\rho^7 \begin{Bmatrix} \cos 7\theta \\ \sin 7\theta \end{Bmatrix}$	

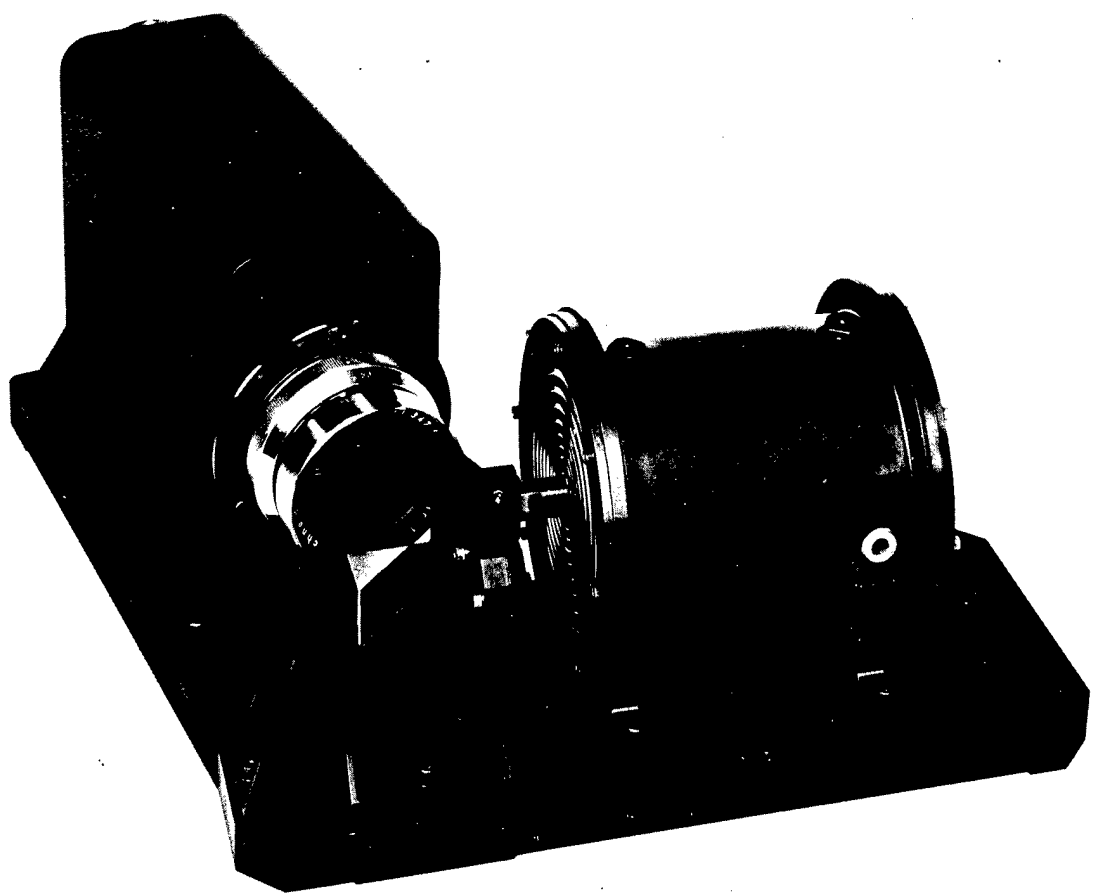
where  $[W]$  is the vector of  $N$  phase measurements made by the interferometer,  $[P]$  is a stored  $N \times M$  matrix, and  $[F]$  is the output vector of  $M$  actuator commands.  $[P]$  is generated in advance by knowing the measurement points and the nature of the actuator influence functions. Simply by changing the  $[P]$  matrix, the output can be actuator forces, values of the wavefront at a given number of points, or polynomial coefficients describing the wavefront. Changing actuator locations or compensating for a "dead" actuator or wavefront sensing point can be accommodated simply by changing the stored matrix,  $[P]$ . It is easily seen that this is ideally suited to the use of digital computation, particularly since the wavefront sensor produces a direct digital output without need for analog to digital conversion.

## 7. TEST RESULTS

The principles of the phase-modulated, diffraction-grating, wavefront-shearing interferometer have been successfully demonstrated in a unit now being used at Itek. A photograph of the device is shown in Fig. 47. A diagram of the interferometer assembly is shown in Fig. 48. The device has been used with an external He-Ne laser source, and also with a self-contained Gallium Arsenide laser diode source shown on the drawing.

Preliminary tests showed that the device operated very well. Results of a through-focus test are shown in Fig. 49. In this case the computer provided values for the number of waves of defocus and for the two components of astigmatism (given by the polynomial terms  $\rho^2 \cos 2\theta$  and  $\rho^2 \sin 2\theta$ ). The amount of defocus is plotted against axial position of the test lens. As predicted for small errors, the result was a straight line, the data falling within 0.01 wave of the line, even in the presence of substantial astigmatism. The astigmatism value was constant through the test, as predicted. In order to determine the rms measurement error for individual points in the wavefront, the defocus and astigmatism were subtracted from the measured wavefront values and the residual measured wavefront error was plotted in an oblique projection in Fig. 50. Here the vertical bar represents 1/10 wave; the rms values of the 35 measured points was less than 1/50 wave. Repeating this at the three center defocus positions gave an rms scatter between measurements also less than 1/50 wave.

This test did not give a measure of the absolute accuracy of the interferometer. It does indicate, however, that any instrumental errors will be small and can at least be removed by calibration. The interferometer has now been modified from the version shown in Fig. 47 to include a laser and provisions for alignment to make it more useful as a laboratory instrument; further tests will be undertaken. In addition, analysis shows that a different version, in which all four gratings are holographically produced on the same surface, will provide a perfect null instrument—that is, systematic instrument errors will tend toward zero as the wavefront being measured approaches a perfect spherical wavefront.



19,661

Fig. 47 — Diffraction grating shearing interferometer

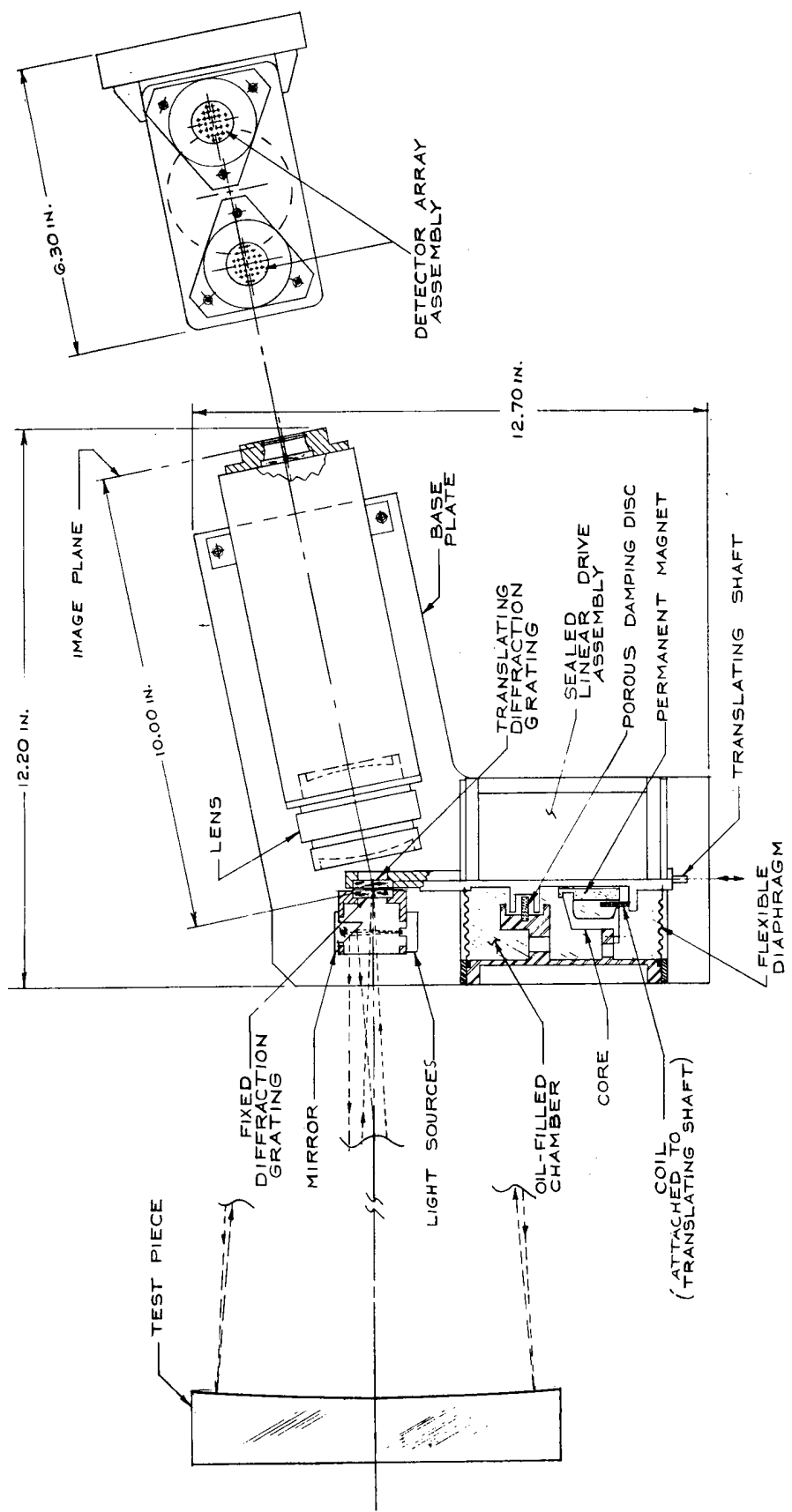


Fig. 48 — Interferometer assembly

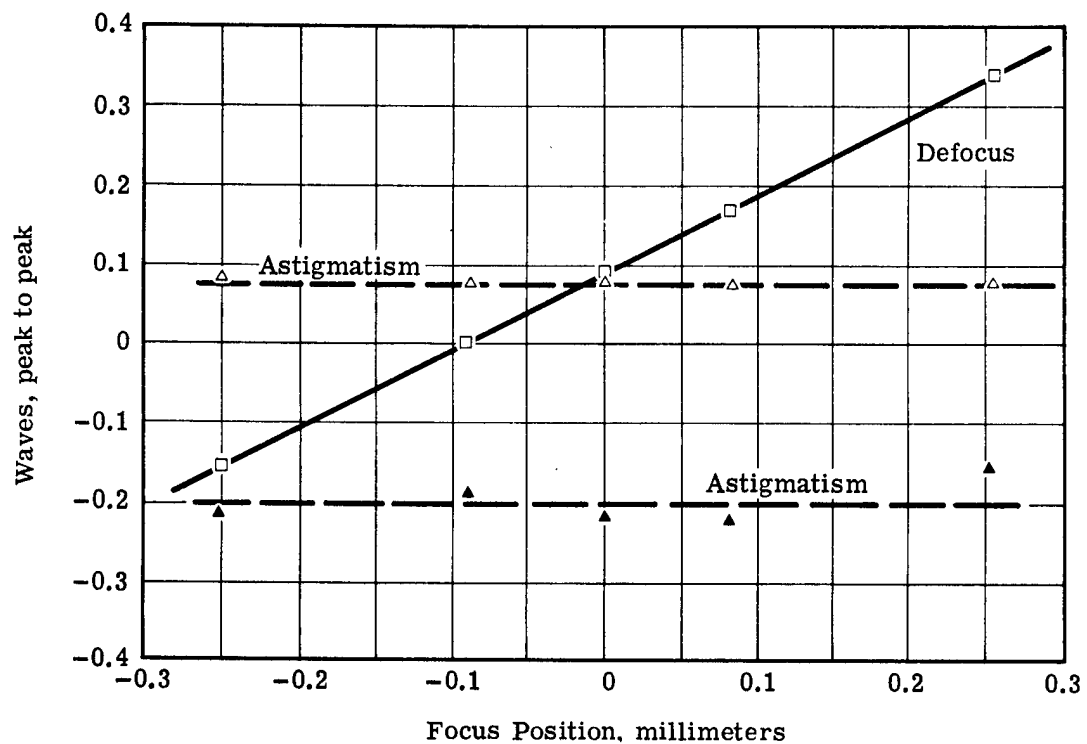


Fig. 49 — Test results for grating shearing interferometer

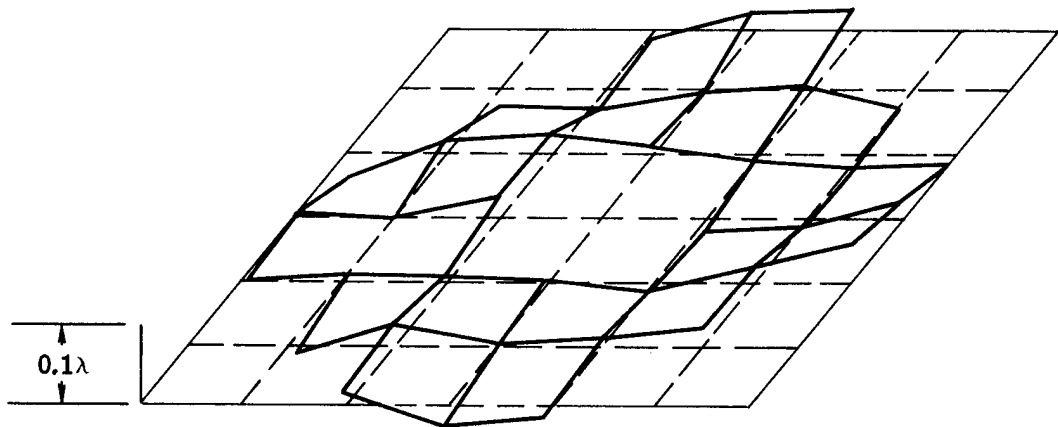


Fig. 50 — Oblique projection of measured wavefront values

1. Report No. NASA CR-134903	2. Government Accession No.	3. Recipient's Catalog No.	
4. Title and Subtitle  Feasibility of a 30-Meter Space Based Laser Transmitter		5. Report Date October 1975	6. Performing Organization Code
7. Author(s)  R. R. Berggren and G. E. Lenertz		8. Performing Organization Report No. 8254-1	10. Work Unit No. R6065
9. Performing Organization Name and Address  Itek Corporation Optical Systems Division 10 Maguire Road Lexington, Massachusetts 02173		11. Contract or Grant No. NAS 3-19400	13. Type of Report and Period Covered Final Report
12. Sponsoring Agency Name and Address  National Aeronautics and Space Administration Washington, D. C. 20546		14. Sponsoring Agency Code	
15. Supplementary Notes  Project Manager, Dr. R. M. Stubbs, NASA Lewis Research Center, Cleveland, Ohio			
16. Abstract  This report presents the results of Itek Corporation's program effort conducted under contract NAS 3-19400 for the NASA Lewis Research Center. The study investigated the application of large expandable mirror structures in future space missions to establish the feasibility and define the potential of high-power laser systems for such applications as propulsion and power transmission. Application of these concepts requires a 30-meter diameter, diffraction limited mirror for transmission of the laser energy. Three concepts for the transmitter are presented. These concepts include consideration of continuous as well as segmented mirror surfaces and the major stow-deployment categories of inflatable, variable geometry and assembled-in-space structures. The mirror surface for each concept would be actively monitored and controlled to maintain diffraction limited performance at 10.6 microns during operation. The proposed mirror configurations are based on existing aerospace state-of-the-art technology. The assembled-in-space concept appears to be the most feasible, at this time. Given further development effort, the inflatable and variable geometry concepts could result in a practical laser-transmitter assembly.			
17. Key Words (Suggested by Author(s))  Laser-transmitter Expandable Mirror Structures Deployable mirror		18. Distribution Statement	
19. Security Classif. (of this report) Unclassified	20. Security Classif. (of this page) Unclassified	21. No. of Pages 110	22. Price* 100

\* For sale by the National Technical Information Service, Springfield, Virginia 22151